

The eROSITA Final Equatorial-Depth Survey (eFEDS): X-ray Properties and Scaling Relations of Galaxy Clusters and Groups

Y. Emre Bahar^{1*}, Esra Bulbul¹, Nicolas Clerc², Vittorio Ghirardini¹, Ang Liu¹, Kirpal Nandra¹, Florian Pacaud³, I-Non Chiu⁴, Johan Comparat¹, Jacob Ider-Chitham¹, Mathias Klein⁵, Teng Liu¹, Andrea Merloni¹, Konstantinos Migkas³, Nobuhiro Okabe^{6,7,8}, Miriam E. Ramos-Ceja¹, Thomas H. Reiprich³, Jeremy S. Sanders¹, Tim Schrabback²

¹Max Planck Institute for Extraterrestrial Physics, Giessenbachstrasse 1, 85748 Garching, Germany

²IRAP, Université de Toulouse, CNRS, UPS, CNES, Toulouse, France

³Argelander-Institut für Astronomie (AIfA), Universität Bonn, Auf dem Hügel 71, 53121 Bonn, Germany

⁴Tsung-Dao Lee Institute, and Key Laboratory for Particle Physics, Astrophysics and Cosmology, Ministry of Education, Shanghai Jiao Tong University, Shanghai 200240, China

⁵Universitaets-Sternwarte Muenchen, Fakultaet fuer Physik, LMU Munich, Scheinerstr. 1, 81679 Munich, Germany

⁶Physics Program, Graduate School of Advanced Science and Engineering, Hiroshima University, 1-3-1 Kagamiyama, Higashi-Hiroshima, Hiroshima 739-8526, Japan

⁷Hiroshima Astrophysical Science Center, Hiroshima University, 1-3-1 Kagamiyama, Higashi-Hiroshima, Hiroshima 739-8526, Japan

⁸Core Research for Energetic Universe, Hiroshima University, 1-3-1, Kagamiyama, Higashi-Hiroshima, Hiroshima 739-8526, Japan

October 20, 2021

ABSTRACT

Context. Scaling relations establish power-law relations between observables of galaxy groups and clusters at different redshift and mass scales. These relations between X-ray observables are used to link physical properties of clusters at cosmic scales, probe evolution of the large-scale structure, and constrain cosmological parameters through cluster counts.

Aims. In this work, we investigate the scaling relations between X-ray observables of the clusters detected in the eFEDS field using Spectrum-Roentgen-Gamma/eROSITA observations taking into account the selection effects and the distributions of observables with cosmic time.

Methods. We extract X-ray observables (L_X , L_{bol} , T , M_{gas} , Y_X) within R_{500} for the sample of 542 clusters in the eFEDS field. By applying detection and extent likelihoods, we construct a subsample of 265 clusters with a contamination level of $< 10\%$ (including AGNs and spurious fluctuations) to be utilized in the scaling relation analysis. The selection function based on the state-of-the-art simulations of the eROSITA sky is fully accounted for in our work.

Results. We provide the X-ray observables in the core-included $< R_{500}$ and core-excised $0.15R_{500} - R_{500}$ apertures for 542 galaxy clusters and groups detected in the eFEDS field. Additionally, we present our best-fit results for the normalization, slope, redshift evolution and intrinsic scatter parameters of the X-ray scaling relations between $L_X - T$, $L_X - M_{\text{gas}}$, $L_X - Y_X$, $L_{\text{bol}} - T$, $L_{\text{bol}} - M_{\text{gas}}$, $L_{\text{bol}} - Y_X$ and $M_{\text{gas}} - T$. We find that the best-fit slopes significantly deviate from the self-similar model at a $> 3\sigma$ confidence level however, our results are in good agreement with the simulations including non-gravitational physics and the recent results that take into account selection effects.

Conclusions. Strong deviations we find from the self-similar scenario indicate that the non-gravitational effects play an important role in shaping the observed physical state of clusters. This work extends the scaling relations to low mass, low luminosity galaxy cluster and group regime using eFEDS observations, demonstrating eROSITA's ability to measure ICM emission out to R_{500} with survey-depth exposures and constrain the scaling relations in a wide mass-luminosity-redshift range.

Key words. Galaxies: clusters: general – Galaxies: groups: general – Galaxies: clusters: intracluster medium – X-rays: galaxies: clusters

1. Introduction

Galaxy clusters, formed by the gravitational collapse of the largest density peaks in the primordial density field, represent the largest virialized objects in the Universe. Embedded in the cosmic web, they evolve and grow through mergers and by accreting smaller subhaloes via the surrounding large scale structure (e.g. Kravtsov & Borgani 2012). The number counts of

clusters of galaxies as a function of redshift and their mass is a powerful cosmological probe that is orthogonal and complementary to the other cosmological geometrical experiments (e.g. Pillepich et al. 2012; Mantz et al. 2015; Schellenberger & Reiprich 2017; Pacaud et al. 2018, also see Pratt et al. 2019 for a review). Additionally, based on the current Lambda cold dark matter (Λ CDM) cosmological model, galaxy clusters are among the structures formed last, therefore capture the formation history and the growth of the structure in the Universe.

* e-mail: ebahar@mpe.mpg.de

Well-established scaling relations between cluster mass and observables provide a way forward for cosmological investigations using clusters of galaxies. Accurate estimates of cluster total masses are crucial ingredients for exploiting the cluster number counts as cosmological probes. However, measurements of masses of individual clusters through multi-wavelength (X-ray, optical, weak lensing, and radio) observations can be expensive for larger cluster samples. Scaling relations aid this problem and bridge cluster number counts with cosmology. On the other hand, the scaling relations between observables and their evolution allow us to constrain intra-cluster medium (ICM) physics and theoretical models based on gravitational collapse (e.g. Kaiser 1986; Ascasibar et al. 2006; Short et al. 2010; Capelo et al. 2012). Kaiser (1986) modeled the formation of clusters as scale-free collapses of initial density peaks and derived relations between ICM properties that results in clusters at different redshifts and masses to be scaled versions of each other. This is called the self-similar model in the literature. Other non-gravitational physical processes, such as radiative cooling, galactic winds, turbulence, and AGN feedback, that affect the formation and evolution of these objects throughout the cosmic time may have imprints on these relations. In observational studies, these imprints are quantified by measuring deviations from the self-similar scaling relations. Clusters of galaxies owing to their deep potential well are less prone to these non-gravitational processes, while the intra-group gas in galaxy groups can be significantly impacted by the non-gravitational physics (e.g. Tozzi & Norman 2001; Borgani et al. 2002; Babul et al. 2002; Puchwein et al. 2008; Biffi et al. 2014; Barnes et al. 2017).

The majority of the baryonic content of the clusters is in the form of X-ray emitting hot ionized plasma, the ICM. Being in the fully ionized state reaching up to 10^8 Kelvin in temperature, the ICM emits primarily in X-rays through thermal Bremsstrahlung offering an opportunity to measure clusters ICM's physical properties, to establish scaling relations between these properties and mass, and to constrain their evolution through cosmic time. The scaling relations between X-ray observables and mass have been extensively explored for massive clusters in the literature, selected in various ways by the multi-wavelength large area surveys (e.g. Mantz et al. 2010b; Bulbul et al. 2019). However, samples including a sufficient number of uniformly selected groups covering the low-mass, low-redshift and low-luminosity range with adequate count rates are limited. The studies of scaling relations of galaxy groups and clusters spanning a wide mass, luminosity, and redshift range with large area surveys with a well-understood selection will allow understanding the interplay between galaxy evolution, AGN feedback, and gravitational processes in these deep potential wells. XMM-Newton's largest observational programme XXL (Pierre et al. 2011) served as a bridge between narrow-deep observations (e.g. CDF-S, Finoguenov et al. 2015) and very wide moderately deep observations (e.g. RASS, Ebeling et al. 1998) by populating the intermediate parameter space with detected clusters. Most recently, extended ROentgen Survey with an Imaging Telescope Array (eROSITA, Merloni et al. 2012; Predehl et al. 2021) carried out its eROSITA Final Equatorial-Depth Survey (eFEDS) observations and provided numerous cluster detections that span a large mass-redshift space. eROSITA on-board the Spectrum-Roentgen-Gamma (SRG) mission continues to detect large numbers of clusters spanning a wide range of redshift, mass since its launch in 2019. It will provide sufficient statistical power, and place the tightest constraints on these scaling relations for probing their mass and redshift evolution.

The eFEDS was performed during eROSITA's calibration and performance verification phase (Predehl et al. 2021; Brunner et al. 2021; Liu et al. 2021a). eFEDS, the first (mini)survey of eROSITA, aims to serve as a demonstration of the observational capabilities of the telescope to the scientific community. The survey area is located at (approximately) $126^\circ < \text{R.A.} < 146^\circ$ and $-3^\circ < \text{Dec.} < +6^\circ$ and covers a total of $\sim 140 \text{ deg}^2$. The exposure time of the survey area is mostly uniform with average vignetted and unvignetted exposure times of ~ 1.3 and $\sim 2.2 \text{ ks}$ respectively (Brunner et al. 2021). The eFEDS area is also covered in survey programs of other telescopes such as the Hyper Supreme-Cam Subaru Strategic Program (HSC-SSP; Aihara et al. 2018), DECaLS (Dark Energy Camera Legacy Survey, Dey et al. 2019), SDSS (Sloan Digital Sky Survey, Blanton et al. 2017; Ider-Chitham et al. 2021), 2MRS (2MASS Redshift Survey, Huchra et al. 2012), and GAMA (Galaxy And Mass Assembly, Driver et al. 2009). These observations are used to optically confirm the detected clusters and measure their redshifts (Klein et al. 2021; Ider-Chitham et al. 2021). Besides the optical confirmation and redshift determination, HSC-SSP observations are also utilized in measuring the weak lensing mass estimates of the detected clusters. The observables presented in this work are measured using R_{500} ¹ values inferred from these weak lensing measurements (Chiu et al. 2021). In this work, we provide X-ray properties of the 542 galaxy clusters and groups in the full eFEDS extent selected sample in two apertures ($r < R_{500}$ and $0.15R_{500} < r < R_{500}$) (Liu et al. 2021a). Additionally, we investigate the scaling relations between core-included ($r < R_{500}$) X-ray observables in a subsample of 265 galaxy clusters and groups with a lower level of contamination by non-cluster detections. This work expands the scaling relation studies to the poorly explored mass ($6.86 \times 10^{12} \text{ M}_\odot < M_{500} < 7.79 \times 10^{14} \text{ M}_\odot$), luminosity ($8.64 \times 10^{40} \text{ erg s}^{-1} < L_X < 3.96 \times 10^{44} \text{ erg s}^{-1}$), and redshift ($0.017 < z < 0.94$) ranges with the largest number of galaxy groups and clusters, paving the way forward for these studies for the eROSITA All-Sky survey (eRASS) observations. We note that the scaling relations between X-ray observables and weak lensing masses have been already published in our companion paper, Chiu et al. (2021). The selection function is based on the realistic full sky simulations of eROSITA and fully accounted for in our results (Comparat et al. 2020). Throughout this paper, the best-fitting thermal plasma temperature to the cluster spectra is marked with T , L_X stands for soft band X-ray luminosity calculated in the $0.5 - 2.0 \text{ keV}$ energy band, L_{bol} stands for the bolometric luminosity calculated in the $0.01 - 100 \text{ keV}$ energy band, the errors correspond to 68% and, we adopt a flat ΛCDM cosmology using the Planck Collaboration et al. (2016) results, namely $\Omega_m = 0.3089$, $\sigma_8 = 0.8147$ and $H_0 = 67.74 \text{ km s}^{-1} \text{ Mpc}^{-1}$

2. Data Analysis

2.1. Data Reduction and the Sample Selection

The eFEDS observations were performed by eROSITA between the 4th and 7th of November 2019. Observation strategy allowed the eFEDS field to be surveyed nearly uniformly with a vignetted exposure of $\sim 1.3 \text{ ks}$ which is similar to the expected vignetted exposure of the final eROSITA All-Sky Survey (eRASS8) at the equatorial regions. First processing of the eFEDS observations are carried out by the eROSITA Standard Analysis Software

¹ R_{500} is the overdensity radius within which the density of the cluster is 500 times the critical density of the Universe at the cluster's redshift.

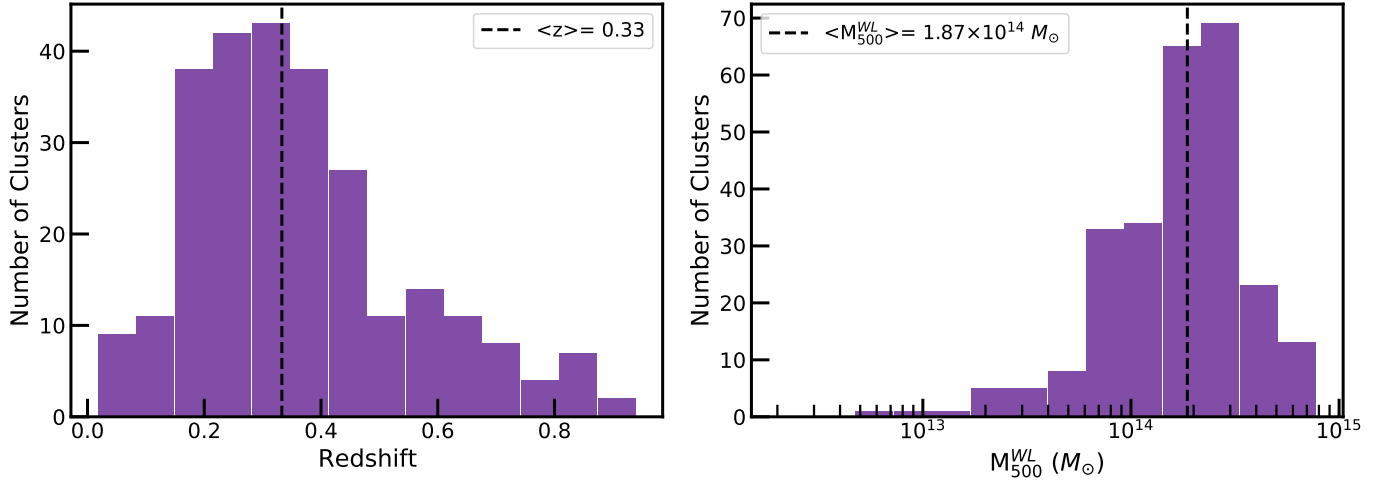


Fig. 1: *Left:* Redshift histogram of the $\mathcal{L}_{\text{det}} > 15$, $\mathcal{L}_{\text{ext}} > 15$ sample used in this work. *Right:* Weak lensing calibrated total mass (M_{500}^{WL}) histogram of the $\mathcal{L}_{\text{det}} > 15$, $\mathcal{L}_{\text{ext}} > 15$ sample used in this work excluding upper limit measurements. Medians of the measurements are marked with dashed line. The overdensity radii of R_{500} within which we measure the X-ray observables are calculated from these mass measurements (see Chiu et al. 2021).

System (eSASS, version eSASSusers_201009, Brunner et al. 2021). In this paper, we only present an outline of the summary of the data reduction and source detection. We refer the reader to Brunner et al. (2021) and Liu et al. (2021a) for more detailed explanations of these steps. We first applied filtering to X-ray data, removing dead time intervals and frames, corrupted events, and bad pixels. Images created in 0.2 – 2.3 keV band using all available telescope modules (TMs) are passed to eSASS source detection tools in order to perform the source detection procedure and provide extension and detection likelihoods. After applying a detection likelihood (\mathcal{L}_{det}) threshold of 5 and an extension likelihood (\mathcal{L}_{ext}) threshold of 6, we obtained 542 cluster candidates in the eFEDS field (Brunner et al. 2021). The physical properties of these clusters, such as soft-band and bolometric luminosities, ICM temperature measurements within a physical radius of 300 kpc and 500 kpc are provided in Liu et al. (2021a).

We used realistic simulations of the eFEDS field (Liu et al. 2021b) in order to measure the contamination fractions of samples with different \mathcal{L}_{det} and \mathcal{L}_{ext} cuts. According to these simulations, the eFEDS cluster catalog, which consists of 542 clusters, has a contamination fraction of $\sim 20\%$. This is a relatively high contamination rate for statistical studies. For the results not to be biased heavily by the non-cluster sources present in the sample (e.g. AGNs and spurious sources), we applied $\mathcal{L}_{\text{det}} > 15$ and $\mathcal{L}_{\text{ext}} > 15$ cuts that give us a sample of 265 clusters with an expected contamination fraction of 9.8%. The final sample covers total mass range of $(6.86 \times 10^{12} \text{ M}_\odot < M_{500} < 7.79 \times 10^{14} \text{ M}_\odot)$, luminosity range of $8.64 \times 10^{40} \text{ erg s}^{-1} < L_X < 3.96 \times 10^{44} \text{ erg s}^{-1}$, and redshift range of $(0.017 < z < 0.94)$. The redshift and mass histograms of this final subsample is shown in Fig 1. Consisting of 68 low-mass ($< 10^{14} \text{ M}_\odot$) galaxy groups, this work extends the scaling relation studies to the low-mass range with one of the largest group sample detected uniformly to date.

2.2. X-ray Observables within R_{500}

One of the main goals of this paper is to provide X-ray properties of eFEDS clusters within the overdensity radius of R_{500} . Here we provide a short summary of the methods we employed to

extract X-ray observables. For a complete description, we refer the reader to Ghirardini et al. (2021b) and Liu et al. (2021a).

The measurements of R_{500} used in this work are obtained from the weak lensing calibrated cluster masses presented in our companion paper Chiu et al. (2021). Calibration is applied by using the eFEDS observations of the same cluster sample used in this work which enables the R_{500} measurements to be self-consistent. Mass estimates are obtained by jointly modeling the eROSITA X-ray count-rate (η) and HSC shear profile (g_+) as a function of cluster mass (M_{500}) and obtaining a scaling relation between $\eta - M_{500} - z$. After obtaining the mass estimates, R_{500} measurements are calculated by $R_{500} = \left(\frac{3}{4\pi} \frac{M_{500}}{500\rho_c}\right)^{1/3}$ where ρ_c is the critical density at the given redshift and cosmology. We refer the reader to Chiu et al. (2021) for a more detailed description of the HSC weak-lensing mass calibration analysis.

X-ray spectra of clusters are extracted within R_{500} , both core-included ($r < R_{500}$) and core-excised ($0.15R_{500} < r < R_{500}$), using the eSASS code `srctool1`. The background spectra are extracted from an annular region that is $4 - 6 R_{500}$ away from the clusters' centroid. We fit the X-ray spectra with an absorbed apec thermal plasma emission model (Smith et al. 2001; Foster et al. 2012) to represent the ICM emission. The fitting band of 0.5 – 8 keV used for TMs 1,2,3,4,6 and a more restricted band of 0.8 – 8 keV used for TMs 5 and 7 in the spectral fits due to the light leak noticed during the commissioning phase (see Predehl et al. 2021). The Galactic hydrogen absorption is modeled using `tbabs` (Wilms et al. 2000), where the column density n_{H} used is fixed to $n_{\text{H,tot}}$ (Willingale et al. 2013), estimated at the position of the cluster center. The metallicity of the clusters is fixed to $0.3 Z_\odot$, adopting the solar abundance table of Asplund et al. (2009). The background spectra and spectra are simultaneously fit to account for the background in the total spectra as described in detail in (Ghirardini et al. 2021b). The background spectra are modeled with a set of apec and power-law models representing instrumental background based on the filter-wheel closed data (see Freyberg et al. 2020)², cosmic background (local bubble, galactic halo, and emission from unresolved AGN). The best-fit values and standard deviations of the ICM temper-

² <https://erosita.mpe.mpg.de/edr/eROSITAObservations/EDRFWC/>

atures (T) are measured using the Markov chain Monte Carlo (MCMC) method within XSPEC (version 12.11.0k).

We extract images and exposure maps in the 0.5 – 2.0 keV energy band to obtain cluster density profiles. We model the two-dimensional distribution of photons by projecting the [Vikhlinin et al. \(2006\)](#) density model. Point sources are either modeled or masked depending on their fluxes, see [Ghirardini et al. \(2021a\)](#) for further details. The cosmic background contribution is added to the total model as a constant. The resulting total image is finally convolved with eROSITA's vignetted exposure map, while the instrumental background model folded with the un-vignetted exposure map. A Poisson log-likelihood in MCMC is used to estimate best-fit cluster model parameters. Finally, the electron density (n_e) profile of the gas is obtained by measuring the emissivity using the temperature information recovered from the spectral analysis. Best-fit parameters of clusters to the [Vikhlinin et al. \(2006\)](#) electron density profile model are presented in Table 5. In order to obtain luminosity profiles, $L_X(r)$ and $L_{\text{bol}}(r)$, we calculated conversion factors from count rate to luminosity in soft (0.5 – 2.0 keV) and bolometric (0.01 – 100 keV) energy bands.

Gas mass (or ICM mass) of the clusters enclosed within R_{500} is computed by integrating the gas electron density assuming spherical symmetry

$$M_g = \mu_e m_p \int_0^{R_{500}} n_e(r) 4\pi r^2 dr \quad (1)$$

where n_e is the number density of electrons, m_p is the proton mass, and $\mu_e = 1.1548$ is the mean molecular weight per electron, calculated using the [Asplund et al. \(2009\)](#) abundance table ([Bulbul et al. 2010](#)).

Lastly, Y_X is calculated by multiplying the gas mass (M_{gas}) with the gas temperature (T) as

$$Y_X = M_{\text{gas}} \cdot T \quad (2)$$

which is introduced by [Kravtsov et al. \(2006\)](#) as a low scatter mass estimator.

We note that in our analysis, uncertainties in R_{500} measurements are fully propagated using the MCMC chains and the redshift errors are neglected. We use the single temperature in our calculations as the survey data do not have sufficient depth to recover the temperature profiles as a function of radius. For all eFEDS clusters, we provide the core-included ($r < R_{500}$) X-ray observables within R_{500} , including T , L_X , L_{bol} , M_{gas} , Y_X as well as the core-excluded X-ray observables extracted between $0.15R_{500} - R_{500}$ (T_{cex} , $L_{X,\text{cex}}$, $L_{\text{bol,cex}}$) in Table 4. eROSITA's field of view averaged point spread function (PSF) half energy width is $\sim 26''$ which is comparable to the cores ($0.15R_{500}$) of the majority of clusters. This has a mild effect on the $L_{X,\text{cex}}$ measurements since we deconvolve the surface brightness profiles with the PSF and used the best fit core included temperatures for the emissivity. However, given the limited photon statistics, only a first-order PSF correction is applied to the T_{cex} measurements where the flux change at different energies are compensated by assuming the spectrum to be similar over the whole of the source. Therefore, we advise reader to approach T_{cex} measurements with caution.

In this work, we focus on the scaling relations between X-ray observables, namely $L - T$, $L - M_{\text{gas}}$, $L - Y_X$, $M_{\text{gas}} - T$. The scaling relations between observables and cluster mass (M_{500}) obtained from weak lensing observations are already provided in the companion paper by [Chiu et al. \(2021\)](#). Although we provide

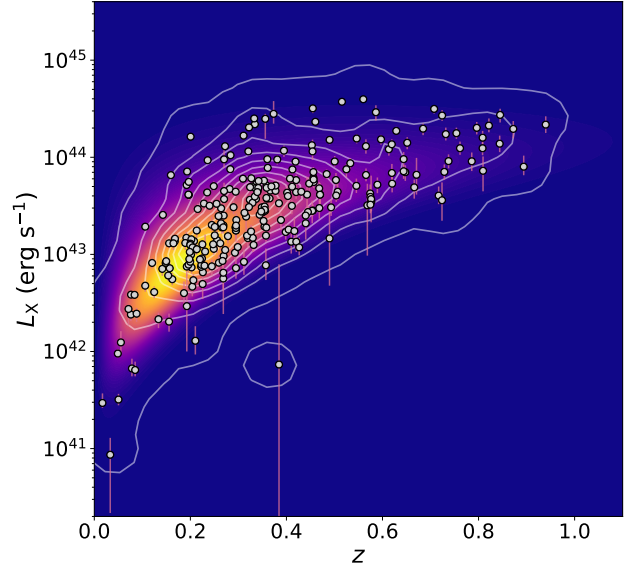


Fig. 2: Soft band (0.5 – 2.0 keV) X-ray luminosity and redshift measurements of the clusters in the eFEDS field that satisfies the $\mathcal{L}_{\text{det}} > 15$ and $\mathcal{L}_{\text{ext}} > 15$ condition. Luminosities are measured within apertures of R_{500} . White solid curves are smoothed contours of the $L_X - z$ data points and the color is proportional to pdf of the hypothetical $L_X - z$ distribution modeled as $P(I, L_X, z) = P(I|L_X, z)P(L_X|z)P(z)$ (see Sect. 3.3 for the description of the model).

measurements of the core-excluded observables in this paper in Table 4, we only use the core-included observables in our further analysis for the scaling relations. The reason is twofold - one the selection function, and two the decrease in the statistics. Our selection function is built using the core-included observables from the simulations of eROSITA sky ([Comparat et al. 2020](#)). Constructing selection functions with the core-excised observables relies on modeling the PSF accurately in simulations. Our imaging analysis and spectral fits account for the PSF spilling, however, this analysis is not available yet in simulations. As a workaround, one could model the relation between the core excised and core included observables (e.g. $P(Y_{X,\text{cex}}|Y_X)$) however, a significant fraction of eFEDS clusters populate a previously poorly explored parameter space and such an approach requires a good understanding of the surface brightness profiles of these clusters. Secondly, when the core is excised, the temperature measurements become either loose or lost due to the decrease in photon statistics. This affects the reliability of the X-ray observable measurements used in our fits and may lead to biased constraints on the scaling relations. The full analysis with the core-excised observables will be done for the clusters detected in the eRASS observations, where we expect to have a larger sample of clusters with a higher depth around the ecliptic poles ([Ghirardini et al. 2022, in prep.](#)).

3. Modeling and Fitting of the Scaling Relations

We model the scaling relations and the likelihoods for different pairs of observables in a similar manner with minor tweaks. Therefore, in this section, we present the general form of the

Table 1: Self-similar expected model parameter values of scaling relations of the form $Y = A Y_{\text{piv}} \left(\frac{X}{X_{\text{piv}}} \right)^B \left(\frac{E(z)}{E(z_{\text{piv}})} \right)^C$

Relation			
Y	X	B_{self}	C_{self}
L_X	T	3/2	1
L_X	M_{gas}	1	2
L_X	Y_X	3/5	8/5
L_{bol}	T	2	1
L_{bol}	M_{gas}	4/3	7/3
L_{bol}	Y_X	4/5	9/5
M_{gas}	T	3/2	-1

scaling relations and the structure of the likelihood for two hypothetical observables: X and Y .

3.1. General Form of the Scaling Relations

Kaiser (1986) derived simple forms of scaling relations, self-similar relations, by assuming gravitational interactions to be the driving force of the evolution of groups and clusters. These relations suggest the observables of clusters to follow these simple power-law relations. Departures from these relations are often interpreted as a result of non-gravitational physical processes, such as radiative cooling, galactic winds, and AGN feedback that can have a significant impact on the distribution of baryons in the ICM and energy budget of the system (Bhattacharya et al. 2008; McCarthy et al. 2010; Fabjan et al. 2010; Bulbul et al. 2016; Giordini et al. 2013; Lovisari et al. 2020).

In this work, we use a relation that takes into account the power-law dependence and the redshift evolution of the form

$$Y = A Y_{\text{piv}} \left(\frac{X}{X_{\text{piv}}} \right)^B \left(\frac{E(z)}{E(z_{\text{piv}})} \right)^C \quad (3)$$

where Y_{piv} , X_{piv} , z_{piv} are the pivot values of the sample. A , B , C are the normalization, power-law slope, and redshift evolution exponent, respectively. The redshift evolution is modeled using the evolution function which is defined as $E(z) = H(z)/H_0$ where $H(z)$ is the Hubble-Lemaître parameter and H_0 is the Hubble constant.

3.2. Likelihood

In our fits to the scaling relations, we take into account various observational and physical effects by adding the relevant components to the corresponding likelihood function similar to the method presented in Giles et al. (2016) for the XXL clusters. The joint probability function in terms of the measured values (\hat{X} , \hat{Y}) of the true values of the observables X and Y is given by

$$P(\hat{Y}, \hat{X}, Y, X, I|\theta, z) = P(I|Y, z)P(\hat{Y}, \hat{X}|Y, X)P(Y|X, \theta, z)P(X|z) \quad (4)$$

where $P(I|Y, z)$ is the probability of a cluster to be included (I) in our sample, i.e. the selection function, $P(\hat{Y}, \hat{X}|Y, X)$ is the two-dimensional measurement uncertainty, $P(Y|X, \theta, z)$ is the modeled $Y - X$ relation, and the $P(X|z)$ term is the cosmological distribution of the observable X . The variable θ in the scaling relation term marks the free parameters of the scaling relation, such

as A , B , C , the scatter $\sigma_{Y|X}$. We note that in this work, correlations between the the measurement uncertainties of observables X and Y are fully considered using the MCMC chains. We also note that the cosmological parameters are frozen throughout our analysis. More than 65% of the clusters in our sample have spectroscopic redshifts and the rest of the sample have photometric redshift measurements using the high signal-to-noise HSC data that provides uncertainties of the order of 0.3% (see Klein et al. 2021; Ider-Chitham et al. 2021). Therefore, we assume that the errors on the redshifts have negligible effects on our measurements, i.e. $z = \hat{z}$. The variance in exposure time due to the overlapping regions and the missed observations due to malfunctions of telescope modules (TMs) (see Brunner et al. 2021, for details) are accounted for by using the exposure time (t_{exp}) at the X-ray center of each cluster when calculating $P(I|Y, z)$.

We model the $Y - X$ relation such that the observable Y is distributed around the power-law scaling relation log-normally. The assumption of the log-normal distribution of X-ray observables is widely used in the literature (e.g. Pacaud et al. 2007; Giles et al. 2016; Bulbul et al. 2019; Bocquet et al. 2019). Then the scaling relation term $P(Y|X, \theta, z)$ in Eqn. 4 becomes

$$P(Y|X, \theta, z) = \mathcal{LN} \left(\mu = A Y_{\text{piv}} \left(\frac{X}{X_{\text{piv}}} \right)^B \left(\frac{E(z)}{E(z_{\text{piv}})} \right)^C, \sigma = \sigma_{Y|X} \right). \quad (5)$$

To obtain the cosmological distribution of the observable X ($P(X|z)$), i.e. the expected distribution of X as function of redshift given a fixed cosmology and an assumed $X - M$ scaling relation, we convert the Tinker et al. (2008) mass function to a Tinker X function using the Chiu et al. (2021) weak lensing mass calibrated scaling relations obtained from the same cluster sample consistently. This conversion is applied such that the intrinsic scatter of the $X - M$ relation is taken into account by the following equation

$$P(X|\theta_{\text{WL}}, z) = \int_M P(X|M, \theta_{\text{WL}}, z)P(M|z)dM \quad (6)$$

where θ_{WL} is the best-fit result of the weak lensing mass calibrated scaling relation $X - M_{500}$. We note that the form of the $X - M$ relation presented in Chiu et al. (2021) is different than the form we use in our $Y - X$ relation. From hereon, we will omit including the θ_{WL} term in $P(X|\theta_{\text{WL}}, z)$, since it is fixed throughout the analysis. After properly defining all the terms in the joint distribution in Eqn. 4, we marginalize over the nuisance variables (X , Y) in order to get the likelihood of obtaining the measured observables (\hat{X} , \hat{Y} , I). Then the final likelihood of a single cluster becomes

$$P(\hat{Y}, \hat{X}, I|\theta, z) = \int \int_{Y, X} P(I|Y, z) \\ \times P(\hat{Y}, \hat{X}|Y, X)P(Y|X, \theta, z)P(X|z)dYdX. \quad (7)$$

To avoid the results to be biased significantly by the assumed cosmological model and the exact form of the $X - M$ relation, we do not use the observed number of detected clusters as data, instead, we take it as a model parameter. In Bayesian framework, this corresponds to using a likelihood that quantifies the probability of measuring \hat{X}_i and \hat{Y}_i observables given that the cluster is

Table 2: Median values of observables measured for the $\mathcal{L}_{\text{det}} > 15$, $\mathcal{L}_{\text{ext}} > 15$ clusters.

Parameters	Median/Pivots
L_X	$3.20 \times 10^{43} \text{ erg s}^{-1}$
L_{bol}	$9.49 \times 10^{43} \text{ erg s}^{-1}$
T	3.26 keV
M_{gas}	$1.04 \times 10^{13} M_\odot$
Y_X	$3.75 \times 10^{13} M_\odot \text{ keV}$
z	0.33

Notes. These values are used as pivot values of observables in Eqn. 3

detected. Such a likelihood can be obtained by using the Bayes theorem where the likelihood for the i 'th cluster becomes

$$\mathcal{L}(\hat{Y}_i, \hat{X}_i | I, \theta, z_i) = \frac{P(\hat{Y}_i, \hat{X}_i, I | \theta, z_i)}{\int \int_{\hat{Y}_i, \hat{X}_i} P(\hat{Y}_i, \hat{X}_i, I | \theta, z_i) d\hat{Y}_i d\hat{X}_i} \quad (8)$$

Lastly, the overall likelihood of the sample is obtained by multiplying the likelihoods of all clusters

$$\mathcal{L}(\hat{Y}_{\text{all}}, \hat{X}_{\text{all}} | I, \theta, z) = \prod_i^{\hat{N}_{\text{det}}} \mathcal{L}(\hat{Y}_i, \hat{X}_i | I, \theta, z_i) \quad (9)$$

where \hat{Y}_{all} and \hat{X}_{all} are the measurements observables of all clusters in the sample and \hat{N}_{det} is the number of detected clusters in our sample.

This form of the likelihood is similar to ones used in the literature, e.g. Mantz et al. (2010a). The most fundamental difference is the goal of this work, i.e. to fit the scaling relations at a fixed cosmology rather than simultaneously fitting scaling relations and cosmological parameters. Using this likelihood allows us to avoid including terms as in Mantz et al. (2010b) that have a strong dependence on cosmology such as the probability of not detecting the model-predicted, undetected clusters, $P(\bar{I}|\theta)$, possible combinations of detecting observed many clusters, $\binom{N}{\hat{N}_{\text{det}}}$, and the prior distribution of the total number of clusters in the field, $P(N)$ (see Mantz 2019, for the use of these parameters). Another benefit of using this likelihood is it allows the results to be less sensitive to the accuracy of the normalization of the $X - M$ relation and therefore makes our analysis more robust for the goal of this work.

3.3. Modeling the Selection Function

The selection function model, $P(I|Y, z)$ in Eqn. 7, adopted here is similar to that described in Liu et al. (2021a). It relies on multiple mock realizations of the eFEDS field (Liu et al. 2021b). The simulations faithfully reproduce instrumental characteristics of eROSITA and features induced by the scanning strategy (exposure variations, point-spread function, effective area, and grasps of the seven telescopes.) Realistic source, fore- and background models are associated with a full-sky light-cone N-body simulation assuming Planck-CMB cosmology. These sources include stars, active galactic nuclei (AGN), and galaxy clusters. The method to associate AGN spectral templates to sources is derived from abundance matching techniques. For clusters and groups, the association between a massive dark matter halo and an emissivity profile drawn from a library of observed templates

depends on the mass, redshift, and dynamical state of the halo. In particular, relaxed halos are associated with gas distributions with higher central projected emission measures. The steps leading to the AGN and cluster simulations are extensively described in Comparat et al. (2019, 2020). The SIXTE engine (Dauser et al. 2019) serves in converting sources into event lists, while the eSASS software (Brunner et al. 2021) is used to process those lists and to deliver source catalogs.

The next steps are identical to Liu et al. (2021a), except for the definition of an extended detection which assumes $\mathcal{L}_{\text{det}} > 15$ and $\mathcal{L}_{\text{ext}} > 15$. In particular, pairs of the simulated and detected sources are searched in the plane of the sky, accounting for their relative positions, their extents and favoring association between bright sources in case of ambiguity. Securely identified matches are flagged as a successful detection.

The modeling of the detection probabilities involves interpolation across the multi-dimensional parameter space describing galaxy cluster properties, which includes their intrinsic soft-band or bolometric luminosity, their redshift, the local exposure time and optionally the central emission measure. Other parameters are marginalized over, making the assumption that their distributions are correctly reflected in the simulations. To this end, we make use of Gaussian Process classifiers, a class of non-parametric models which captures the variations of the detection probability under the assumption of the covariance function (kernel) being a squared exponential function. One advantage of using such models, over the multi-dimensional spline interpolation, for example, is a more appropriate mathematical treatment of uncertainties, particularly in poorly populated areas of the parameter space. Two-thirds of the simulated clusters are used for training the classifiers, and the remaining third provides the material to test the performance of the classifiers and to assess their behavior on a realistic population of halos. In particular, we check that systems assigned a given detection probability by the classifier display a detection rate with a value close to that probability – the classifier is said to be well-calibrated.

These models are designed to emulate the whole chain of computationally expensive steps needed in performing an eFEDS end-to-end simulation (Liu et al. 2021b). It is worth noting that such selection functions have a range of applicability that is set by the simulation.

In order to demonstrate the representativeness of the selection function, we model the luminosity distribution of the $\mathcal{L}_{\text{det}} > 15$, $\mathcal{L}_{\text{ext}} > 15$ clusters and compare it with the observed cluster distribution. We model it as $P(I, L_X, z) = P(I|L_X, z)P(L_X|z)P(z)$ where we calculate $P(L_X|z)$ using the Eqn. 6 and the best-fit $L_X - M$ relation presented in Chiu et al. (2021). For the redshift distribution, we assume the comoving cluster density to be constant within our redshift span ($0 < z < 0.9$) so that $P(z)$ is proportional to the comoving volume shell $dV_c(z) = \frac{c}{H_0} \frac{(1+z)^2 d_A(z)^2}{E(z)} \Omega_s dz$ (Hogg 1999) where c is the light speed, H_0 is the Hubble constant, $d_A(z)$ is the angular diameter distance and Ω_s is the solid angle of the eFEDS survey. A comparison between the distribution of the luminosity measurements for the cluster sample with $\mathcal{L}_{\text{det}} > 15$, $\mathcal{L}_{\text{ext}} > 15$ selection and our model predicted by our selection function is shown in Fig. 2. The figure visually demonstrates the consistency of the luminosity distribution with redshift predicted from the selection function (plotted as the background color), and measurements from the eFEDS data (white data points and white contours).

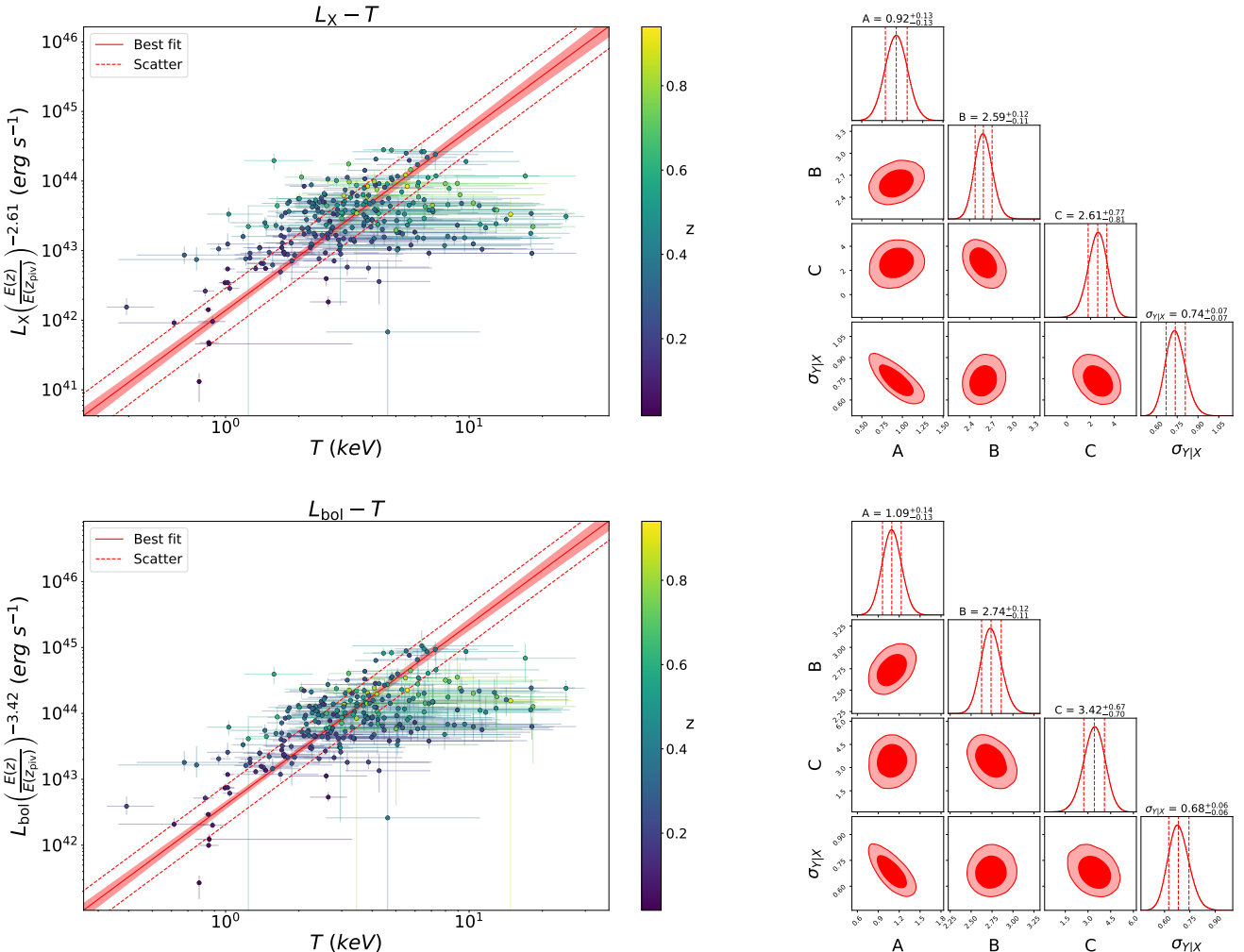


Fig. 3: *Left:* Soft band ($0.5 - 2.0$ keV) X-ray luminosity (L_X), bolometric ($0.01 - 100$ keV) luminosity (L_{bol}), temperature (T) and redshift (z) measurements of the $\mathcal{L}_{\text{det}} > 15$, $\mathcal{L}_{\text{ext}} > 15$ sample and the best-fit scaling relation models. Light-red shaded area indicating 1σ uncertainty of the mean of the log-normal model (see Eqn. 5) and dashed red line indicating the best-fit standard deviation ($\sigma_{L|T}$) around the mean. *Right:* The parameter constraints of the $M_{\text{gas}} - T$ relation obtained from the second half of the MCMC chains. Marginalized posterior distributions are shown on the diagonal plots and the joint posterior distributions are shown on off-diagonal plots. Red dashed vertical lines indicate 32th, 50th and 68th percentiles and contours indicate 68 and 95% credibility regions.

3.4. Fitting

We fit scaling relations using the MCMC sampler package `emcee` (Foreman-Mackey et al. 2013) with a likelihood described in Sect. 3.2. Before we fit the real data, we validate our fitting code on simulated clusters. For the tests, we mock X-ray observables of a sample of 265 clusters corresponding to the same number of clusters in the sample selected with the criteria of $\mathcal{L}_{\text{det}} > 15$ and $\mathcal{L}_{\text{ext}} > 15$. We sample the observables, X , and Y , from a bivariate distribution of the form using the observed redshifts as priors,

$$P(Y, X, I|\theta_{\text{sim}}, z) = P(I|Y, z)P(Y|X, \theta_{\text{sim}}, z)P(X|z) \quad (10)$$

where $P(Y|X, \theta_{\text{sim}}, z)$ is the scaling relation term including intrinsic scatter and θ_{sim} is the input scaling relations parameters for the simulated clusters. We then scatter the X and Y observables to mimic observational uncertainty and assign conservative error

bars to model our observable measurements. We then run our fitting code on the simulated clusters with 100 walkers for 10000 steps and compare the best-fit θ values with the input parameters (θ_{sim}). We find that the fitting code successfully recovers all input parameters with a deviation within one sigma validating the performance and the accuracy of the code.

After the test run, we fit the X-ray scaling relations using the eFEDS measurements using flat priors for all scaling relations parameters; $\mathcal{U}(-4, 4)$ for the normalization (A), $\mathcal{U}(-10, 10)$ for the slope (B), $\mathcal{U}(-10, 10)$ for the redshift evolution exponent (C), and $\mathcal{U}(0.1, 3.0)$ for the scatter ($\sigma_{Y|X}$). The median values of the observables are used as the pivot values in our fits that are provided in Table 2.

In total, we perform two fits for each scaling relation with: the first fits are performed with free redshift evolution exponents, C , and the second fits where the parameter C is fixed to the self-similar values. The self-similar expectations are given in Table 1 for all scaling relations used in this work. The best-fit parameters

of these seven relations can be found in Table 3. We provide our results and comparisons with the literature in Section 4.

4. Results

Scaling relations between X-ray observables are tools for understanding the ICM physics for various mass scales and evolution of the ICM with redshift, while the relations between observables and cluster mass are used for facilitating cosmology with cluster number counts. In this section we examine the $L - T$, $L - M_{\text{gas}}$, $L - Y_X$, $M_{\text{gas}} - T$ scaling relations, using both L_X and L_{bol} , and provide extensive comparisons with the literature. Owing to the high soft-band sensitivity of the eROSITA, we were able to include a large number of low-mass/luminosity clusters in our study, down to the soft band luminosities of 8.64×10^{40} ergs s $^{-1}$ and masses (M_{500}) of $6.86 \times 10^{12} M_{\odot}$. In the eFEDS field alone, we detect a total of 68 low-mass groups with $M_{500} < 10^{14} M_{\odot}$ that are fully included in our analysis. eROSITA will be revolutionary in both ICM studies and cosmology in this regard as it will extend clusters samples to much lower luminosities and lower masses than ever reached before. We first describe our method and lay the groundwork with the eFEDS sample with this work, and will push the mass and luminosity limits down with our ongoing work on the eRASS1 sample. One other important aspect is the fact that eROSITA group and cluster samples are uniformly selected and the selection function is well-understood with the help of our full-sky eROSITA simulations.

There are several complications comparing scaling relations results in the literature with our results: the form of the fitted scaling relations, energy band of extracted observables, the assumed cosmology, or instrument calibration varies from one study to another. To overcome these difficulties, we apply corrections before we compare them with our results. In these comparison plots, we use the self-similar redshift evolution as the common reference point and convert the observables accordingly. The standard energy band we use in this paper for the extraction of observables is the 0.5 – 2.0 keV band. To convert normalizations of scaling relations involving luminosities obtained in the 0.1 – 2.4 keV energy band ($L_{0.1-2.4}$), we fake an unabsorbed APEC spectra within XSPEC and calculated a conversion factor of 1.64 for a cluster at a redshift of 0.33, has a temperature of 3.26 keV and has an abundance of 0.3 where redshift and the temperature values are medians of our sample (see Table 2). Changing the temperatures and redshifts affects the conversion factor by a few percent, consistent with the findings of Lovisari et al. (2020) therefore we applied the same conversion factor to all other works using 0.1 – 2.4 keV energy band. Lastly, we convert the relations assuming the dimensionless Hubble constant to be 0.6774 which is the value we use in this work. The corrections are only applied to the normalizations, therefore the slopes and redshift evolution exponents of previously reported relations remain unchanged.

Another challenge in comparisons of scaling relations involving the ICM temperature is the calibration differences between various X-ray telescopes. It has been shown that calibration differences between *Chandra* and *XMM-Newton* are band dependent and can be as large as a factor of two for hot clusters with temperatures > 10 keV in the soft band (0.7–2 keV) (Schellenberger et al. 2015). This difference, however, is small 10–15% in the full 0.7 – 7 keV band for low temperature clusters (< 4 keV) to which we are sensitive to in the eFEDS observations. Our preliminary, calibration studies with eROSITA showed that in general, eROSITA temperatures are in good agreement with

Chandra and *XMM-Newton* temperatures (Sanders et al. 2021; Veronica et al. 2021; Iljenkarevic et al. 2021; Whelan et al. 2021). Turner et al. (2021) recently cross matched the eFEDS cluster catalog (Liu et al. 2021a) with the *XMM-Newton* Cluster Survey (XCS, Romer et al. 2001) sample and found luminosities of 29 cross-matched clusters to be in excellent agreement. They also compared temperatures of 8 clusters that are measured with both telescopes and found *XMM* measurements to have slightly higher temperatures on average. In order to understand the instrumental differences better, more extensive studies should be performed with a cluster sample containing larger range of temperatures using the survey data. This will be further investigated in future eROSITA projects.

4.1. $L_X - T$ and $L_{\text{bol}} - T$ Relations

The two main observables from X-rays, luminosity, and temperature, reflect different but complexly related features of the ICM in clusters. On one hand, luminosity is proportional to the square of the electron density, therefore it is highly sensitive to the distribution of the hot gas. On the other hand, the temperature is related to the average kinetic energy of the baryons in the ICM. Both luminosity and temperature are subject to gravitational and non-gravitational effects in a different manner and this makes their relation non-trivial (see Giodini et al. 2013, for a more detailed discussion). Hence, a better understanding of the $L - T$ relation will shed light on the history of the heating and cooling mechanisms of clusters.

In the self-similar scenario (Kaiser 1986), the relation between luminosity, temperature and redshift follows as

$$L_X \propto T^{3/2} E(z) \quad (11)$$

and

$$L_{\text{bol}} \propto T^2 E(z). \quad (12)$$

however, there are plethora of studies in the literature report steeper $L_X - T$ ($B \sim 2.5$) and $L_{\text{bol}} - T$ ($B \sim 3.0$) relations compared to their self similar predictions (e.g. Pratt et al. 2009; Eckmiller et al. 2011; Maughan et al. 2012; Hilton et al. 2012; Kettula et al. 2015; Lovisari et al. 2015; Zou et al. 2016; Giles et al. 2016; Molham et al. 2020).

Our best-fit results for the $L_X - T$ relation are presented in Table 3 where we report a slope of $B = 2.59^{+0.12}_{-0.11}$, a redshift evolution dependence of $C = 2.61^{+0.77}_{-0.81}$ and a scatter of $\sigma_{L_X|T} = 0.74 \pm 0.07$. The best-fit model is shown in Fig. 3. In general, our results agree well with studies that account for the selection biases. A comparison of our results with some others can be found in Fig. 4. Our best-fit slope is significantly steeper at a $\sim 9\sigma$ confidence level than the self-similar expectation ($B_{\text{self}} = 3/2$). However, it is in very good agreement with the slopes reported for the XXL sample, $B = 2.63 \pm 0.15$, (Giles et al. 2016) and the combined Northern ROSAT All-Sky Survey (NORAS) plus ROSAT-ESO Flux Limited X-ray Survey (REFLEX) samples, $B = 2.67 \pm 0.11$, (Lovisari et al. 2015). We note that they fully account for selection effects in their analysis and both of these samples are the most similar to the eFEDS sample since they also contain a significant fraction of low-mass clusters. Our slope is slightly steeper than the slopes found in Eckmiller et al. (2011) ($B = 2.52 \pm 0.17$) and Kettula et al. (2015) ($B = 2.52 \pm 0.17$) but consistent within 1σ . The slope of $B = 2.24 \pm 0.25$ reported in Pratt et al. (2009) is $< 1.5\sigma$ shallower than our results. Our best-fit redshift evolution for the $L_X - T$ relation is 2σ shallower than the self-similar scenario

Table 3: Best-fit parameters of the scaling relations

Relation		Best fit parameters							
		Free redshift evolution				Self-similar redshift evolution			
Y	X	A	B	C	$\sigma_{Y X}$	A	B	$C = C_{self}$	$\sigma_{Y X}$
L_X	T	$0.92^{+0.13}_{-0.13}$	$2.59^{+0.12}_{-0.11}$	$2.61^{+0.77}_{-0.81}$	$0.74^{+0.07}_{-0.07}$	$0.87^{+0.14}_{-0.14}$	$2.69^{+0.12}_{-0.11}$	1	$0.79^{+0.07}_{-0.07}$
L_X	M_{gas}	$0.89^{+0.02}_{-0.02}$	$1.10^{+0.03}_{-0.02}$	$1.44^{+0.25}_{-0.26}$	$0.30^{+0.02}_{-0.02}$	$0.88^{+0.02}_{-0.02}$	$1.07^{+0.02}_{-0.02}$	2	$0.30^{+0.02}_{-0.02}$
L_X	Y_X	$1.20^{+0.04}_{-0.04}$	$0.80^{+0.02}_{-0.02}$	$1.83^{+0.31}_{-0.32}$	$0.28^{+0.03}_{-0.03}$	$1.20^{+0.04}_{-0.04}$	$0.81^{+0.02}_{-0.02}$	$8/5$	$0.28^{+0.03}_{-0.03}$
L_{bol}	T	$1.09^{+0.14}_{-0.13}$	$2.74^{+0.12}_{-0.11}$	$3.42^{+0.67}_{-0.70}$	$0.68^{+0.06}_{-0.06}$	$1.02^{+0.15}_{-0.14}$	$2.90^{+0.12}_{-0.12}$	1	$0.77^{+0.07}_{-0.06}$
L_{bol}	M_{gas}	$0.96^{+0.03}_{-0.03}$	$1.19^{+0.03}_{-0.03}$	$1.86^{+0.29}_{-0.30}$	$0.32^{+0.02}_{-0.02}$	$0.95^{+0.03}_{-0.03}$	$1.16^{+0.02}_{-0.02}$	$7/3$	$0.31^{+0.02}_{-0.02}$
L_{bol}	Y_X	$1.24^{+0.04}_{-0.04}$	$0.88^{+0.02}_{-0.02}$	$2.05^{+0.26}_{-0.27}$	$0.28^{+0.02}_{-0.02}$	$1.25^{+0.04}_{-0.04}$	$0.89^{+0.02}_{-0.02}$	$9/5$	$0.28^{+0.02}_{-0.02}$
M_{gas}	T	$0.83^{+0.11}_{-0.11}$	$2.17^{+0.10}_{-0.10}$	$1.03^{+0.65}_{-0.70}$	$0.65^{+0.06}_{-0.06}$	$0.73^{+0.12}_{-0.11}$	$2.25^{+0.11}_{-0.10}$	-1	$0.73^{+0.06}_{-0.06}$

Notes. Fitted relation is of the form $Y = A Y_{\text{piv}} \left(\frac{X}{X_{\text{piv}}} \right)^B \left(\frac{E(z)}{E(z_{\text{piv}})} \right)^C$ with a log-normal intrinsic scatter $\sigma_{Y|X}$ (in natural log). Pivot values of the observables are provided in Table 2. Each relation is fitted twice; first with leaving the redshift evolution exponent (C) free, second with a redshift evolution exponent fixed to the corresponding self-similar value (see Table 1 for the self-similar exponents). Details of the modeling and fitting the scaling relations can be found in Sect. 3. Errors are 1σ uncertainties calculated from the second half of the MCMC chains.

($C_{\text{self}} = 1$) and it agrees well with Giles et al. (2016) within 1σ . Furthermore, our redshift evolution agrees also well with most of the other results due to the large error bars which indicate the redshift evolution could not be constrained as well as other parameters. When we fix the evolution term to the self-similar value, we find a steeper slope of ($B = 2.69^{+0.12}_{-0.11}$). This slope is $\sim 2\sigma$ away from the slope reported in Migkas et al. (2020) ($B = 2.38 \pm 0.08$) if their temperature correction is taken into account. Our best-fit intrinsic scatter for the $L_X - T$ relation agrees very well with Pratt et al. (2009) ($\sigma_{L_X|T} = 0.76 \pm 0.14$) whereas it is in 2.5σ tension with Giles et al. (2016) ($\sigma_{L_X|T} = 0.47 \pm 0.07$). Lovisari et al. (2015) ($\sigma_{L_X|T} = 0.56$) and Eckmiller et al. (2011) ($\sigma_{L_X|T} = 0.63$) also reported slightly smaller intrinsic scatter results compared to our findings however, a statistical comparison cannot be made due to the lack of the errorbars in their scatter measurements.

For the $L_{\text{bol}} - T$ relation, we find a slope of $B = 2.74^{+0.12}_{-0.11}$, redshift evolution term of $C = 3.42^{+0.67}_{-0.70}$ and a scatter of $\sigma_{L_{\text{bol}}|T} = 0.68 \pm 0.06$. Similarly, both the slope and the redshift evolution are steeper than the self-similar expectation of $B_{\text{self}} = 2$ at a 6σ level and $C_{\text{self}} = 1$ at a 3.5σ level. Due to the temperature dependence of the X-ray emissivity, the $L - T$ scaling relation involving the bolometric luminosity is expected to be steeper relative to that of the soft-band luminosity for the same cluster about a factor of $\propto n_e^2 T^{0.5}$. The slope in this case is consistent with Pratt et al. (2009) ($B = 2.70 \pm 0.24$). When we fix the redshift evolution to the self-similar value, we obtain a much steeper slope of $B = 2.90 \pm 0.12$. Our best-fit slope are consistent with the slopes in Giles et al. (2016) ($B = 3.08 \pm 0.15$) and Zou et al. (2016) ($B = 3.29 \pm 0.33$) within uncertainties whereas Migkas et al. (2020) found a 3σ shallower slope ($B = 2.46 \pm 0.09$). Maughan et al. (2012) ($B = 3.63 \pm 0.27$) on the other hand, found a significantly steeper slope than both the self-similar model and our results when they included the cluster cores. Maughan et al. (2012) reported that when they limit their sample to relaxed cool core clusters, they find a slope of $B = 2.44 \pm 0.43$, i.e. consistent with our results within the given uncertainties, indicating that the discrepancy observed here could be due to their samples be-

ing heavily affected by the selection effects which we take into account by using realistic simulations in our analysis. Intrinsic scatter of the $L_{\text{bol}} - T$ relation is slightly lower compared to the best-fit value of our $L_X - T$ relation however they agree within the errorbars. Pratt et al. (2009) reported $\sigma_{L_{\text{bol}}|T} = 0.73 \pm 0.14$ that is consistent with our results for the $L_{\text{bol}} - T$ relation within uncertainties. Our best-fit intrinsic scatter is slightly higher but within 1.5 and 2σ statistical agreement with the findings reported in Zou et al. (2016) ($\sigma_{L_{\text{bol}}|T} = 0.47 \pm 0.11$) and Giles et al. (2016) ($\sigma_{L_{\text{bol}}|T} = 0.47 \pm 0.07$) respectively.

4.2. $L_X - M_{\text{gas}}$ and $L_{\text{bol}} - M_{\text{gas}}$ Relations

Luminosity and gas mass are two tightly related observables because of their mutual dependence on electron density therefore, a strong correlation between them is expected. Measurement of their correlation by taking into account the selection effects and the mass function with a large sample allows to test the theorized relation between these observables. According to the self-similar model, they are connected as

$$L_X \propto M_{\text{gas}} E(z)^2 \quad (13)$$

and

$$L_{\text{bol}} \propto M_{\text{gas}}^{4/3} E(z)^{7/3}. \quad (14)$$

Our best-fit results for the $L_X - M_{\text{gas}}$ and $L_{\text{bol}} - M_{\text{gas}}$ relations are provided in Table 3 and in Fig. 5. Comparisons of the results with the previous work in Fig. 4. We report a slope of $B = 1.10^{+0.03}_{-0.02}$, redshift evolution term of $C = 1.44^{+0.25}_{-0.26}$, and scatter $\sigma_{L_X|M_{\text{gas}}} = 0.30 \pm 0.02$. Slope is in tension with the self-similar expectation at a 5σ level, however, the redshift evolution is consistent the self-similar model within 2σ confidence for the $L_X - M_{\text{gas}}$ relation. When we fix the redshift evolution to the self-similar value, the slope does not change significantly ($B = 1.07 \pm 0.02$). Zhang et al. (2011) obtained a slope of $B = 1.11 \pm 0.03$ from the 62 clusters in the HIFLUGCS sample which is consistent with our measurements. Their slope for the cool-core clusters ($B = 1.09 \pm 0.05$) is similar to what they

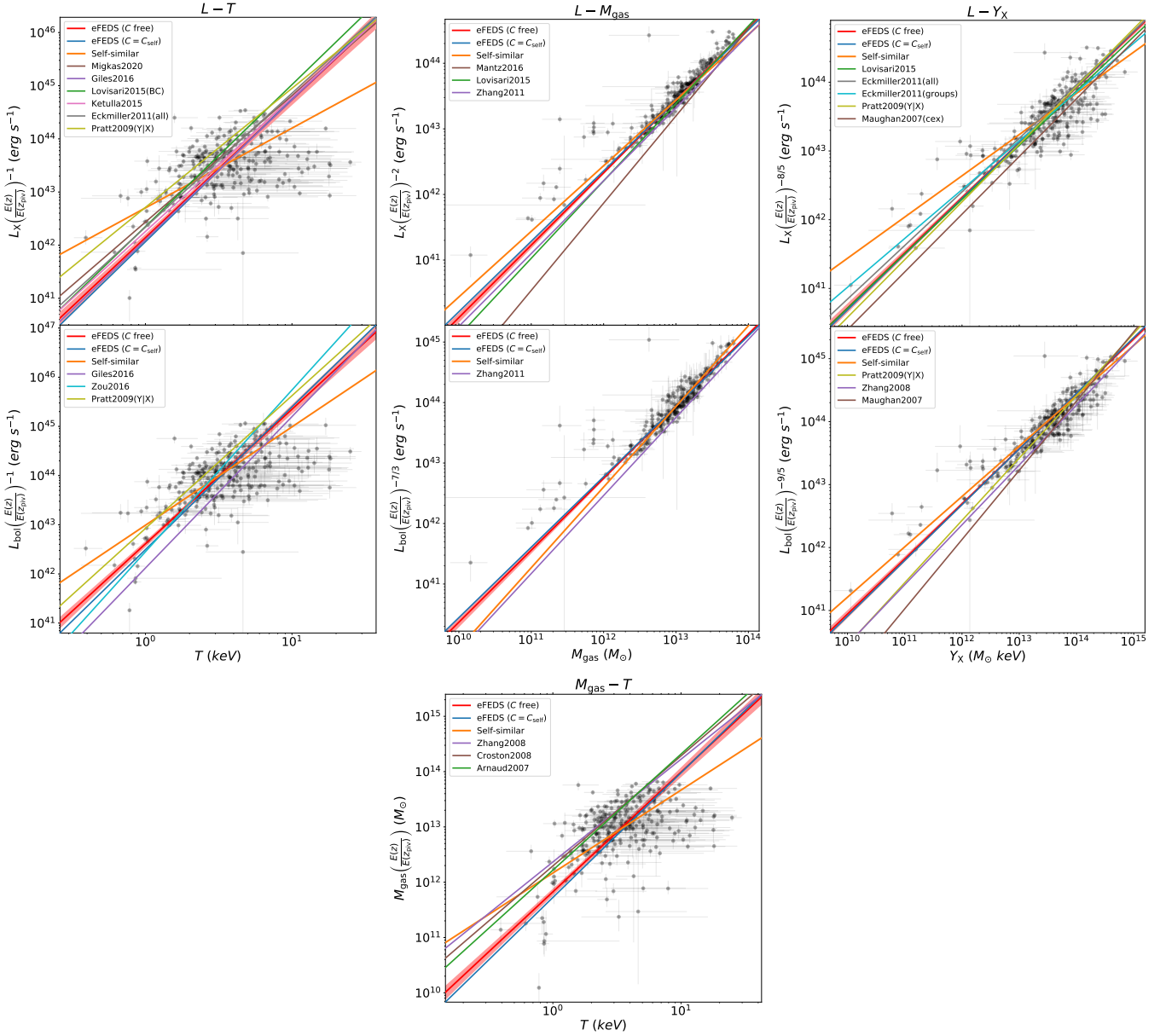


Fig. 4: Top: Comparison between our best-fit $L_X - M_{\text{gas}}$, $L_X - M_{\text{gas}}$, $L_X - Y_X$, and $M_{\text{gas}} - T$ relations in comparison to the self-similar model and the other studies in the literature (Maughan 2007; Arnaud et al. 2007; Zhang et al. 2008; Pratt et al. 2009; Eckmiller et al. 2011; Zhang et al. 2011; Lovisari et al. 2015; Mantz et al. 2016). Grey circles are the eFEDS clusters. In order to achieve consistency, cosmology and energy band conversion is applied to the previously reported results (see Sect. 4 for the details).

found for their all sample however, the best-fit slope for their non-cool-core clusters is steeper ($B = 1.20 \pm 0.06$). Lovisari et al. (2015) studied the scaling properties of a complete X-ray selected galaxy group sample and found that the slope of $L_X - M_{\text{gas}}$ relation for galaxy groups, $B = 1.02 \pm 0.24$, which is slightly shallower but still consistent with the result they obtained for more massive clusters, $B = 1.18 \pm 0.07$. Both of these measurements are consistent with our slope. On the other hand, a flux-limited sample of 139 clusters compiled from the ROSAT All-Sky Survey catalog has a steeper slope with $B = 1.34 \pm 0.05$ for $L_X - M_{\text{gas}}$ relation (Mantz et al. 2016). Their result is more than 4σ away from our measurement. This discrepancy might be due to the fact that the Mantz et al. (2016) sample is dominated by massive luminous clusters (their lowest luminosity system is about as bright as our most luminous systems), while the

eFEDS sample is composed of low-mass clusters and groups. There are not many studies in the literature reporting intrinsic scatter of the $L_X - M_{\text{gas}}$ relation. Therefore we were only able to compare our results with Zhang et al. (2011) where they found $\sigma_{L_X|M_{\text{gas}}} = 0.14 \pm 2$ that is significantly less (5.5σ) than our results.

On the other hand, we find the best-fit parameters of the slope, evolution term, and scatter of the $L_{\text{bol}} - M_{\text{gas}}$ relation are $B = 1.19 \pm 0.03$, $C = 1.86^{+0.29}_{-0.30}$, and $\sigma_{L_{\text{bol}}|M_{\text{gas}}} = 0.32 \pm 0.02$, respectively. Similarly, the slope is $\sim 5\sigma$ away from the self-similar model, while the redshift evolution is fully consistent with the model. This relation is studied much less in the literature. Zhang et al. (2011) found a slope of $B = 1.29 \pm 0.05$ when they fitted their all sample. Their reported slope is less steep for cool-core clusters ($B = 1.24 \pm 0.05$) relative to the non-cool-

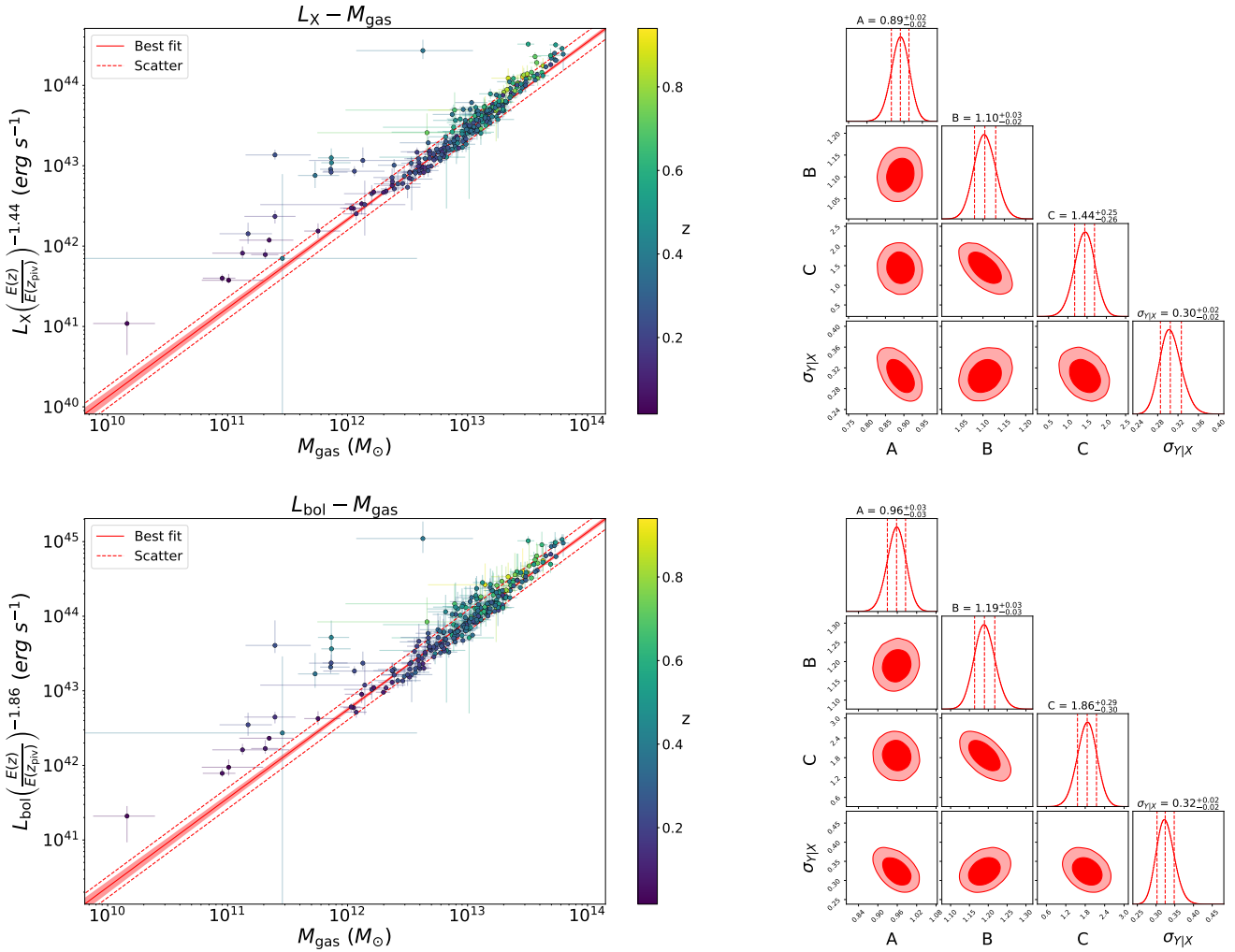


Fig. 5: *Left:* Soft band (0.5 – 2.0 keV) X-ray luminosity (L_X), bolometric (0.01 – 100 keV) luminosity (L_{bol}), gas mass (M_{gas}) and redshift (z) measurements of the $\mathcal{L}_{\text{det}} > 15$, $\mathcal{L}_{\text{ext}} > 15$ sample and the best-fit scaling relation models. Light-red shaded area indicating 1σ uncertainty of the mean of the log-normal model (see Eqn. 5) and dashed red line indicating the best-fit standard deviation ($\sigma_{L|M_{\text{gas}}}$) around the mean. *Right:* The parameter constraints of the $L_X - M_{\text{gas}}$ and $L_{\text{bol}} - M_{\text{gas}}$ relations obtained from the second half of the MCMC chains. Marginalized posterior distributions are shown on the diagonal plots and the joint posterior distributions are shown on off-diagonal plots. Red dashed vertical lines indicate 32th, 50th and 68th percentiles and contours indicate 68 and 95% credibility regions.

core clusters ($B = 1.42 \pm 0.06$). The slope of the all sample is fully consistent with our measurements within 2σ . Similar to the $L_X - M_{\text{gas}}$ relation, we could only compare our best-fit intrinsic scatter for the $L_{\text{bol}} - M_{\text{gas}}$ relation with Zhang et al. (2011) where they report $\sigma_{L_{\text{bol}}|M_{\text{gas}}} = 0.21 \pm 2$ that is in 4σ tension with our results.

One additional point is that there is a noticeable deviation around the gas mass of $\sim 10^{12} M_\odot$ in Fig. 5. The low-mass groups below tend to have higher luminosity relative to the mass determined from the scaling relations. The slope and normalization of this power-law relation are mostly governed by the higher mass clusters. The low-mass groups would prefer shallower $L_X - M_{\text{gas}}$ power-law slope relative to the high-mass clusters. This observed trend is fully consistent with the $L_X - M_{\text{gas}}$ relation reported in (Lovisari et al. 2015) where they similarly observed the relation getting shallower at group scale but within errorbars.

4.3. $L_X - Y_X$ and $L_{\text{bol}} - Y_X$ Relations

An accurate mass indicator, Y_X , first introduced by Kravtsov et al. (2006), shows a low intrinsic scatter with mass and has a tight relation with the Sunyaev Zel'dovich (SZ) effect observable Compton-y parameter, Y_{SZ} (e.g. Maughan 2007; Benson et al. 2013; Mantz et al. 2016; Bulbul et al. 2019; Andrade-Santos et al. 2021). Due to this strong correlation, scaling relations involving Y_X can be used as a connection in multi-wavelength studies of galaxy clusters. Numerical simulations suggest that non-gravitational effects have a small influence on this mass proxy compared to other X-ray observables (Nagai et al. 2007).

According to the self-similar model, luminosity is expected to depend on Y_X and redshift as

$$L_X \propto Y_X^{3/5} E(z)^{8/5} \quad (15)$$

and

$$L_{\text{bol}} \propto Y_X^{4/5} E(z)^{9/5}. \quad (16)$$

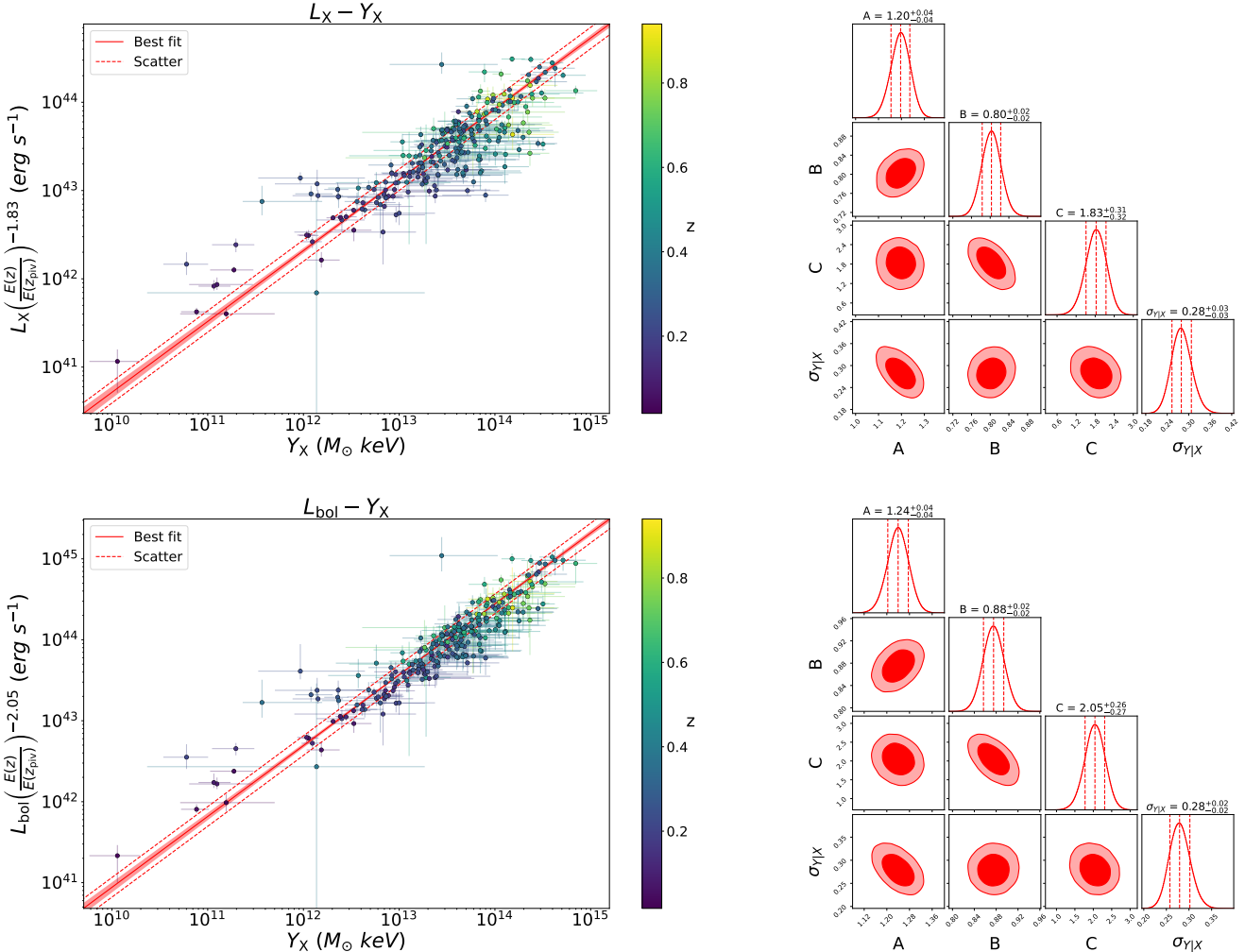


Fig. 6: *Left:* Soft band ($0.5 - 2.0$ keV) X-ray luminosity (L_X), bolometric ($0.01 - 100$ keV) luminosity (L_{bol}), integrated Compton- γ parameter (Y_X) and redshift (z) measurements of the $\mathcal{L}_{\text{det}} > 15$, $\mathcal{L}_{\text{ext}} > 15$ sample and the best-fit scaling relation models. Light-red shaded area indicating 1σ uncertainty of the mean of the log-normal model (see Eqn. 5) and dashed red line indicating the best-fit standard deviation ($\sigma_{L_X|Y_X}$) around the mean. *Right:* The parameter constraints of the $L_X - Y_X$ and $L_{\text{bol}} - Y_X$ relations obtained from the second half of the MCMC chains. Marginalized posterior distributions are shown on the diagonal plots and the joint posterior distributions are shown on off-diagonal plots. Red dashed vertical lines indicate 32th, 50th and 68th percentiles and contours indicate 68 and 95% credibility regions.

Our results for the best-fit $L_X - Y_X$ relations are listed in Table 3 and plotted in Fig. 6, while a comparison with the literature is provided in Fig. 4. We find a slope of $B = 0.80 \pm 0.02$ and a redshift evolution exponent of $C = 1.83^{+0.31}_{-0.32}$ and an intrinsic scatter of $\sigma_{L_X|Y_X} = 0.28 \pm 0.03$ for the $L_X - Y_X$ scaling relation. Our slope for the $L_X - Y_X$ relation is 10σ steeper than the one predicted by the self-similar model. The redshift evolution of the $L_X - Y_X$ relation is also slightly steeper than the self-similar expectation but consistent within the uncertainties. Our slope is consistent with the results presented in Maughan (2007), ($B = 0.84 \pm 0.03$) and with Lovisari et al. (2015) ($B = 0.79 \pm 0.03$). Our results for the same relation is within uncertainties with the HI-FLUGCS+groups sample of Eckmiller et al. (2011) and in 1.7σ agreement with their only groups sample. They find slopes of $B = 0.78 \pm 0.02$ and $B = 0.71 \pm 0.05$ for the HI-FLUGCS+groups and only groups samples respectively where the later is in $\sim 2\sigma$ with the self-similar expectation. Our best-fit intrinsic scatter is in good agreement ($< 2\sigma$) with the findings of Pratt et al. (2009)

($\sigma_{L_X|Y_X} = 0.41 \pm 0.07$). Eckmiller et al. (2011) ($\sigma_{L_X|Y_X} = 0.46$) and Lovisari et al. (2015) ($\sigma_{L_X|Y_X} = 0.51$) report higher values for the intrinsic scatter of the $L_X - Y_X$ relation however, these measurements are presented without errorbars therefore a statistical comparison with our findings cannot be made.

For the $L_{\text{bol}} - Y_X$ relation, we find a slope of $B = 0.88 \pm 0.02$, a redshift evolution exponent of $C = 2.05^{+0.26}_{-0.27}$ and an intrinsic scatter of $\sigma_{L_{\text{bol}}|Y_X} = 0.28 \pm 0.02$. The slope shows a 4σ deviation from self-similarity. When we fix the redshift evolution to its self-similar value, we find that the tension reaches up to a 5σ significance. Maughan (2007) find an even larger deviation from the self-similarity, measuring a slope of $B = 1.10 \pm 0.04$. Also in Zhang et al. (2008), the authors reported a significantly steeper slope of $B = 0.95 \pm 0.08$. Pratt et al. (2009) also found a significant deviation from the self-similar model, measuring a slope of $B = 1.04 \pm 0.06$. These results are all significantly steeper than our results and the self-similar model. Numerical simulations show a similar scenario, Biffi et al. (2014) reports

this slope to be $B = 0.94 \pm 0.02$, also steeper than our results and self-similarity. Our redshift evolution for the $L_{\text{bol}} - Y_{\text{X}}$ relation is consistent with the self-similar prediction within the uncertainties. A similar redshift evolution was measured in Maughan (2007), with $C = 2.2 \pm 0.1$. Our best-fit intrinsic scatter for the $L_{\text{bol}} - Y_{\text{X}}$ relation is slightly smaller (1.5σ) compared to the value reported in Pratt et al. (2009) ($\sigma_{L_{\text{bol}}|Y_{\text{X}}} = 0.38 \pm 0.06$). Maughan (2007) reported a similar value ($\sigma_{L_{\text{bol}}|Y_{\text{X}}} = 0.36 \pm 0.03$) for the intrinsic scatter that is in 2.2σ tension with our best-fit value.

4.4. $M_{\text{gas}} - T$ relation

$M_{\text{gas}} - T$ and $L_{\text{X}} - T$ relations are conjugates of each other due to the tight correlation between M_{gas} and L_{X} . However, we still expect to see differences as M_{gas} has a linear dependence on electron density whereas L has a quadratic dependence. We fit the $M_{\text{gas}} - T$ relation following the similar framework as in the sections above with minor changes. We use the L_{X} flavored selection function by converting M_{gas} to L_{X} since we do not have a selection function involving M_{gas} from simulations. This one-to-one conversion in principle should not introduce a large bias to our results since L_{X} and M_{gas} are tightly correlated and the scatter between them is relatively low.

Based on the self-similar model, gas mass and temperature should be related to each other via

$$M_{\text{gas}} \propto T^{3/2} E(z)^{-1}. \quad (17)$$

Our results for the $M_{\text{gas}} - T$ relation are listed in Table 3 and shown in Fig. 7. We obtain a slope of $B = 2.17 \pm 0.10$, a redshift evolution exponent of $C = 1.03^{+0.65}_{-0.70}$ and a scatter of $\sigma_{M_{\text{gas}}|T} = 0.65 \pm 0.06$. Our slope is 7σ steeper than the self-similar model. We find a positive redshift evolution which is expected to be negative in the self-similar case that results in a 3σ tension. Comparison of our results with literature is given in Fig. 4. In general, the slope of the $M_{\text{gas}} - T$ relation reported in the literature is close to ~ 1.9 , steeper than the self-similar expectation. Reported slopes in the literature show a dependency on the mass range of the parent sample. For instance, Arnaud et al. (2007) reports a slope of 2.10 ± 0.05 based on the XMM-Newton observations of 10 relaxed nearby clusters. Consistently, Croston et al. (2008) found 1.99 ± 0.11 using the 31 clusters in the REXCESS sample and Zhang et al. (2008) obtained 1.86 ± 0.19 with XMM-Newton data for 37 LoCuSS clusters. These slopes are broadly consistent with the results reported here within 1.5σ uncertainties. The slight discrepancy could be due to the different selection of the samples compared here.

We find a factor of ~ 2 difference when we compare our best-fit normalization results with Arnaud et al. (2007) and Croston et al. (2008) at their pivot temperature value (5 keV). To investigate the difference and test our results, we reconstruct the $M_{\text{gas}} - T$ relation using our best-fit $L_{\text{X}} - T$ and $L_{\text{X}} - M_{\text{gas}}$ relations that are in agreement with the most recent studies in the literature taking into account the selection effects. We obtain a relation of

$$M_{\text{gas}} = 1.04 M_{\text{gas,piv}} \left(\frac{T}{T_{\text{piv}}} \right)^{2.35} \left(\frac{E(z)}{E(z_{\text{piv}})} \right)^{1.06}. \quad (18)$$

The normalization, slope, and evolution terms are $< 2\sigma$ away from the best-fit $M_{\text{gas}} - T$ relation which indicates that our results for the $M_{\text{gas}} - T$ relation would be in good agreement with the previous results if the selection effects were taken into account. We argue that the observed discrepancy arises due to the combined effect of two main differences between our and previous

analyses. The first difference is, we include selection effects in our work and therefore measure a steeper slope for the $M_{\text{gas}} - T$ relation compared to the previously reported results. Our slope being steeper agrees well with previous findings since M_{gas} is a very good L_{X} proxy and many studies, including us, show that the best-fit slope of the $L_{\text{X}} - T$ relation is measured steeper when the selection effects are taken into account. The second difference is, our sample includes a larger fraction of low-mass clusters compared to the other samples. If the cluster populations were similar, we would not observe such a difference in normalization even if the slopes did not match. Therefore, in our case, the populations and the slopes being different combine and result in the observed mismatch. Additionally, using a converted flavored selection function might have also contributed on the discrepancy however its effect is expected to be much smaller since the relation between L_{X} and M_{gas} is tight and the scatter is low.

5. Discussion

Slopes of the scaling relations between X-ray observables studied in this work show deviations from the self-similar model by $3 - 9$ confidence levels. These deviations are often attributed to the departures from the assumptions in the self-similar (Kaiser 1986) model in the literature. We discuss two potential reasons for the observed discrepancy in the eFEDS sample in this section.

The most commonly proposed explanations in the literature for the departures from self-similarity challenge two major assumptions in the model. First, clusters are assumed to have a spherically symmetric gas distribution that is in hydrostatic equilibrium. Secondly, physical processes are majorly driven by the gravitational force, and that the other effects are negligible in shaping the observed physical state of clusters. Observational data and numerical simulations indicate that both of these assumptions may not hold, and this can lead to departures from the self-similar expectation. Non-gravitational processes such as AGN feedback, galactic winds, or star formation introduce extra energy to the system, heat the gas, and increase the entropy in the core (e.g. Voit 2005; Walker et al. 2012; Bulbul et al. 2016). AGN feedback, in particular, can play an important role in shaping the gas physics in especially low mass clusters and groups that dominate the eFEDS extended source sample. AGN activity can expel gas to the outskirts for lower mass haloes due to their shallower potential wells. As the larger fraction of gas is removed from the centers of low-mass haloes, their luminosity gets lower (e.g. Puchwein et al. 2008). The most massive clusters with deeper potential wells, higher total mass, and the ICM temperature, are less affected by the non-gravitational effects. When the clusters and groups are fit together, lower luminosity of groups and low mass clusters lead to a steeper slope of the $L_{\text{X}} - T$ scaling relations when the cores are included. This result is consistent with numerical simulations (Puchwein et al. 2008; Schaye et al. 2010; Biffi et al. 2014; Truong et al. 2018; Henden et al. 2018, 2019), and the observational data in the literature (Eckmiller et al. 2011; Maughan et al. 2012; Pratt et al. 2009; Zou et al. 2016; Giles et al. 2016; Migkas et al. 2020; Lovisari et al. 2021). Another proposed reason for these steep slopes is the use of the overdensity radii R_{500} derived from the X-ray masses calculated assuming the hydrostatic equilibrium (see Lovisari et al. 2021, for discussion). If the radius R_{500} is biased low due to unaccounted non-thermal pressure in the ICM, the luminosity extracted in this radius would be lower. The temperatures are less impacted by this effect due to large uncertainties. How-

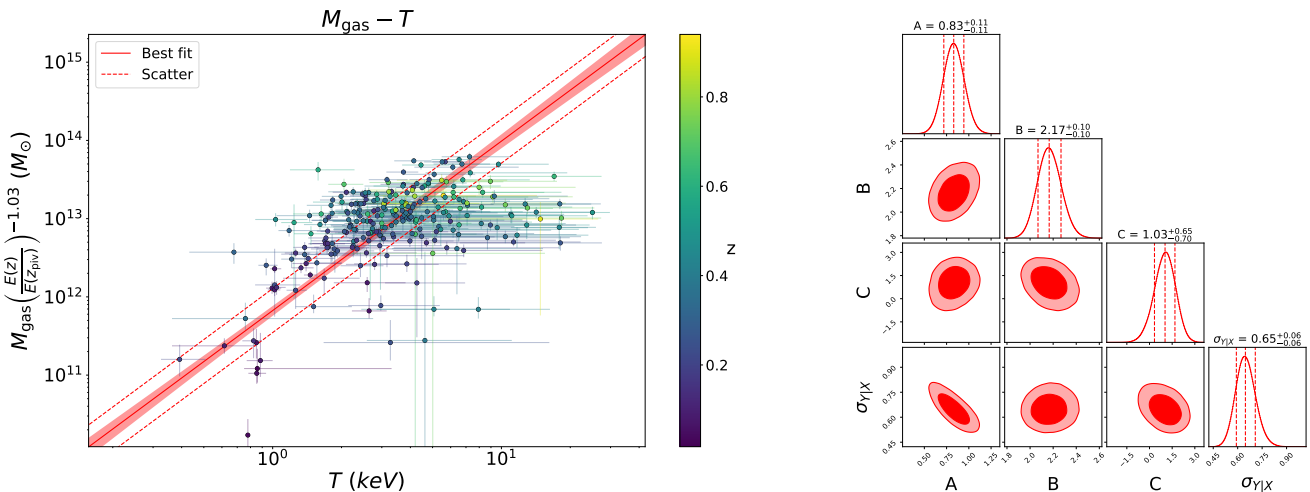


Fig. 7: *Left:* Gas mass (M_{gas}), temperature (T) and redshift (z) measurements of the $\mathcal{L}_{\text{det}} > 15$, $\mathcal{L}_{\text{ext}} > 15$ sample and the best-fit scaling relation models. Light-red shaded area indicating 1σ uncertainty of the mean of the log-normal model (see Eqn. 5) and dashed red line indicating the best-fit standard deviation ($\sigma_{L|M_{\text{gas}}}$) around the mean. *Right:* The parameter constraints of the $L_{\text{X}} - M_{\text{gas}}$ and $L_{\text{bol}} - M_{\text{gas}}$ relations obtained from the second half of the MCMC chains. Marginalized posterior distributions are shown on the diagonal plots and the joint posterior distributions are shown on off-diagonal plots. Red dashed vertical lines indicate 32th, 50th and 68th percentiles and contours indicate 68 and 95% credibility regions.

ever, in this work, we use the overdensity radii R_{500} obtained from the HSC weak lensing measurements uniformly for low mass groups and clusters in the eFEDS sample (Chiu et al. 2021). We argue that the (mass-dependent) hydrostatic equilibrium bias and radius of extraction do not play a major effect in this work and cannot explain the steepening of the $L_{\text{X}} - T$ scaling relations. The $M_{\text{gas}} - T$ relations should be affected by the AGN feedback similarly but less prominent relative to the $L_{\text{X}} - T$ relation due to the linear dependence of M_{gas} on the number density of electrons, i.e. $M_{\text{gas}} \propto n_e$ while $L_{\text{X}} \propto n_e^2$ through X-ray emissivity. The expected steepening in $M_{\text{gas}} - T$ should be less prominent as a result of this effect. This is fully consistent with our results assuming that the discrepancy is attributed to non-gravitational effects. Another important issue in comparing various results in the literature is the calibration differences between X-ray telescopes. The number density and luminosity measurements are expected to be consistent between X-ray telescopes, e.g. *Chandra* and *XMM-Newton* (Bulbul et al. 2019), however, significant band-dependent disagreements have been reported for cluster ICM temperature measurements (Schellenberger et al. 2015). Given the reported discrepancies between X-ray instruments are small in the soft X-ray band where the temperature measurements of most of our clusters lie, we do not expect that the slope differences are due to these calibration effects.

For $L_{\text{X}} - Y_{\text{X}}$ and $L_{\text{X}} - M_{\text{gas}}$ scaling relations, the effect of Malmquist bias, i.e. preferential sampling of bright objects, can clearly be seen that is often prominent in X-ray selected samples. We note that these biases and selection effects are fully accounted for in our selection function, thus should not bias our best-fit scaling relations. We observe mild deviations from the self-similar model on both scaling relations in low M_{gas} and Y_{X} regimes. The mass proxy Y_{X} shows low intrinsic scatter with cluster mass in the literature (Kravtsov et al. 2006; Eckmiller et al. 2011; Bulbul et al. 2019). As the ICM temperature scales with total mass, we expect to see a similar trend with low-scatter in the $L_{\text{X}} - Y_{\text{X}}$ scaling relations. Indeed, the $L_{\text{X}} - Y_{\text{X}}$ scaling relations show a tight correlation for massive clusters. Along

the lines of what we observe, as the group scales dominate the sample, the intrinsic scatter becomes larger. We find that the departures from the self-similarity are significant for both of the relations which is consistent with the results reported in the literature and numerical simulations (Eckmiller et al. 2011; Biffi et al. 2014; Lovisari et al. 2015).

The self-similar model predicts cosmology-dependent redshift evolution for the scaling relations between observables and cluster mass. This dependence is introduced through the overdensity radius (and the critical density) which is inversely related to the evolution of the Hubble parameter with redshift z , $E(z) = H(z)/H_0$. We do not find significant departures from the self-similar evolution with redshift in any of our relations. All show self-similar redshift evolution at a 2.5σ confidence level except the $L_{\text{bol}} - T$ relation. The evolution of scaling relations has contradictory reports in the literature. Some studies report self-similar redshift evolution with redshift (Giodini et al. 2013), while some studies report no evolution (Maughan 2007; Pacaud et al. 2007). Larger samples, covering a wide redshift range, will be available with the eRASS data, which will constrain the redshift evolution of scaling relations and test the self-similar model.

In this work, we investigate the scaling relations between X-ray observables of the clusters of galaxies and galaxy groups by fully modeling the selection effects. Our method of obtaining the selection function relies on the realistic simulations of the eROSITA observations. This is the most robust way of modeling the selection effects as long as the simulated population of sources is representative of the observed sample. The advantage of this method lies in the fact that the same detection and reduction methods are applied to both simulated observations and the eROSITA data self-consistently (Clerc et al. 2018; Comparat et al. 2020). In these simulations, cluster surface brightness profiles are created by making use of the previously measured profiles of cluster and group samples at a wide mass and redshift scales, they use X-COP, SPT, XXL, and HiFLUGCS cluster samples. This method allows the profiles to be consis-

tent with the observations except the low-L, low-z regime where we probe a mass and redshift space that is poorly explored by previous X-ray observations. This led to a slight excess in the number of detected simulated clusters by the pipeline at this parameter space which can be barely seen in Fig. 2. The mild difference does not have any effect on our best fitting relations since our likelihood takes the redshift (z) and detection (I) information of clusters as givens, $\mathcal{L}(\hat{Y}_{\text{all}}, \hat{X}_{\text{all}} | I, \theta, z)$, such that in our analysis, the shape of $P(I|L_X, z)$ as a function of L_X matters rather than the relative normalizations at different redshifts, $P(I|z) = \int P(I|L_X, z)P(L_X|z)dL_X$. Following our analysis of the eFEDS observations, this less populated mass-luminosity range will be filled with eFEDS clusters, and therefore surface brightness profiles of simulated clusters at these regimes will be improved for modeling the selection function for the future eRASS observations. Proper modeling of the selection effects will be particularly important for placing constraints on cosmological parameters using eROSITA observations (Clerc et al. 2018).

We also test our method by comparing the model predicted number of detected clusters (N_{det}) and the number of clusters in our observed sample (\hat{N}_{det}) as also presented in Giles et al. (2016). However, we find that comparing the predicted and observed cluster numbers is not informative since the predictions have large uncertainties driven mostly by the propagated errors from our scaling relations analysis and the weak lensing mass calibrated scaling relations analysis (Chiu et al. 2021). To give an example, we compare the observed number of detected clusters for the $\mathcal{L}_{\text{det}} > 15$, $\mathcal{L}_{\text{ext}} > 15$ sample (265) with the model predicted number for the $L_X - T$ relation similar to the Giles et al. (2016). We calculated N_{det} as

$$N_{\text{det}} = \int \int \int_{L_X, T, z} P(I|L_X, z)P(L_X|T, \theta_{L_X T}, z) \frac{dn}{dT} \frac{dV_c}{dz} dL_X dT dz \quad (19)$$

where $\frac{dV_c}{dz}$ is the differential comoving volume shell spanning a solid angle of $\Omega_{\text{eFEDS}} = 140/(180/\pi)^2$, $\frac{dn}{dT}$ is the temperature function calculated as described in Sect. 3.2 and $\theta_{L_X T}$ is the best-fit parameters of the $L_X - T$ relation. While calculating N_{det} , first we only propagate the errors of the best-fit parameters ($\theta_{L_X T}$) using MCMC chains and we find the model-predicted number of detected clusters to be $N_{\text{det}, L_X T} = 347.8^{+48.1}_{-49.0}$. When we further propagate both the uncertainties of $\theta_{L_X T}$ and the best-fit weak lensing mass calibrated scaling relations parameters (A_X, B_X, γ_X), we find the new measurement to be $N_{\text{det}, L_X T} = 367.8^{+169.8}_{-109.1}$. In this case, the observed number of clusters is consistent with the predicted number of clusters within the uncertainties. The difference in the absolute values might be due to the selection function, or the cosmology-dependent normalization of the mass function. In this work and simulations, we use the Planck cosmology (Planck Collaboration et al. 2016) with the Tinker et al. (2008) mass function. Larger samples of clusters of galaxies will soon be available through the eROSITA All-Sky observations will provide sufficient statistics to constrain the cosmology simultaneously with the scaling relations (see Pillepich et al. 2012, for the cosmology forecast).

Decreasing the scatter is of importance to reduce the systematics on the constraints of cosmological parameters through cluster counts. The use of cool-core and relaxed clusters are reported to show less scatter on the scaling relations relative to the mergers (Vikhlinin et al. 2009; Mantz et al. 2010b). The dynamical states of the eFEDS clusters and groups are already presented in (Ghirardini et al. 2021b). The dynamically relaxed clusters

compose of 30% to 40% of this sample, therefore using them reduces the statistical power on our measurements. Additionally, the use of the relaxed cluster in the scaling relations fits requires a selection function characterized in terms of these morphological parameters and a dynamical state dependent mass function (e.g. Seppi et al. 2021). This form of the selection function is not available yet. We, therefore, leave this work for the future studies on the eRASS data.

6. Conclusions

The eFEDS is at a similar depth with the the final eROSITA All-Sky Survey in Equatorial regions. In this field, we detect 542 clusters galaxies and groups in the extent selected sample with an addition of 347 clusters of galaxies in the point source samples (Liu et al. 2021a; Klein et al. 2021; Bulbul et al. 2021). In this work, we present the X-ray properties ($L_X, L_{\text{bol}}, T, M_{\text{gas}}, Y_X$) of the all eFEDS clusters and groups measured in two apertures; core-included ($r < R_{500}$) and core-excluded ($0.15R_{500} < r < R_{500}$). The overdensity radius R_{500} is obtained from the HSC weak lensing mass estimates provided in (Chiu et al. 2021), allowing our measurements to be bias-free of the hydrostatic equilibrium assumption. This work clearly demonstrates that the cluster ICM emission will be significantly detected for most of the clusters in the mass redshift range out to R_{500} at this depth.

Additionally, we provide the $L - T$, $L - M_{\text{gas}}$, $L - Y_X$, and $M_{\text{gas}} - T$ scaling relations between these (core-included) X-ray observables for a subsample of clusters. We only consider the extent selected sample, where we can characterize the selection effects using the state-of-the art simulations. The contamination of the main eFEDS clusters and groups sample is in the order of 20% due to AGNs and false detections due to fluctuations (see Liu et al. 2021a,b, for details). To reduce the contamination of the sample under 10%, we further apply the cuts on the extent and detection likelihoods of $\mathcal{L}_{\text{det}} > 15$ and $\mathcal{L}_{\text{ext}} > 15$. We note that besides the \mathcal{L}_{det} and \mathcal{L}_{ext} cuts, we haven't applied any any further cleaning to the sample such as optical cross matching. These cuts reduce the sample size to 265 clusters and groups spanning a redshift range of $0.017 < z < 0.94$, soft band luminosity range of $8.64 \times 10^{40} \text{ erg s}^{-1} < L_X < 3.96 \times 10^{44} \text{ erg s}^{-1}$, and a mass range of $6.86 \times 10^{12} M_\odot < M_{500} < 7.79 \times 10^{14} M_\odot$. In this sample, we find 68 low mass galaxy groups with $< 10^{14} M_\odot$, that are uniformly selected with the rest of the massive clusters in the sample. We investigate these seven relations by taking into account both the selection effects and the cosmological distributions of observables. Fitting is performed twice for each of the seven relation first with a redshift evolution exponent left free and the second with a redshift evolution exponent fixed to the corresponding self-similar value. Main conclusions of our analysis are as follows:

- The eFEDS scaling relations results between X-ray observables in general are in good agreement with the recently reported results. However, we find significant tension with the self-similar expectation for all scaling relations studied here. We suggest that these deviations indicate that the non-gravitational effects such as the feedback mechanisms play a key, non-negligible role in shaping the observed physical properties of the clusters, especially in the low- mass group regime. Specifically, scaling relations results we present in this paper for the $L - T$ relation agrees well with the results from the samples that are similar to the eFEDS sample when the selection function is taken into account (Giles et al. 2016;

Lovisari et al. 2015; Eckmiller et al. 2011) with which our cluster sample is most similar. Our results for the $L - T$ relation also agree well with the FABLE and MACSIS simulations where they include baryonic feedback (Puchwein et al. 2008; Henden et al. 2019; Biffi et al. 2014; Barnes et al. 2017).

- The largest scatter we measured is for $L_X - T$ and $L_{\text{bol}} - T$ relations. We found $\sigma_{L_X|T} = 0.79 \pm 0.07$, $\sigma_{L_{\text{bol}}|T} = 0.77^{+0.07}_{-0.06}$ when fix the redshift evolution to the self-similar value and $\sigma_{L_X|T} = 0.74 \pm 0.07$, $\sigma_{L_{\text{bol}}|T} = 0.68 \pm 0.06$ when the evolution is let free. This intrinsic scatter is mostly driven by the groups. The lowest scatter is measured for the $L_X - Y_X$ and $L_{\text{bol}} - Y_X$ relations with $\sigma_{L_{X(\text{bol})}|Y_X} = 0.28 \pm 0.03(0.02)$. This result shows that besides Y_X being a good mass indicator, it is also a good proxy for the X-ray properties of the ICM.
- The redshift evolution of the scaling relations of the seven scaling relations we examined are broadly consistent with the self-similar model. Fixing the redshift evolution exponent to the corresponding self-similar value only changed the best-fit slopes $< 1\sigma$ from its previous value obtained with a free exponent. Larger samples of clusters and groups are required for constraining the evolution of these relations with redshift.
- We find a factor of ~ 2 normalization difference for the $M_{\text{gas}} - T$ relation with the previous results in the literature. This could be driven due to the lack of proper consideration of the selection effects in the previously reported results and the eFEDS sample containing much more low-mass clusters and groups than the compared samples. This difference might partially also be due to the lack of a selection function with the M_{gas} flavor. Ingesting X-ray observables other than L_X and L_{bol} on the simulations is ongoing which will help understanding the effect.

This work extends the study of X-ray scaling relations to a sample that is dominated by the low mass clusters and groups. It opens a door to study ICM physics for a new population of low-mass cluster and groups, as well as massive clusters at a wide redshift range. These initial results demonstrate the capability of eROSITA to detect the ICM emission out to R_{500} for a large number of clusters detected at the final depth of the All Sky Survey. We note that this depth will be exceeded on the first All Sky Survey for a limited area allowing the observables to be measured out to R_{500} or beyond for a subsample of clusters. These measurements will allow the most stringent constraints on the mass and redshift evolution of the scaling relations. eFEDS observations not only allow us to put tight constraints on the scaling relations parameters but it also allowed us to test our selection function which will be used in future statistical studies with eROSITA.

Acknowledgements. This work is based on data from eROSITA, the soft X-ray instrument aboard SRG, a joint Russian-German science mission supported by the Russian Space Agency (Roscosmos), in the interests of the Russian Academy of Sciences represented by its Space Research Institute (IKI), and the Deutsches Zentrum für Luft und Raumfahrt (DLR). The SRG spacecraft was built by Lavochkin Association (NPOL) and its subcontractors, and is operated by NPOL with support from the Max Planck Institute for Extraterrestrial Physics (MPE). The development and construction of the eROSITA X-ray instrument was led by MPE, with contributions from the Dr. Karl Remeis Observatory Bamberg & ECAP (FAU Erlangen-Nuernberg), the University of Hamburg Observatory, the Leibniz Institute for Astrophysics Potsdam (AIP), and the Institute for Astronomy and Astrophysics of the University of Tübingen, with the support of DLR and the Max Planck Society. The Argelander Institute for Astronomy of the University of Bonn and the Ludwig Maximilians Universität Munich also participated in the science preparation for eROSITA. The eROSITA data shown here were processed using the eSASS software system developed by the German eROSITA consortium. The Hyper Suprime-Cam (HSC) collaboration includes the astronomical communities of Japan and Taiwan, and Princeton University.

The HSC instrumentation and software were developed by the National Astronomical Observatory of Japan (NAOJ), the Kavli Institute for the Physics and Mathematics of the Universe (Kavli IPMU), the University of Tokyo, the High Energy Accelerator Research Organization (KEK), the Academia Sinica Institute for Astronomy and Astrophysics in Taiwan (ASIAA), and Princeton University. Funding was contributed by the FIRST program from the Japanese Cabinet Office, the Ministry of Education, Culture, Sports, Science and Technology (MEXT), the Japan Society for the Promotion of Science (JSPS), Japan Science and Technology Agency (JST), the Toray Science Foundation, NAOJ, Kavli IPMU, KEK, ASIAA, and Princeton University. This paper makes use of software developed for the Large Synoptic Survey Telescope. We thank the LSST Project for making their code available as free software at <http://dm.lsst.org>. This paper is based [in part] on data collected at the Subaru Telescope and retrieved from the HSC data archive system, which is operated by the Subaru Telescope and Astronomy Data Center (ADC) at National Astronomical Observatory of Japan. Data analysis was in part carried out with the cooperation of Center for Computational Astrophysics (CfCA), National Astronomical Observatory of Japan. The Subaru Telescope is honored and grateful for the opportunity of observing the Universe from Maunakea, which has the cultural, historical and natural significance in Hawaii. E.B. acknowledges financial support from the European Research Council (ERC) Consolidator Grant under the European Union's Horizon 2020 research and innovation programme (grant agreement No 101002585). N.C. is supported by CNES.

References

- Aihara, H., Arimoto, N., Armstrong, R., et al. 2018, PASJ, 70, S4
 Andrade-Santos, F., Pratt, G. W., Melin, J.-B., et al. 2021, ApJ, 914, 58
 Arnaud, M., Pointecouteau, E., & Pratt, G. W. 2007, A&A, 474, L37
 Ascasibar, Y., Sevilla, R., Yepes, G., Müller, V., & Gottlöber, S. 2006, MNRAS, 371, 193
 Asplund, M., Grevesse, N., Sauval, A. J., & Scott, P. 2009, ARA&A, 47, 481
 Babul, A., Balogh, M. L., Lewis, G. F., & Poole, G. B. 2002, MNRAS, 330, 329
 Barnes, D. J., Kay, S. T., Henson, M. A., et al. 2017, MNRAS, 465, 213
 Benson, B. A., de Haan, T., Dudley, J. P., et al. 2013, ApJ, 763, 147
 Bhattacharya, S., Di Matteo, T., & Kosowsky, A. 2008, MNRAS, 389, 34
 Biffi, V., Sembolini, F., De Petris, M., et al. 2014, MNRAS, 439, 588
 Blanton, M. R., Bershadsky, M. A., Abolfathi, B., et al. 2017, AJ, 154, 28
 Bocquet, S., Dietrich, J. P., Schrabback, T., et al. 2019, ApJ, 878, 55
 Borgani, S., Governato, F., Wadsley, J., et al. 2002, MNRAS, 336, 409
 Brunner, H., Liu, T., Lamer, G., et al. 2021, arXiv e-prints, arXiv:2106.14517
 Bulbul, E. and Liu, A., Ghirardini, V., Hoang, D. N., et al. 2021, A&A, A4
 Bulbul, E., Chiu, I. N., Mohr, J. J., et al. 2019, ApJ, 871, 50
 Bulbul, E., Randall, S. W., Bayliss, M., et al. 2016, ApJ, 818, 131
 Bulbul, G. E., Hasler, N., Bonamente, M., & Joy, M. 2010, ApJ, 720, 1038
 Capelo, P. R., Coppi, P. S., & Natarajan, P. 2012, MNRAS, 422, 686
 Chiu, I.-N., Ghirardini, V., Liu, A., et al. 2021, arXiv e-prints, arXiv:2107.05652
 Clerc, N., Ramos-Ceja, M. E., Ridl, J., et al. 2018, A&A, 617, A92
 Comparat, J., Eckert, D., Finoguenov, A., et al. 2020, The Open Journal of Astrophysics, 3, 13
 Comparat, J., Merloni, A., Salvato, M., et al. 2019, MNRAS, 487, 2005
 Croston, J. H., Pratt, G. W., Böhringer, H., et al. 2008, A&A, 487, 431
 Dauser, T., Falkner, S., Lorenz, M., et al. 2019, A&A, 630, A66
 Dey, A., Schlegel, D. J., Lang, D., et al. 2019, AJ, 157, 168
 Driver, S. P., Norberg, P., Baldry, I. K., et al. 2009, Astronomy and Geophysics, 50, 5.12
 Ebeling, H., Edge, A. C., Böhringer, H., et al. 1998, MNRAS, 301, 881
 Eckmiller, H. J., Hudson, D. S., & Reiprich, T. H. 2011, A&A, 535, A105
 Fabjan, D., Borgani, S., Tornatore, L., et al. 2010, MNRAS, 401, 1670
 Finoguenov, A., Tanaka, M., Cooper, M., et al. 2015, A&A, 576, A130
 Foreman-Mackey, D., Hogg, D. W., Lang, D., & Goodman, J. 2013, PASP, 125, 306
 Foster, A. R., Ji, L., Smith, R. K., & Brickhouse, N. S. 2012, ApJ, 756, 128
 Freyberg, M., Perinati, E., Pacaud, F., et al. 2020, in Society of Photo-Optical Instrumentation Engineers (SPIE) Conference Series, Vol. 11444, Society of Photo-Optical Instrumentation Engineers (SPIE) Conference Series, 114441O
 Ghirardini, V., Bahar, E., Bulbul, E., et al. 2021a, arXiv e-prints, arXiv:2106.15086
 Ghirardini, V., Bulbul, E., Hoang, D. N., et al. 2021b, A&A, 647, A4
 Giles, P. A., Maughan, B. J., Pacaud, F., et al. 2016, A&A, 592, A3
 Giordini, S., Lovisari, L., Pointecouteau, E., et al. 2013, Space Sci. Rev., 177, 247
 Henden, N. A., Puchwein, E., Shen, S., & Sijacki, D. 2018, MNRAS, 479, 5385
 Henden, N. A., Puchwein, E., & Sijacki, D. 2019, MNRAS, 489, 2439
 Hilton, M., Romer, A. K., Kay, S. T., et al. 2012, MNRAS, 424, 2086
 Hogg, D. W. 1999, arXiv e-prints, astro
 Huchra, J. P., Macri, L. M., Masters, K. L., et al. 2012, ApJS, 199, 26

- Ider-Chitham, J., Comparat, J., Dwelly, T., & Clerc, N. 2021, arXiv e-prints, arXiv:
- Iliejkarevic, J., Reiprich, T. H., Pacaud, F., et al. 2021, arXiv e-prints, arXiv:2106.14544
- Kaiser, N. 1986, MNRAS, 222, 323
- Kettula, K., Giordini, S., van Uitert, E., et al. 2015, MNRAS, 451, 1460
- Klein, M., Oguri, M., Mohr, J. J., et al. 2021, arXiv e-prints, arXiv:2106.14519
- Kravtsov, A. V. & Borgani, S. 2012, ARA&A, 50, 353
- Kravtsov, A. V., Vikhlinin, A., & Nagai, D. 2006, ApJ, 650, 128
- Liu, A., Bulbul, E., Ghirardini, V., et al. 2021a, arXiv e-prints, arXiv:2106.14518
- Liu, T., Merloni, A., Comparat, J., et al. 2021b, arXiv e-prints, arXiv:2106.14528
- Lovisari, L., Ettori, S., Gaspari, M., & Giles, P. A. 2021, Universe, 7, 139
- Lovisari, L., Reiprich, T. H., & Schellenberger, G. 2015, A&A, 573, A118
- Lovisari, L., Schellenberger, G., Sereno, M., et al. 2020, ApJ, 892, 102
- Mantz, A., Allen, S. W., Ebeling, H., Rapetti, D., & Drlica-Wagner, A. 2010a, MNRAS, 406, 1773
- Mantz, A., Allen, S. W., Rapetti, D., & Ebeling, H. 2010b, MNRAS, 406, 1759
- Mantz, A. B. 2019, MNRAS, 485, 4863
- Mantz, A. B., Allen, S. W., Morris, R. G., et al. 2016, MNRAS, 463, 3582
- Mantz, A. B., von der Linden, A., Allen, S. W., et al. 2015, MNRAS, 446, 2205
- Maughan, B. J. 2007, ApJ, 668, 772
- Maughan, B. J., Giles, P. A., Randall, S. W., Jones, C., & Forman, W. R. 2012, MNRAS, 421, 1583
- McCarthy, I. G., Schaye, J., Ponman, T. J., et al. 2010, MNRAS, 406, 822
- Merloni, A., Predehl, P., Becker, W., et al. 2012, arXiv e-prints, arXiv:1209.3114
- Migkas, K., Schellenberger, G., Reiprich, T. H., et al. 2020, A&A, 636, A15
- Molham, M., Clerc, N., Takey, A., et al. 2020, MNRAS, 494, 161
- Nagai, D., Kravtsov, A. V., & Vikhlinin, A. 2007, ApJ, 668, 1
- Pacaud, F., Pierre, M., Adamo, C., et al. 2007, MNRAS, 382, 1289
- Pacaud, F., Pierre, M., Melin, J. B., et al. 2018, A&A, 620, A10
- Pierre, M., Pacaud, F., Juin, J. B., et al. 2011, MNRAS, 414, 1732
- Pillepich, A., Porciani, C., & Reiprich, T. H. 2012, MNRAS, 422, 44
- Planck Collaboration, Ade, P. A. R., Aghanim, N., et al. 2016, A&A, 594, A13
- Pratt, G. W., Arnaud, M., Biviano, A., et al. 2019, Space Sci. Rev., 215, 25
- Pratt, G. W., Croston, J. H., Arnaud, M., & Böhringer, H. 2009, A&A, 498, 361
- Predehl, P., Andritschke, R., Arefiev, V., et al. 2021, A&A, 647, A1
- Puchwein, E., Sijacki, D., & Springel, V. 2008, ApJ, 687, L53
- Romer, A. K., Viana, P. T. P., Liddle, A. R., & Mann, R. G. 2001, ApJ, 547, 594
- Sanders, J. S., Biffi, V., Brüggen, M., et al. 2021, arXiv e-prints, arXiv:2106.14534
- Schaye, J., Dalla Vecchia, C., Booth, C. M., et al. 2010, MNRAS, 402, 1536
- Schellenberger, G. & Reiprich, T. H. 2017, MNRAS, 469, 3738
- Schellenberger, G., Reiprich, T. H., Lovisari, L., Nevalainen, J., & David, L. 2015, A&A, 575, A30
- Seppi, R., Comparat, J., Nandra, K., et al. 2021, A&A, 652, A155
- Short, C. J., Thomas, P. A., Young, O. E., et al. 2010, MNRAS, 408, 2213
- Smith, R. K., Brickhouse, N. S., Liedahl, D. A., & Raymond, J. C. 2001, ApJ, 556, L91
- Tinker, J., Kravtsov, A. V., Klypin, A., et al. 2008, ApJ, 688, 709
- Tozzi, P. & Norman, C. 2001, ApJ, 546, 63
- Truong, N., Rasia, E., Mazzotta, P., et al. 2018, MNRAS, 474, 4089
- Turner, D. J., Giles, P. A., Romer, A. K., et al. 2021, arXiv e-prints, arXiv:2109.11807
- Veronica, A., Su, Y., Biffi, V., et al. 2021, arXiv e-prints, arXiv:2106.14543
- Vikhlinin, A., Burenin, R. A., Ebeling, H., et al. 2009, ApJ, 692, 1033
- Vikhlinin, A., Kravtsov, A., Forman, W., et al. 2006, ApJ, 640, 691
- Voit, G. M. 2005, Reviews of Modern Physics, 77, 207
- Walker, S. A., Fabian, A. C., Sanders, J. S., & George, M. R. 2012, MNRAS, 427, L45
- Whelan, B., Reiprich, T. H., Pacaud, F., et al. 2021, arXiv e-prints, arXiv:2106.14545
- Willingale, R., Starling, R. L. C., Beardmore, A. P., Tanvir, N. R., & O'Brien, P. T. 2013, MNRAS, 431, 394
- Wilms, J., Allen, A., & McCray, R. 2000, ApJ, 542, 914
- Zhang, Y. Y., Andernach, H., Caretta, C. A., et al. 2011, A&A, 526, A105
- Zhang, Y. Y., Finoguenov, A., Böhringer, H., et al. 2008, A&A, 482, 451
- Zou, S., Maughan, B. J., Giles, P. A., et al. 2016, MNRAS, 463, 820

Table 4: X-ray observables of eFEDS clusters measured within R_{500} and between $0.15R_{500} - R_{500}$.

Cluster (eFEDS I+)	ID_SRC	RA (deg)	Dec (deg)	\mathcal{L}_{ext}	\mathcal{L}_{ext} (deg)	R_{500} (arcmin)	T (keV)	L_X (10^{42} erg s $^{-1}$)	L_{bol} (10^{42} erg s $^{-1}$)	M_{gas} (10^{12} M $_{\odot}$)	Y_X (10^{12} M $_{\odot}$ keV)	T_{ex} (keV)	$L_{\text{X,ex}}$ (10^{42} erg s $^{-1}$)	$L_{\text{bol,ex}}$ (10^{42} erg s $^{-1}$)	t_{exp} (s)	
082626.5-003429	28993	126.6108	-0.5748	8.5	5.0	0.161	2.404	5.1 $^{+3.4}_{-3.4}$	< 5.7	< 30	< 2.5	< 36	4.1 $^{+12.9}_{-4.8}$	< 4.9	< 24	184
082751.7-002853	11248	126.9635	-0.4816	12.8	27.9	0.257	2.620	1.80 $^{+2.11}_{-2.11}$	< 12	< 33	< 5.0	< 15	1.73 $^{+9.17}_{-0.63}$	< 7.0	< 21	707
082808.7-001003	4800	127.0366	-0.1677	28.5	62.5	0.076	5.487	0.994 $^{+0.63}_{-0.38}$	2.40 $^{+0.48}_{-0.48}$	4.58 $^{+0.09}_{-0.09}$	1.13 $^{+0.31}_{-0.31}$	1.62 $^{+0.52}_{-0.52}$	3.22 $^{+1.12}_{-1.12}$	1.08 $^{+0.63}_{-0.63}$	1.62 $^{+0.52}_{-0.52}$	675
082820.5-000721	4169	127.0856	-0.1228	42.4	81.4	0.845	1.894	5.5 $^{+3.3}_{-3.3}$	2.73 $^{+0.34}_{-0.34}$	990 $^{+332}_{-332}$	42.5 $^{+2.9}_{-2.9}$	23.3 $^{+2.2}_{-2.2}$	4.9 $^{+0.74}_{-0.74}$	23.2 $^{+0.34}_{-0.34}$	790 $^{+310}_{-310}$	748
082840.6-000500	7991	127.1692	-0.0836	18.4	37.5	0.320	2.504	8.7 $^{+2.0}_{-2.0}$	14.7 $^{+2.7}_{-2.7}$	65 $^{+4.4}_{-4.4}$	5.7 $^{+1.8}_{-1.8}$	7.0 $^{+1.2}_{-1.2}$	8.3 $^{+1.4}_{-1.4}$	8.3 $^{+1.4}_{-1.4}$	35 $^{+26}_{-26}$	856
082859.9+010756	14973	127.2500	+1.1323	19.2	14.4	0.354	2.522	6.9 $^{+2.9}_{-2.9}$	27.4 $^{+3.8}_{-3.8}$	115 $^{+21}_{-21}$	11.9 $^{+1.2}_{-1.2}$	< 420	5.7 $^{+1.8}_{-1.8}$	25.9 $^{+2.9}_{-2.9}$	95 $^{+13}_{-13}$	464
082952.7+002139	7528	127.4697	+0.3611	7.7	38.6	0.420	1.874	6.3 $^{+3.4}_{-3.4}$	14.3 $^{+4.9}_{-4.9}$	58 $^{+14}_{-14}$	3.7 $^{+1.6}_{-1.6}$	< 130	6.0 $^{+3.4}_{-3.4}$	7.5 $^{+4.8}_{-4.8}$	31 $^{+27}_{-27}$	1099
082955.4+004131	3810	127.4810	+0.6922	24.2	80.3	0.940	1.555	5.6 $^{+0.7}_{-0.7}$	21.7 $^{+4.6}_{-4.6}$	790 $^{+210}_{-210}$	28.8 $^{+4.6}_{-4.6}$	152 $^{+269}_{-269}$	4.1 $^{+1.1}_{-1.1}$	180 $^{+46}_{-46}$	580 $^{+160}_{-160}$	1020
083040.7+023219	9837	127.6697	+2.5388	11.5	23.7	0.111	3.431	10.4 $^{+0.9}_{-0.9}$	20.1 $^{+1.8}_{-1.8}$	0.64 $^{+0.25}_{-0.25}$	< 0.48	< 5.1	< 1.9	< 1.9	718	
083110.5+015616	5601	127.7940	+1.9378	11.8	34.1	0.420	2.172	11.3 $^{+1.4}_{-1.4}$	37.1 $^{+0.8}_{-0.8}$	18 $^{+0.8}_{-0.8}$	13.0 $^{+2.5}_{-2.5}$	< 540	7.7 $^{+1.8}_{-1.8}$	31.0 $^{+9.1}_{-9.1}$	137 $^{+112}_{-112}$	1016
083120.5+005257	9594	127.8354	+0.8825	7.0	25.9	0.664	1.510	3.0 $^{+0.2}_{-0.2}$	33.6 $^{+0.3}_{-0.3}$	98 $^{+27}_{-27}$	7.6 $^{+2.8}_{-2.8}$	22.6 $^{+4.8}_{-4.8}$	2.69 $^{+4.57}_{-4.57}$	22.1 $^{+5.0}_{-5.0}$	63 $^{+34}_{-34}$	1205
083120.5+030949	11134	127.8355	+3.1639	32.8	27.7	0.568	2.243	1.24 $^{+0.25}_{-0.25}$	< 75	< 160	< 23	< 31	1.24 $^{+0.88}_{-0.88}$	< 62	< 130	746
083125.9+015533	2659	127.8580	+1.9259	47.5	110.5	0.684	1.930	2.05 $^{+0.14}_{-0.14}$	197 $^{+26}_{-26}$	482 $^{+61}_{-61}$	34.1 $^{+4.9}_{-4.9}$	71 $^{+14}_{-14}$	170 $^{+25}_{-25}$	1.95 $^{+0.74}_{-0.74}$	417 $^{+56}_{-56}$	1095
083137.9+004632	3725	127.9081	+0.7758	17.2	66.1	0.293	2.379	1.38 $^{+0.31}_{-0.31}$	23.0 $^{+3.9}_{-3.9}$	23.0 $^{+0.8}_{-0.8}$	3.39 $^{+0.55}_{-0.55}$	4.8 $^{+2.3}_{-2.3}$	5.5 $^{+2.6}_{-2.6}$	12.3 $^{+4.6}_{-4.6}$	1207	
083146.7-012849	4403	127.9449	-1.4805	6.0	30.1	0.405	4.4 $^{+2.0}_{-2.0}$	0.117 $^{+0.049}_{-0.049}$	30.7 $^{+0.8}_{-0.8}$	0.40 $^{+0.03}_{-0.03}$	< 0.16	< 1.3	3.0 $^{+0.23}_{-0.23}$	< 0.12	< 3.9	1684
083149.4+002230	5463	127.9559	+0.8751	13.1	41.5	0.398	2.204	1.84 $^{+0.75}_{-0.75}$	12.8 $^{+0.8}_{-0.8}$	30.9 $^{+0.5}_{-0.5}$	2.72 $^{+0.98}_{-0.98}$	< 14	2.4 $^{+1.1}_{-1.1}$	< 9.3	< 27	1205
083153.6+012530	2600	127.9734	+1.4253	48.4	94.5	0.2699	3.209	2.41 $^{+0.75}_{-0.75}$	25.1 $^{+2.7}_{-2.7}$	64.2 $^{+11.3}_{-11.3}$	10.4 $^{+2.5}_{-2.5}$	25.6 $^{+12.2}_{-12.2}$	7.72 $^{+2.4}_{-2.4}$	17.5 $^{+3.2}_{-3.2}$	47.1 $^{+11.4}_{-11.4}$	1207
083204.4+041907	3593	128.0185	+4.3188	66.0	118.6	0.197	4.511	2.54 $^{+0.36}_{-0.36}$	40.9 $^{+5.8}_{-5.8}$	105 $^{+14}_{-14}$	18.1 $^{+2.4}_{-2.4}$	46.8 $^{+16.8}_{-16.8}$	2.56 $^{+1.1}_{-1.1}$	68 $^{+15}_{-15}$	34.7 $^{+4.1}_{-4.1}$	524
083228.0-000656	7396	128.1169	-0.1157	13.6	42.4	0.206	2.026	3.4 $^{+0.36}_{-0.36}$	18.2 $^{+6.4}_{-6.4}$	53 $^{+26}_{-26}$	6.7 $^{+1.8}_{-1.8}$	20.9 $^{+3.5}_{-3.5}$	3.7 $^{+0.8}_{-0.8}$	190 $^{+55}_{-55}$	1204	
083238.8-003200	8565	128.1617	-0.5336	15.8	32.6	0.399	2.122	6.2 $^{+1.7}_{-1.7}$	17.0 $^{+3.5}_{-3.5}$	66 $^{+20}_{-20}$	7.4 $^{+2.4}_{-2.4}$	< 200	4.0 $^{+1.5}_{-1.5}$	44 $^{+12}_{-12}$	1213	
083249.9+031737	10398	128.2928	+3.2939	7.7	29.0	0.828	1.363	3.9 $^{+0.44}_{-0.44}$	< 76	7.5 $^{+1.3}_{-1.3}$	< 300	7.5 $^{+1.6}_{-1.6}$	< 260	1.66	1166	
083310.2+030136	15959	128.2928	+3.0269	6.7	18.4	0.748	1.376	1.03 $^{+0.30}_{-0.30}$	39 $^{+19}_{-19}$	95 $^{+43}_{-43}$	7.4 $^{+3.0}_{-3.0}$	13.1 $^{+7.8}_{-7.8}$	371 $^{+16}_{-16}$	89 $^{+38}_{-38}$	1206	
083315.5+006623	6869	128.3148	+0.1065	16.5	42.0	0.470	1.970	1.03 $^{+0.30}_{-0.30}$	41.3 $^{+8.3}_{-8.3}$	82 $^{+16}_{-16}$	10.6 $^{+2.0}_{-2.0}$	10.8 $^{+4.9}_{-4.9}$	1.19 $^{+0.34}_{-0.34}$	33.1 $^{+7.9}_{-7.9}$	1212	
083322.8-000656	2879	128.3382	+1.4456	18.7	43.6	0.566	1.912	8.2 $^{+2.19}_{-2.19}$	65.7 $^{+8.0}_{-8.0}$	28 $^{+18}_{-18}$	16.2 $^{+2.6}_{-2.6}$	< 540	6.8 $^{+1.6}_{-1.6}$	47.0 $^{+7.7}_{-7.7}$	1214	
083322.6-011128	6302	128.3444	-1.1912	11.6	22.5	0.288	2.489	2.16 $^{+0.53}_{-0.53}$	12.5 $^{+2.5}_{-2.5}$	30.9 $^{+0.8}_{-0.8}$	5.1 $^{+2.2}_{-2.2}$	10.9 $^{+6.2}_{-6.2}$	2.30 $^{+1.46}_{-1.46}$	9.0 $^{+2.6}_{-2.6}$	22.8 $^{+6.8}_{-6.8}$	1185
083330.4+030427	2528	128.3767	+0.5744	50.1	123.3	0.318	3.476	1.676	17.6 $^{+2.3}_{-2.3}$	66.2 $^{+25}_{-25}$	7.8 $^{+1.4}_{-1.4}$	< 180	6.7 $^{+1.6}_{-1.6}$	31.4 $^{+8.8}_{-8.8}$	891	
083334.0-002943	6767	128.4211	-0.4954	7.2	32.3	0.318	2.067	1.61 $^{+0.67}_{-0.67}$	< 19	< 45	< 5.8	< 15	3.5 $^{+0.48}_{-0.48}$	12.5 $^{+2.1}_{-2.1}$	3780	1207
083345.8+004208	29844	128.4409	+0.7025	29.3	90.5	0.384	2.344	2.33 $^{+0.53}_{-0.53}$	33.6 $^{+5.3}_{-5.3}$	85 $^{+15}_{-15}$	9.5 $^{+2.2}_{-2.2}$	21.8 $^{+9.3}_{-9.3}$	2.35 $^{+0.79}_{-0.79}$	22.9 $^{+4.4}_{-4.4}$	58 $^{+13}_{-13}$	1204
083401.5-001337	4258	128.5065	-0.2271	8.3	23.2	0.314	0.629	7.9 $^{+1.4}_{-1.4}$	< 6.6	< 34	< 0.73	< 11	6.2 $^{+0.49}_{-0.49}$	< 4.2	< 20	1184
083402.5+023437	6409	128.5105	+2.5772	9.2	36.8	0.362	0.2020	5.0 $^{+1.6}_{-1.6}$	11.6 $^{+2.9}_{-2.9}$	30.6 $^{+0.8}_{-0.8}$	2.9 $^{+1.1}_{-1.1}$	< 76	6.1 $^{+1.3}_{-1.3}$	18.1 $^{+12.3}_{-12.3}$	1205	
083430.7+012131	4634	128.5155	+1.3588	15.4	65.4	0.671	1.676	4.2 $^{+3.6}_{-3.6}$	17.6 $^{+2.7}_{-2.7}$	64.2 $^{+14.5}_{-14.5}$	4.3 $^{+1.8}_{-1.8}$	< 120	7.5 $^{+1.3}_{-1.3}$	< 380	1207	
083441.7+035856	1092	128.5590	+3.9825	20.7	30.6	0.201	2.785	5.8 $^{+2.4}_{-2.4}$	23.3 $^{+4.8}_{-4.8}$	9.9 $^{+2.0}_{-2.0}$	40 $^{+3.3}_{-3.3}$	23.4 $^{+9.8}_{-9.8}$	6.9 $^{+1.7}_{-1.7}$	31 $^{+22}_{-22}$	1187	
083442.7+034537	3240	128.5946	+3.7603	10.0	77.7	0.338	2.222	1.50 $^{+0.42}_{-0.42}$	14.1 $^{+2.0}_{-2.0}$	31.3 $^{+5.5}_{-5.5}$	5.7 $^{+1.6}_{-1.6}$	< 10	1.37 $^{+0.57}_{-0.57}$	< 23	1193	
083427.0-015612	12633	128.6129	-1.9369	13.4	21.8	0.573	1.661	6.4 $^{+2.4}_{-2.4}$	25.7 $^{+6.4}_{-6.4}$	103 $^{+10.6}_{-10.6}$	9.1 $^{+2.0}_{-2.0}$	< 260	4.0 $^{+0.92}_{-0.92}$	25.0 $^{+6.6}_{-6.6}$	1574	
083434.0+034208	8206	128.6296	+3.7023	6.8	18.1	0.215	2.188	5.0 $^{+3.20}_{-3.20}$	20.6 $^{+5.8}_{-5.8}$	3.0 $^{+0.83}_{-0.83}$	11.1 $^{+10.0}_{-10.0}$	1.59 $^{+0.50}_{-0.50}$	< 49	5.6 $^{+1.47}_{-1.47}$	2.95 $^{+0.98}_{-0.98}$	1205
083435.6+05159	4593	128.6484	+5.0332	7.7	62.3	0.091	3.805	2.48 $^{+0.28}_{-0.28}$	15.3 $^{+6.1}_{-6.1}$	60.5 $^{+3.9}_{-3.9}$	1.66 $^{+0.55}_{-0.55}$	< 1.4	< 3.8	3.8 $^{+0.72}_{-0.72}$	< 1.6	1266
083457.7+02420	12572	128.7406	+5.3425	15.4	19.3	0.410	2.103	2.26 $^{+0.68}_{-0.68}$	13.5 $^{+4.0}_{-4.0}$	34.3 $^{+0.59}_{-0.59}$	5.4 $^{+1.5}_{-1.5}$	12.0 $^{+7.3}_{-7.3}$	3.1 $^{+2.8}_{-2.8}$	9.3 $^{+1.6}_{-1.6}$	985	
083503.2+010756	3874	128.7406	+1.3225	36.9	85.8	0.296	4.648	4.2 $^{+0.57}_{-0.57}$	22.6 $^{+3.7}_{-3.7}$	74 $^{+8.0}_{-8.0}$	9.4 $^{+1.6}_{-1.6}$	40 $^{+8.2}_{-8.2}$	2.28 $^{+0.67}_{-0.67}$	18.8 $^{+3.3}_{-3.3}$	46.6 $^{+7.6}_{-7.6}$	1188
083509.0+001542	1360	128.7876	+0.2619	74.8	213.1</											

Table 4: continued.

Cluster (eFEDS I+)	ID_SRC	RA (deg)	Dec (deg)	\mathcal{L}_{ext}	\mathcal{L}_{ext} (deg)	R_{500} (arcmin)	z	T (keV)	L_X ($10^{42} \text{ erg s}^{-1}$)	L_{bol} ($10^{42} \text{ erg s}^{-1}$)	M_{gas} (10^{12} M_\odot)	Y_X ($10^{12} \text{ M}_\odot \text{ keV}$)	T_{ex} (keV)	$L_{\text{bol,ex}}$ ($10^{42} \text{ erg s}^{-1}$)	t_{exp} (s)	
083817.4+041821	6136	129.5727	+4.3060	21.1	56.6	0.211	3.028	$3.4^{+6.0}_{-1.4}$	$11.3^{+1.4}_{-1.4}$	$32.7^{+19.4}_{-13.4}$	$5.45^{+0.93}_{-0.82}$	$18.5^{+33.3}_{-8.74}$	$4.4^{+8.7}_{-2.1}$	$28.8^{+22.1}_{-7.3}$	1214	
083817.5-021704	6195	129.5732	-2.2845	33.7	71.2	0.565	2.177	$4.6^{+1.4}_{-1.4}$	130^{+168}_{-13}	440^{+168}_{-94}	$30.1^{+5.0}_{-4.5}$	$13.9^{+1.7}_{-1.7}$	$3.5^{+3.0}_{-1.2}$	$11.7^{+2.2}_{-1.2}$	639	
083834.1+020643	3905	129.6425	+2.1121	29.1	67.2	0.457	2.181	$3.7^{+1.9}_{-1.9}$	$55.6^{+1.6}_{-1.6}$	169^{+51}_{-51}	$15.2^{+4.5}_{-4.5}$	$4.6^{+1.2}_{-1.2}$	$41.2^{+4.2}_{-4.2}$	140^{+53}_{-53}	1188	
083840.3+04416	81186	129.6681	+4.7380	17.9	34.1	0.455	1.946	$2.59^{+1.3}_{-1.3}$	$28.3^{+4.4}_{-3.3}$	76^{+21}_{-21}	$10.0^{+1.3}_{-1.3}$	$26.4^{+2.3}_{-2.3}$	$2.27^{+2.7}_{-2.7}$	63.1^{+21}_{-21}	1341	
083840.6-004134	7463	129.6694	-0.6930	9.5	36.9	0.462	1.919	$12.5^{+0.7}_{-0.7}$	$19.2^{+6.9}_{-6.9}$	106^{+67}_{-67}	$8.3^{+2.3}_{-2.3}$	$18.0^{+0.77}_{-0.71}$	$13.0^{+0.77}_{-0.73}$	102^{+73}_{-73}	1207	
083856.9+030743	7902	129.7327	+3.1287	6.7	31.1	0.241	2.239	$2.3^{+0.6}_{-0.6}$	$3.70^{+0.6}_{-0.6}$	$9.5^{+4.0}_{-3.8}$	$1.77^{+0.98}_{-0.98}$	< 310	$5.4^{+1.72}_{-1.72}$	$5.4^{+1.72}_{-1.72}$	1190	
083857.5+020846	1806	129.7398	+2.1464	92.8	192.1	0.360	3.019	$4.3^{+1.5}_{-1.5}$	$95.6^{+0.88}_{-0.88}$	298^{+54}_{-54}	$28.5^{+3.7}_{-3.7}$	120^{+31}_{-31}	$4.7^{+2.9}_{-2.9}$	$77.3^{+9.7}_{-7.8}$	255 ⁺⁶⁹ ₋₃₆	
083858.5-015032	6026	129.7441	-1.8424	7.4	49.5	0.135	3.038	$1.18^{+1.39}_{-1.39}$	$1.09^{+0.84}_{-0.84}$	81^{+108}_{-108}	$2.24^{+0.95}_{-0.95}$	< 1.5	< 1.8	$1.48^{+1.75}_{-1.75}$	< 3.4	1223
083859.3+022841	3315	129.7473	+2.4782	11.5	26.8	0.359	2.122	$2.3^{+1.3}_{-1.3}$	$23.6^{+2.0}_{-2.0}$	$5.6^{+1.2}_{-1.2}$	$32.2^{+1.5}_{-1.5}$	$3.9^{+0.8}_{-0.8}$	$16.0^{+0.42}_{-0.42}$	51^{+35}_{-35}	1187	
083900.6+020507	736	129.7527	+2.0159	39.3	313.3	0.359	2.701	$3.46^{+1.36}_{-1.36}$	$51.2^{+6.0}_{-6.0}$	$149^{+1.8}_{-1.8}$	$9.2^{+1.4}_{-1.4}$	142^{+29}_{-29}	$4.7^{+1.6}_{-1.6}$	$20.5^{+3.5}_{-3.5}$	72^{+40}_{-40}	1201
083903.5-011454	7445	129.7649	-1.2485	13.0	38.9	0.437	1.883	$4.4^{+0.78}_{-0.78}$	$27.1^{+0.8}_{-0.8}$	$94^{+0.8}_{-0.8}$	$9.4^{+1.3}_{-1.3}$	41^{+80}_{-80}	$4.4^{+0.86}_{-0.86}$	$24.4^{+3.3}_{-3.3}$	82^{+16}_{-16}	1173
083914.7-021226	5360	129.8117	-2.2073	21.4	45.0	0.187	2.850	$1.68^{+0.72}_{-0.72}$	$4.0^{+1.96}_{-1.96}$	$9.0^{+1.2}_{-1.2}$	$1.59^{+0.87}_{-0.87}$	$2.5^{+1.8}_{-1.8}$	< 4.0	$1.40^{+0.86}_{-0.86}$	< 8.9	1086
083916.7-020552	7669	129.8198	-2.0979	24.9	29.6	0.269	2.508	$1.56^{+0.57}_{-0.57}$	$5.6^{+1.2}_{-1.2}$	$12.8^{+6.1}_{-6.1}$	$2.62^{+0.65}_{-0.65}$	$4.4^{+1.25}_{-1.25}$	$1.55^{+0.58}_{-0.58}$	$3.1^{+3.2}_{-1.2}$	$6.9^{+7.1}_{-7.1}$	1198
083917.9-020839	15489	129.8247	-2.1442	18.2	15.0	0.269	2.266	$1.87^{+0.74}_{-0.74}$	< 18	43	$3.4^{+0.96}_{-0.96}$	$6.4^{+1.7}_{-1.7}$	< 17	$1.81^{+0.48}_{-0.48}$	< 40	1183
083921.0-014149	12407	129.8377	-1.6978	18.5	26.5	0.269	2.990	$3.95^{+1.26}_{-1.26}$	$19.9^{+2.6}_{-2.6}$	60^{+12}_{-10}	$9.6^{+1.5}_{-1.5}$	$38.1^{+1.40}_{-1.40}$	$17.1^{+2.2}_{-2.2}$	54^{+13}_{-13}	1180	
083927.0-021357	10377	129.8627	-2.2328	9.3	22.5	0.567	1.767	$2.70^{+0.87}_{-0.87}$	$20.1^{+21.6}_{-21.6}$	56^{+10}_{-10}	< 15	< 60	< 17	< 130	1156	
083929.0+043001	3677	129.8711	+4.5003	20.1	76.6	0.249	2.582	$1.86^{+0.72}_{-0.72}$	$11.4^{+1.54}_{-1.54}$	26.8^{+10}_{-10}	$3.90^{+0.79}_{-0.79}$	$7.2^{+3.3}_{-3.3}$	$2.00^{+0.95}_{-0.95}$	$7.5^{+1.7}_{-1.7}$	$18.3^{+5.5}_{-5.5}$	1216
083929.6-015005	15946	129.8736	-1.8348	16.4	21.3	0.575	1.907	$5.7^{+1.5}_{-1.5}$	$39.1^{+1.53}_{-1.53}$	$142^{+2.9}_{-2.9}$	$14.2^{+2.9}_{-2.9}$	$2.62^{+0.65}_{-0.65}$	$2.5^{+1.7}_{-1.7}$	$35.1^{+7.0}_{-7.0}$	151^{+113}_{-113}	1198
083930.3-014348	6979	129.8763	-1.7302	7.8	22.5	0.271	2.243	$1.93^{+1.41}_{-1.41}$	$1.93^{+1.41}_{-1.41}$	$6.8^{+1.39}_{-1.39}$	$16.1^{+0.99}_{-0.99}$	$2.5^{+2.1}_{-2.1}$	< 14	$1.79^{+0.36}_{-0.36}$	< 15	1178
083933.8-014044	356	129.8909	-1.6790	245.8	663.7	0.272	4.501	$3.73^{+0.72}_{-0.72}$	$130.0^{+1.0}_{-1.0}$	$38.6^{+0.53}_{-0.53}$	$38.0^{+1.59}_{-1.59}$	142^{+29}_{-29}	$3.56^{+0.73}_{-0.73}$	265^{+36}_{-36}	1126	
083936.0+011445	2898	129.9001	+1.7459	7.4	42.1	0.149	2.836	$1.72^{+0.58}_{-0.58}$	$4.2^{+0.45}_{-0.45}$	$4.2^{+0.45}_{-0.45}$	$4.2^{+0.45}_{-0.45}$	< 4.0	$1.44^{+0.67}_{-0.67}$	< 1.7	< 3.8	1216
083937.8+014631	7652	129.9074	+1.7754	17.6	38.0	0.389	2.088	$2.73^{+0.74}_{-0.74}$	$22.6^{+0.59}_{-0.59}$	62^{+14}_{-14}	$7.7^{+0.53}_{-0.53}$	$21.5^{+4.35}_{-4.35}$	$2.07^{+0.37}_{-0.37}$	$17.5^{+4.4}_{-4.4}$	44^{+14}_{-14}	1213
083940.8+010416	2832	129.9201	+1.0714	27.3	84.0	0.157	3.349	$2.57^{+0.88}_{-0.88}$	$7.20^{+0.66}_{-0.66}$	$19.2^{+1.12}_{-1.12}$	$3.30^{+0.66}_{-0.66}$	$3.0^{+1.0}_{-1.0}$	$2.5^{+2.1}_{-2.1}$	$3.7^{+1.6}_{-1.6}$	$15.6^{+6.2}_{-6.2}$	1206
083945.5+031556	7213	129.9396	+3.2657	11.0	32.9	0.425	1.859	$0.90^{+0.61}_{-0.61}$	$9.0^{+0.92}_{-0.92}$	$17.3^{+1.6}_{-1.6}$	< 3.6	< 4.0	$1.01^{+0.43}_{-0.43}$	< 16	1193	
083955.0+024245	3270	129.9793	+2.4071	9.0	12.3	0.189	3.258	$1.22^{+0.36}_{-0.36}$	$3.34^{+0.33}_{-0.33}$	$7.0^{+0.62}_{-0.62}$	$1.97^{+0.84}_{-0.84}$	$1.97^{+0.84}_{-0.84}$	$2.28^{+1.7}_{-1.7}$	$4.9^{+3.0}_{-3.0}$	1215	
084000.0-013109	7217	130.0002	-1.5194	26.2	55.8	0.266	3.130	$1.70^{+0.59}_{-0.59}$	$19.0^{+0.58}_{-0.58}$	$4.9^{+0.88}_{-0.88}$	$9.2^{+0.88}_{-0.88}$	$19.0^{+0.52}_{-0.52}$	$16.0^{+0.52}_{-0.52}$	$34.8^{+8.9}_{-8.9}$	1096	
084001.6+024242	4839	130.0070	+4.4145	14.8	51.2	0.259	2.452	$3.2^{+0.42}_{-0.42}$	$8.0^{+0.24}_{-0.24}$	$8.0^{+0.19}_{-0.19}$	$22.4^{+7.1}_{-7.1}$	$2.96^{+0.75}_{-0.75}$	$2.9^{+1.7}_{-1.7}$	$4.4^{+2.36}_{-2.36}$	$13.3^{+6.4}_{-6.4}$	1221
084003.2+003008	2568	130.0137	+0.5023	19.1	104.0	0.385	2.223	$4.6^{+1.45}_{-1.45}$	< 15	< 55	< 7.3	< 36	$7.2^{+1.87}_{-1.87}$	< 7.2	< 31	1211
084003.8+013751	10272	130.0203	+1.6309	13.1	17.4	0.342	2.210	$5.0^{+1.4}_{-1.4}$	$13.4^{+9.5}_{-9.5}$	$13.4^{+9.5}_{-9.5}$	$2.63^{+0.77}_{-0.77}$	$2.63^{+0.77}_{-0.77}$	$2.63^{+0.77}_{-0.77}$	$2.9^{+1.5}_{-1.5}$	$8.9^{+8.5}_{-8.5}$	1213
084006.1+025913	2388	130.0258	+2.9871	41.9	117.5	0.456	2.307	$3.76^{+0.36}_{-0.36}$	$1.22^{+0.36}_{-0.36}$	$61.5^{+8.6}_{-8.6}$	$1.74^{+0.18}_{-0.18}$	$1.74^{+0.18}_{-0.18}$	$0.222^{+0.13}_{-0.13}$	172^{+74}_{-74}	1208	
084011.6+034837	5544	130.0487	+3.8104	12.5	39.3	0.825	1.469	$1.71^{+0.55}_{-0.55}$	$17.1^{+0.55}_{-0.55}$	$45.3^{+7.9}_{-7.9}$	$7.7^{+2.4}_{-2.4}$	$21.1^{+0.82}_{-0.82}$	$2.28^{+0.74}_{-0.74}$	$14.7^{+2.4}_{-2.4}$	1215	
084016.6+039591	6282	130.0695	+3.6644	9.4	35.5	0.805	1.443	$17.1^{+0.55}_{-0.55}$	$17.1^{+0.55}_{-0.55}$	46^{+13}_{-13}	300^{+14}_{-14}	$11.8^{+2.8}_{-2.8}$	< 470	$3.9^{+0.24}_{-0.24}$	217^{+134}_{-134}	1199
084021.6-022948	5406	130.0901	-2.4967	12.5	29.3	0.184	2.978	$2.65^{+0.88}_{-0.88}$	$7.2^{+1.10}_{-1.10}$	$7.2^{+1.10}_{-1.10}$	$3.70^{+0.69}_{-0.69}$	$19.1^{+4.0}_{-4.0}$	$10.1^{+5.7}_{-5.7}$	$2.31^{+1.0}_{-1.0}$	$15.9^{+3.5}_{-3.5}$	1209
084021.6+020132	5639	130.0903	+2.0256	31.1	17.7	0.357	0.565	$0.76^{+0.40}_{-0.40}$	$1.75^{+0.55}_{-0.55}$	$17.3^{+4.4}_{-4.4}$	$0.54^{+0.15}_{-0.15}$	$0.37^{+0.15}_{-0.15}$	$0.37^{+0.15}_{-0.15}$	$7.2^{+3.0}_{-3.0}$	$14.5^{+4.2}_{-4.2}$	1215
084034.5+023638	250	130.1441	+2.6108	114.6	661.8	0.049	7.565	$0.849^{+0.032}_{-0.032}$	$0.92^{+0.032}_{-0.032}$	$0.92^{+0.032}_{-0.032}$	$1.74^{+0.018}_{-0.018}$	$0.222^{+0.013}_{-0.013}$	$0.188^{+0.012}_{-0.012}$	$0.154^{+0.084}_{-0.084}$	< 2.0	1217
084035.8+044036	5844	130.1493	+4.6768	8.6	39.8	0.793	1.448	$3.34^{+0.34}_{-0.34}$	$4.37^{+0.091}_{-0.091}$	$43^{+2.0}_{-2.0}$	$2.73^{+0.97}_{-0.97}$	< 51	< 53	$3.4^{+3.4}_{-3.4}$	< 160	1320
084044.7+024108	8131	130.1863	+2.6858	8.6	19.8	1.104	1.220	$2.9^{+0.4}_{-0.4}$	$16.7^{+0.4}_{-0.4}$	167^{+43}_{-43}	$10.0^{+1.5}_{-1.5}$	510^{+10}_{-10}	$19.0^{+1.5}_{-1.5}$	55^{+113}_{-113}	1216	
084051.7+014122	7662	130.295														

Table 4: continued.

Cluster	ID_SRC	RA (deg)	Dec (deg)	\mathcal{L}_{ext}	\mathcal{L}_{ext}	R_{500} (arcmin)	T (keV)	L_X (10^{42} erg s $^{-1}$)	L_{bol} (10^{42} erg s $^{-1}$)	M_{gas} (10^{12} M $_{\odot}$)	Y_X (10^{12} M $_{\odot}$ keV)	T_{ex} (keV)	$L_{\text{bol,ex}}$ (10^{42} erg s $^{-1}$)	t_{exp} (s)
084151.7+004351	6543	130.4656	+0.7311	12.5	25.5	0.237	2.312	$1.92^{+1.32}_{-0.88}$	<34	<36	$5.2^{+9.3}_{-2.4}$	<11	1133	
084151.9-010156	6071	130.4665	-1.0323	9.1	36.8	0.270	2.240	$9.3^{+6.1}_{-3.9}$	$23.1^{+17.7}_{-8.8}$	$2.03^{+0.44}_{-0.38}$	<80	<10	$17.9^{+11.5}_{-7.2}$	1603
084201.3+040534	6988	130.5036	+4.0928	6.6	36.5	0.758	1.432	$6.1^{+3.2}_{-2.0}$	$39^{+1.2}_{-1.2}$	$4.9^{+1.1}_{-0.8}$	<180	<46	<160	1208
084201.8+005941	3334	130.5076	+0.9950	7.5	9.9	0.887	1.940	$5.6^{+1.2}_{-1.0}$	<0.45	<1.7	$6.8^{+0.8}_{-0.5}$	<2.3	$4.4^{+0.2}_{-0.1}$	<1.5
084210.5+020558	7967	130.5439	+2.0558	6.8	28.0	0.421	1.748	$3.4^{+3.4}_{-3.2}$	<12	<43	$6.4^{+0.2}_{-0.1}$	<27	$3.4^{+3.5}_{-3.4}$	<29
084220.9+013844	3295	130.5875	+1.6457	27.7	64.5	0.421	0.498	$7.9^{+4.4}_{-4.4}$	$13.5^{+3.9}_{-3.9}$	57^{+36}_{-36}	<22	$5.8^{+0.8}_{-0.7}$	$12.8^{+3.6}_{-3.6}$	48 ⁺³² ₋₁₅
084223.1+003340	4993	130.5963	+0.5613	11.0	55.3	1.077	1.317	$3.2^{+2.8}_{-2.8}$	247^{+78}_{-78}	720^{+40}_{-290}	<33	$5.8^{+2.4}_{-2.4}$	<350	<950
084240.7-011643	2859	130.6698	-1.2787	18.5	16.5	0.210	0.876	$0.392^{+0.17}_{-0.067}$	$1.29^{+0.53}_{-0.53}$	$3.1^{+0.6}_{-0.6}$	$0.148^{+0.086}_{-0.062}$	$0.060^{+0.041}_{-0.026}$	$0.38^{+0.042}_{-0.034}$	<3.4
084246.9-000916	4861	130.6956	-0.1548	31.3	45.7	0.420	2.485	$6.8^{+1.0}_{-0.9}$	$43.8^{+0.6}_{-0.6}$	167^{+37}_{-36}	$17.4^{+2.2}_{-2.2}$	$2.6^{+0.5}_{-0.5}$	$3.7^{+0.9}_{-0.9}$	148 ⁺¹⁰⁶ ₋₄₁
084253.7+022006	6903	130.7388	+0.3350	6.6	29.7	0.345	1.970	$3.0^{+0.9}_{-0.9}$	$6.9^{+0.4}_{-0.4}$	$21.2^{+20.5}_{-20.5}$	<6.3	<53	$3.4^{+4.6}_{-4.6}$	<38
084255.6+022332	2475	130.7317	+4.3924	32.3	129.4	0.484	2.202	$2.34^{+1.2}_{-1.2}$	$67.1^{+1.8}_{-1.8}$	172^{+55}_{-55}	$41.4^{+9.7}_{-9.7}$	$2.37^{+1.7}_{-1.7}$	$46.3^{+1.1}_{-1.1}$	120 ⁺²³ ₋₂₃
084258.3-004037	4269	130.7432	-0.6772	7.7	55.4	0.407	1.986	$2.24^{+0.67}_{-0.67}$	$16.5^{+6.3}_{-6.3}$	43^{+20}_{-20}	$4.4^{+1.0}_{-1.0}$	$2.80^{+0.85}_{-0.85}$	$15.3^{+3.8}_{-3.8}$	45 ⁺³¹ ₋₂₁
084301.4+025741	11065	130.7560	+2.9615	7.8	31.3	0.539	1.613	$2.08^{+0.56}_{-0.56}$	$18.6^{+5.7}_{-5.7}$	47^{+16}_{-16}	<7.9	<28	$2.37^{+1.4}_{-1.4}$	<20
084307.1+002839	3336	130.7797	+0.4777	28.1	87.0	0.264	2.866	$8.9^{+1.2}_{-1.2}$	98^{+30}_{-30}	$9.0^{+1.4}_{-1.4}$	$8.0^{+1.4}_{-1.4}$	$9.3^{+0.8}_{-0.8}$	$15.3^{+4.0}_{-4.0}$	72 ⁺⁴⁴ ₋₃₄
084324.2-001438	9590	130.8511	-0.2441	16.3	31.7	0.350	2.191	$4.1^{+1.8}_{-1.8}$	$14.8^{+3.0}_{-3.0}$	47^{+36}_{-36}	$6.4^{+1.4}_{-1.4}$	$3.2^{+2.6}_{-2.6}$	$13.4^{+3.5}_{-3.5}$	1057
084346.2+010833	12839	130.9425	+1.1425	11.2	21.1	0.342	2.095	$3.8^{+1.6}_{-1.6}$	$12.6^{+3.0}_{-3.0}$	40^{+21}_{-21}	$5.8^{+1.4}_{-1.4}$	$21.9^{+3.7}_{-3.7}$	$3.4^{+2.6}_{-2.6}$	135
084349.1+044044	19985	130.9547	+4.0678	12.0	18.2	0.213	2.716	$3.0^{+1.0}_{-1.0}$	<31	<110	$9.5^{+1.3}_{-1.3}$	<59	$3.3^{+1.3}_{-1.3}$	<110
084353.9+031402	19202	130.9747	+3.2341	7.7	11.1	0.374	1.919	$2.62^{+0.96}_{-0.96}$	$6.9^{+3.6}_{-3.6}$	$19.8^{+11.8}_{-8.4}$	$3.3^{+1.4}_{-1.4}$	<38	$2.48^{+0.84}_{-0.84}$	<34
084412.6-026514	3396	131.0526	-2.0874	6.8	80.1	0.382	2.894	$5.0^{+0.6}_{-0.6}$	<180	<25	<200	$9.1^{+0.8}_{-0.8}$	$6.3^{+2.5}_{-2.5}$	135
084417.9+010415	1812	131.0748	+1.0711	26.0	94.6	0.340	2.586	$4.5^{+2.7}_{-2.7}$	45^{+12}_{-12}	131^{+37}_{-37}	$12.9^{+1.6}_{-1.6}$	$44^{+3.6}_{-3.6}$	$32.1^{+4.9}_{-4.9}$	1055
084430.8+021736	3541	131.1295	+2.935	27.5	79.3	0.050	5.678	$0.852^{+0.084}_{-0.084}$	$0.320^{+0.046}_{-0.046}$	$0.590^{+0.122}_{-0.122}$	$0.090^{+0.026}_{-0.028}$	$0.076^{+0.027}_{-0.028}$	$0.074^{+0.030}_{-0.029}$	1085
084443.3+031026	4876	131.1430	+3.1739	9.9	48.9	0.724	1.560	$2.05^{+0.89}_{-0.89}$	91^{+56}_{-56}	222^{+128}_{-128}	<22	$5.6^{+1.1}_{-1.1}$	$2.27^{+1.6}_{-1.6}$	1136
084443.5+041946	11610	131.1606	+4.3295	18.7	28.2	0.577	1.726	$4.2^{+1.4}_{-1.4}$	$34.9^{+7.2}_{-7.2}$	115^{+21}_{-21}	$10.5^{+2.1}_{-2.1}$	$4.9^{+1.0}_{-1.0}$	$27.6^{+3.2}_{-3.2}$	1315
084443.9+043302	5668	131.1625	+4.5507	11.9	47.6	0.517	1.839	$2.9^{+1.8}_{-1.8}$	$27.3^{+7.6}_{-7.6}$	79^{+19}_{-19}	$6.6^{+2.2}_{-2.2}$	$20.3^{+7.4}_{-7.4}$	$17.3^{+3.2}_{-3.2}$	1209
084444.1,3+021701	1778	131.1723	+2.2839	22.1	146.1	0.651	1.913	$6.2^{+1.4}_{-1.4}$	141^{+15}_{-15}	540^{+10}_{-10}	$26.5^{+3.9}_{-3.9}$	$15.9^{+6.5}_{-6.5}$	$7.7^{+3.1}_{-3.1}$	1064
084445.4+010021	4436	131.2253	+1.0059	17.1	59.7	0.295	2.314	$2.70^{+2.22}_{-2.22}$	$47.9^{+12.3}_{-12.3}$	$17.7^{+2.8}_{-2.8}$	$6.4^{+1.2}_{-1.2}$	$4.2^{+4.4}_{-4.4}$	$13.7^{+1.9}_{-1.9}$	160
084449.2-011902	4768	131.2471	-1.3174	48.2	93.5	0.447	2.517	$5.7^{+0.83}_{-0.83}$	$53.6^{+3.0}_{-3.0}$	$19.8^{+1.4}_{-1.4}$	$20.1^{+3.2}_{-3.2}$	$7.0^{+1.2}_{-1.2}$	$45.4^{+2.8}_{-2.8}$	1566
084501.0+012728	1607	131.2542	+1.4578	29.0	78.1	0.420	2.350	$3.08^{+0.91}_{-0.91}$	$58.2^{+8.4}_{-8.4}$	79^{+20}_{-20}	$16.1^{+3.8}_{-3.8}$	$5.0^{+1.7}_{-1.7}$	$14.0^{+3.4}_{-3.4}$	1127
084528.6+032759	144	131.3695	+3.4609	316.7	183.0	0.334	3.872	$6.7^{+1.0}_{-1.0}$	$219.0^{+0.90}_{-0.90}$	$49.9^{+3.6}_{-3.6}$	$6.7^{+1.6}_{-1.6}$	$33.5^{+8.7}_{-8.7}$	$14.9^{+0.6}_{-0.6}$	1093
084531.6+022831	1039	131.3818	+2.4753	98.9	275.7	0.076	6.064	$1.460^{+0.090}_{-0.090}$	$8.51^{+0.61}_{-0.61}$	$8.5^{+0.61}_{-0.61}$	$1.65^{+0.16}_{-0.16}$	$2.43^{+0.35}_{-0.35}$	$4.74^{+0.61}_{-0.61}$	1077
084544.3-002914	2214	131.4349	-0.4874	33.5	103.1	0.156	3.745	$2.31^{+0.83}_{-0.83}$	$13.0^{+3.4}_{-3.4}$	$32.4^{+3.7}_{-3.7}$	$4.78^{+0.49}_{-0.49}$	$11.1^{+1.8}_{-1.8}$	$2.17^{+0.97}_{-0.97}$	1021
084545.5+005535	3660	131.4384	+0.9265	10.7	49.2	0.293	2.122	$6.5^{+2.5}_{-2.5}$	$8.7^{+0.8}_{-0.8}$	<87	<44	<6.4	<33	
084552.4+011714	5804	131.4684	+1.2872	12.8	47.6	0.668	1.596	$4.0^{+2.5}_{-2.5}$	44^{+25}_{-25}	$130^{+7.8}_{-7.8}$	<18	$4.5^{+2.2}_{-2.2}$	<68	
084557.6+041103	25781	131.4901	+4.1843	13.2	13.0	0.284	2.432	$7.0^{+1.5}_{-1.5}$	$4.7^{+2.3}_{-2.3}$	$4.7^{+2.3}_{-2.3}$	<51	$6.9^{+0.6}_{-0.6}$	<45	
084558.1+012443	9771	131.4924	+1.4120	11.2	34.3	0.350	2.135	$3.3^{+0.7}_{-0.7}$	$18.1^{+3.8}_{-3.8}$	$5.8^{+1.6}_{-1.6}$	<130	$3.3^{+1.9}_{-1.9}$	$12.2^{+3.7}_{-3.7}$	1179
084559.7+031321	5281	131.4988	+3.1224	11.4	32.0	0.391	2.014	$4.4^{+1.2}_{-1.2}$	$2.34^{+1.4}_{-1.4}$	$32.4^{+3.4}_{-3.4}$	<74	$11.1^{+1.8}_{-1.8}$	$2.17^{+0.97}_{-0.97}$	1063
084607.6+000651	29318	131.5138	+0.1114	6.1	11.0	0.229	2.561	$0.47^{+0.73}_{-0.73}$	$5.7^{+0.8}_{-0.8}$	$20.3^{+7.0}_{-7.0}$	$3.6^{+1.4}_{-1.4}$	$1.65^{+32.45}_{-32.45}$	$17.2^{+7.9}_{-7.9}$	1060
084630.7+024702	13490	131.6281	+2.7839	8.4	18.8	0.206	2.353	$1.60^{+0.40}_{-0.40}$	$4.9^{+1.17}_{-1.17}$	$11.0^{+2.8}_{-2.8}$	$2.26^{+0.55}_{-0.55}$	$3.66^{+0.50}_{-0.50}$	$9.1^{+3.0}_{-2.3}$	1123
084637.1-002256	2987	131.6546	-0.3824	32.9	63.6	0.256	3.499	$4.5^{+0.5}_{-0.5}$	$14.0^{+1.9}_{-1.9}$	$48^{+2.4}_{-2.4}$	<11	$4.5^{+0.6}_{-0.6}$	<155	
084640.3-010423	9948	131.6681	-1.0733	8.8	19.7	0.244	2.261	$0.91^{+0.59}_{-0.59}$	$6.6^{+1.7}_{-1.7}$	$5.8^{+1.7}_{-1.7}$	<130	$2.55^{+2.41}_{-2.41}$	$19.8^{+1.6}_{-1.6}$	901
084645.6+014947	6215	131.6902	+1.8298	12.4	39.2	0.051	5.077	$2.51^{+0.86}_{-0.86}$	$9.0^{+0.12}_{-0.12}$	$24.1^{+0.12}_{-0.12}$	$0.51^{+0.06}_{-0.06}$	$1.32^{+1.02}_{-1.02}$	$0.76^{+0.32}_{-0.32}$	1173
084647.4+044607	6656	131.6975	+4.7688	19.6	58.7	0.245	3.468	$3.7^{+1.0}_{-1.0}$	$20.1^{+2.8}_{-2.8}$	61^{+36}_{-36}	$9.7^{+0.87}_{-0.87}$	$44^{+4.47}_{-4.47}$	$44^{+4.12}_{-4.12}$	531
084649.0+004946	11018	131.7045	+0.8295	17.1	58.7	0.269	2.426	$0.937^{+0.13}_{-0.13}$	$18.1^{+3.7}_{-3.7}$	$10.1^{+4.4}_{-4.4}$	$2.44^{+0.57}_{-0.57}$	$2.28^{+0.67}_{-0.67}$	$4.9^{+1.19}_{-1.19}$	1178
084655.7-002705	3712	131.7322	-0.6181	21.6	70.1	0.365	2.348	$2.49^{+0.43}_{-0.43}$	$9.0^{+0.37}_{-0.37}$	99^{+37}_{-37}	$10.1^{+0.93}_{-0.93}$	$2.40^{+0.84}_{-0.84}$	$9.1^{+3.0}_{-2.3}$	1043
084657.6-011314	9845	131.7403	-1.2206	6.6	21.4	0.804	1.370	$5.5^{+1.6}_{-1.6}$	45^{+20}_{-20}	167^{+77}_{-77}	$10.1^{+3.5}_{-3.$			

Table 4: continued.

Cluster (eFEDS I+)	ID_SRC	RA (deg)	Dec (deg)	\mathcal{L}_{ext}	\mathcal{L}_{ext} (deg)	R_{500} (arcmin)	T (keV)	L_X (10^{42} erg s $^{-1}$)	L_{bol} (10^{42} erg s $^{-1}$)	M_{gas} (10^{12} M $_{\odot}$)	Y_X (10^{12} M $_{\odot}$ keV)	T_{ex} (keV)	$L_{\text{bol,ex}}$ (10^{42} erg s $^{-1}$)	t_{exp} (s)		
084939.6-005126	2261	132.4151	-0.8573	29.0	108.8	0.613	2.004	$8.3^{+10.0}_{-3.8}$	121^{+19}_{-17}	540^{+300}_{-140}	$25.8^{+4.1}_{-3.4}$	210^{+280}_{-100}	$7.2^{+10.1}_{-3.5}$	380^{+230}_{-100}	868	
084957.4+004524	8524	132.4894	+0.7567	11.0	37.4	1.066	1.360	$14.0^{+10.8}_{-7.0}$	<360	<2300	<33	<760	$11.0^{+15.9}_{-6.7}$	<260	<1500	857
085018.3+020018	5464	132.5764	+2.0053	8.2	48.4	0.421	2.084	$4.3^{+1.0}_{-0.7}$	$3.3^{+1.0}_{-0.7}$	108^{+87}_{-63}	<15	<160	$7.7^{+5.2}_{-5.2}$	<97	<220	856
085020.4+032819	6529	132.5851	+3.4722	26.4	47.3	0.294	2.822	$4.4^{+7.7}_{-4.7}$	$19.0^{+1.6}_{-1.6}$	60^{+38}_{-13}	$7.2^{+1.7}_{-1.4}$	30^{+56}_{-12}	$13.4^{+3.0}_{-2.9}$	$4.2^{+1.5}_{-1.5}$	<43	965
085022.2+001607	8602	132.5927	+0.2687	13.4	18.2	0.196	3.001	$3.86^{+2.20}_{-1.87}$	$11.0^{+3.3}_{-3.3}$	34^{+13}_{-13}	$4.4^{+1.8}_{-1.4}$	$17.5^{+1.6}_{-1.5}$	$4.3^{+1.5}_{-1.5}$	$10.6^{+2.1}_{-2.1}$	$34^{+1.2}_{-1.2}$	862
085027.8+001503	1023	132.6160	+0.2509	128.7	280.4	0.197	4.560	$3.31^{+3.4}_{-1.87}$	$55.8^{+3.4}_{-3.4}$	155^{+15}_{-15}	$20.5^{+2.5}_{-2.5}$	68^{+13}_{-13}	$3.21^{+1.6}_{-1.6}$	$44.8^{+3.2}_{-3.2}$	125^{+13}_{-13}	860
085030.5+003330	6125	132.6272	+0.5584	29.2	62.1	0.192	3.291	$5.2^{+6.4}_{-6.4}$	$14.8^{+2.8}_{-2.8}$	52^{+32}_{-32}	$6.28^{+1.8}_{-1.8}$	32^{+14}_{-14}	$5.3^{+2.7}_{-2.7}$	$11.8^{+2.4}_{-2.4}$	$43^{+2.7}_{-2.7}$	852
085051.8+015331	8679	132.7161	+1.8921	9.8	22.0	0.268	2.270	$14.4^{+10.4}_{-7.7}$	$10.7^{+4.5}_{-4.5}$	61^{+39}_{-20}	$3.7^{+0.97}_{-0.97}$	<150	$14.2^{+20.0}_{-20.0}$	$2.05^{+1.35}_{-1.35}$	<94	862
085056.4+005607	3556	132.7354	+0.9553	9.9	83.5	0.295	2.459	$2.5^{+2.9}_{-2.9}$	$16.4^{+3.2}_{-3.2}$	42^{+14}_{-14}	$6.3^{+1.3}_{-1.3}$	<58	$2.53^{+0.59}_{-0.59}$	$13.4^{+3.9}_{-3.9}$	$25^{+7.8}_{-7.8}$	851
085119.9+022951	2101	132.8333	+2.4977	54.7	133.3	0.381	2.664	$2.25^{+1.54}_{-1.54}$	95^{+21}_{-21}	$23.3^{+2.9}_{-2.9}$	51^{+14}_{-14}	$22.7^{+3.2}_{-3.2}$	$70.9^{+1.2}_{-1.2}$	184^{+37}_{-37}	853	
085121.2+012836	11156	132.8384	+1.4825	10.2	25.2	0.327	2.217	$14.2^{+0.79}_{-0.79}$	$13.7^{+0.7}_{-0.7}$	78^{+27}_{-27}	$5.2^{+2.5}_{-2.5}$	51^{+12}_{-12}	$10.9^{+0.94}_{-0.94}$	$51^{+2.8}_{-2.8}$	860	
085128.4+011501	7355	132.8685	+1.2505	6.9	48.0	0.197	2.817	$9.6^{+5.1}_{-5.1}$	<3.0	<17	<2.9	<37	$7.0^{+4.55}_{-4.55}$	<2.3	<11	861
085130.0-004609	18314	132.8750	-0.7693	12.3	23.7	0.484	1.950	$1.78^{+0.72}_{-0.72}$	84^{+20}_{-20}	$11.3^{+2.3}_{-2.3}$	$20.3^{+9.1}_{-9.1}$	$53.6^{+2.1}_{-2.1}$	$2.05^{+1.35}_{-1.35}$	75^{+21}_{-21}	1010	
085131.0+045239	8633	132.8795	+4.8778	28.0	117.4	0.395	2.566	$2.39^{+3.9}_{-3.9}$	$31.1^{+6.6}_{-6.6}$	$94^{+12.9}_{-12.9}$	$14.8^{+1.9}_{-1.9}$	$35.8^{+16.0}_{-16.0}$	$2.57^{+0.59}_{-0.59}$	$74^{+11.2}_{-11.2}$	199^{+53}_{-53}	827
085138.2-003537	4508	132.9096	-0.5938	6.6	40.1	0.458	1.862	$16.2^{+1.0}_{-1.0}$	$11.0^{+6.6}_{-6.6}$	150^{+13}_{-13}	$1.4^{+0.7}_{-0.7}$	$12.0^{+2.5}_{-2.5}$	$15.7^{+6.4}_{-6.4}$	$87^{+6.0}_{-6.0}$	1007	
085141.9+021438	7280	132.9448	+2.440	9.1	39.3	0.107	3.689	$1.01^{+0.16}_{-0.16}$	<1.3	<2.6	<0.98	<1.0	$0.115^{+0.97}_{-0.97}$	<1.5	<1200000	859
085204.5+012132	6636	133.0188	+1.3590	27.9	54.1	0.401	2.530	$12.7^{+7.6}_{-7.6}$	$10.6^{+3.1}_{-3.1}$	238^{+129}_{-129}	$16.0^{+3.1}_{-3.1}$	<630	$12.3^{+7.4}_{-7.4}$	$33.7^{+7.4}_{-7.4}$	182^{+98}_{-98}	867
085217.0-010131	339	133.0709	-1.0254	209.0	405.9	0.460	3.097	$9.7^{+6.4}_{-6.4}$	$22.2^{+1.9}_{-1.9}$	11.20^{+270}_{-270}	$53.6^{+2.1}_{-2.1}$	520^{+370}_{-370}	163^{+380}_{-380}	$9.0^{+1.3}_{-1.3}$	1133	
085230.6+002457	2524	133.1275	+0.4159	64.5	140.4	0.270	3.364	$2.39^{+3.06}_{-3.06}$	$37.1^{+3.3}_{-3.3}$	$31.1^{+6.6}_{-6.6}$	$14.8^{+1.9}_{-1.9}$	$35.8^{+16.0}_{-16.0}$	$2.57^{+0.59}_{-0.59}$	$74^{+11.2}_{-11.2}$	967	
085231.1-011230	4810	133.1296	-1.2084	25.9	69.7	0.546	1.949	$6.3^{+3.4}_{-3.4}$	$50.8^{+3.6}_{-3.6}$	150^{+23}_{-23}	$1.4^{+0.8}_{-0.8}$	$48^{+5.7}_{-5.7}$	$12.8^{+4.8}_{-4.8}$	$36.4^{+7.8}_{-7.8}$	1172	
085239.6+003240	5477	133.1652	+0.5446	11.6	44.6	0.452	1.921	$4.0^{+1.7}_{-1.7}$	$31.9^{+7.6}_{-7.6}$	99^{+39}_{-39}	$8.9^{+2.9}_{-2.9}$	30^{+26}_{-26}	$22.4^{+5.6}_{-5.6}$	67^{+37}_{-37}	968	
085245.7-020519	5790	133.1905	-2.0888	8.2	44.6	0.761	1.497	$2.40^{+2.07}_{-2.07}$	64^{+22}_{-22}	175^{+65}_{-65}	<18	<74	$3.4^{+10.4}_{-10.4}$	<78	<240	862
085255.1-013737	1376	133.2297	-1.6271	7.4	14.9	0.343	0.586	$4.9^{+1.9}_{-1.9}$	$5.3^{+1.7}_{-1.7}$	$18.7^{+8.8}_{-8.8}$	$0.51^{+0.23}_{-0.23}$	<14	$3.7^{+6.8}_{-6.8}$	$5.0^{+1.5}_{-1.5}$	1668	
085256.8+002741	6642	133.2370	+5.4615	8.2	29.0	0.273	2.401	$10.8^{+2.46}_{-2.46}$	$8.4^{+2.19}_{-2.19}$	41^{+16}_{-16}	$1.43^{+0.83}_{-0.83}$	<65	$7.1^{+3.2}_{-3.2}$	$2.57^{+0.72}_{-0.72}$	<39	545
085323.0-002130	9042	133.3570	+3.1430	7.1	29.7	0.335	2.074	$6.3^{+1.57}_{-1.57}$	$8.5^{+1.88}_{-1.88}$	28^{+21}_{-21}	$1.83^{+0.68}_{-0.68}$	<57	$8.7^{+3.6}_{-3.6}$	$7.0^{+2.2}_{-2.2}$	<52	862
085327.2-002117	6003	133.3634	-0.5549	17.5	52.7	0.193	2.894	$4.0^{+1.67}_{-1.67}$	$7.5^{+1.3}_{-1.3}$	$31.9^{+7.6}_{-7.6}$	$3.61^{+1.98}_{-1.98}$	90^{+39}_{-39}	$3.61^{+1.98}_{-1.98}$	$22.4^{+8.5}_{-8.5}$	61^{+14}_{-14}	1171
085335.2+032214	8596	133.3967	+3.3708	33.7	86.7	0.295	2.421	$12.6^{+3.1}_{-3.1}$	$10.6^{+2.7}_{-2.7}$	57^{+38}_{-38}	$4.8^{+1.5}_{-1.5}$	<14	$3.7^{+6.8}_{-6.8}$	$5.0^{+1.5}_{-1.5}$	1668	
085345.5+014038	8094	133.4191	+2.4032	31.2	48.5	0.196	3.367	$1.73^{+1.39}_{-1.39}$	$7.8^{+1.1}_{-1.1}$	$18.1^{+8.5}_{-8.5}$	$3.93^{+0.85}_{-0.85}$	<65	$7.1^{+3.2}_{-3.2}$	$1.5^{+0.46}_{-0.46}$	1666	
085346.6+003835	3298	133.6526	+0.6431	242.8	688.6	0.106	6.414	$2.68^{+0.43}_{-0.43}$	$2.68^{+0.43}_{-0.43}$	51.0^{+35}_{-35}	$10.8^{+2.1}_{-2.1}$	$31.7^{+4.7}_{-4.7}$	$6.5^{+1.2}_{-1.2}$	$7.6^{+1.6}_{-1.6}$	303^{+25}_{-25}	312
085412.8-021223	1458	133.5536	-2.3566	12.7	61.0	0.377	3.233	$8.1^{+1.2}_{-1.2}$	$11.8^{+1.6}_{-1.6}$	$11.8^{+1.6}_{-1.6}$	$10.8^{+4.2}_{-4.2}$	<1000	$6.5^{+1.2}_{-1.2}$	$7.6^{+1.6}_{-1.6}$	1175	
085419.5-000925	1294	133.5814	-0.1572	56.0	110.0	0.282	3.324	$1.83^{+1.43}_{-1.43}$	$4.7^{+1.3}_{-1.3}$	$47.1^{+1.3}_{-1.3}$	$4.7^{+1.3}_{-1.3}$	$16.8^{+4.2}_{-4.2}$	$31.4^{+8.7}_{-8.7}$	$82.9^{+8.7}_{-8.7}$	1196	
085433.0+004009	3675	133.6376	+0.6693	10.3	46.5	0.109	3.078	$7.2^{+1.3}_{-1.3}$	$6.3^{+1.3}_{-1.3}$	$1.68^{+0.86}_{-0.86}$	<0.33	<0.87	$2.60^{+0.42}_{-0.42}$	$23.8^{+18.9}_{-18.9}$	1166	
085434.5-014038	8094	133.6438	-1.6731	13.6	38.7	0.595	1.698	$1.81^{+0.88}_{-0.88}$	$1.81^{+0.88}_{-0.88}$	47^{+29}_{-29}	$5.2^{+1.7}_{-1.7}$	<190	$12.7^{+11.2}_{-11.2}$	$3.8^{+1.2}_{-1.2}$	$38^{+2.8}_{-2.8}$	854
085436.6+003835	3298	133.6526	+0.6431	242.8	688.6	0.106	6.414	$2.68^{+0.43}_{-0.43}$	$2.68^{+0.43}_{-0.43}$	50.4^{+26}_{-26}	$10.7^{+1.8}_{-1.8}$	$8.13^{+0.97}_{-0.97}$	$21.9^{+7.8}_{-7.8}$	$2.45^{+0.89}_{-0.89}$	$12.50^{+20.0}_{-20.0}$	883
085438.5+001211	5390	133.6608	+0.2032	6.2	21.4	0.178	3.375	$2.1^{+1.8}_{-1.8}$	$2.1^{+1.8}_{-1.8}$	$11.8^{+1.6}_{-1.6}$	$1.4^{+0.8}_{-0.8}$	<29	$2.38^{+0.49}_{-0.49}$	<14	1199	
085440.4-020931	7700	133.6686	-2.1588	7.0	32.4	0.472	1.787	$5.8^{+1.86}_{-1.86}$	$13.0^{+1.4}_{-1.4}$	50.3^{+53}_{-53}	$3.1^{+1.7}_{-1.7}$	<140	$5.0^{+1.7}_{-1.7}$	$14.0^{+2.7}_{-2.7}$	<72	967
085447.0-012132	1797	133.6962	-1.3591	81.5	153.9	0.333	3.015	$1.99^{+1.35}_{-1.35}$	$5.75^{+1.25}_{-1.25}$	177^{+25}_{-25}	$19.5^{+1.4}_{-1.4}$	$39.0^{+8.1}_{-8.1}$	$2.05^{+0.95}_{-0.95}$	$43.8^{+4.6}_{-4.6}$	107^{+15}_{-15}	1204
085508.9-003445	2810	133.7874	+3.4687	9.2	103.6	0.174	2.974	$1.29^{+1.35}_{-1.35}$	$1.29^{+1.35}_{-1.35}$	$10.4^{+1.3}_{-1.3}$	<1.6	<28	$12.0^{+1.5}_{-1.5}$	<3.0	1201	
085517.2+013508	6746	133.9279	+1.5887	36.4	55.0	0.324	2.548	$2.40^{+0.63}_{-0.63}$	$2.40^{+0.$							

Table 4: continued.

Cluster	ID_SRC	RA (deg)	Dec (deg)	\mathcal{L}_{ext}	\mathcal{L}_{ext}	R_{500} (arcmin)	T (keV)	L_X (10^{42} erg s $^{-1}$)	L_{bol} (10^{42} erg s $^{-1}$)	M_{gas} (10^{12} M $_{\odot}$)	Y_X (10^{12} M $_{\odot}$ keV)	T_{ex} (keV)	$L_{\text{bol,ex}}$ (10^{42} erg s $^{-1}$)	t_{exp} (s)		
(eFEDS I+)																
085744.0-022448	12696	134.4337	-2.4134	9.3	20.1	0.162	2.803	1.27 $^{+0.53}_{-0.23}$	1.98 $^{+0.61}_{-0.48}$	1.36 $^{+0.37}_{-0.36}$	1.71 $^{+0.07}_{-0.23}$	1.30 $^{+0.47}_{-0.50}$	3.6 $^{+1.2}_{-1.2}$	1859		
085751.6+031039	108	134.4633	+3.1775	742.2	2053.9	0.201	6.278	5.68 $^{+0.37}_{-0.30}$	163.0 $^{+0.60}_{-0.50}$	590 $^{+1.00}_{-0.75}$	49.3 $^{+0.70}_{-0.60}$	5.13 $^{+0.57}_{-0.63}$	106.0 $^{+0.50}_{-0.50}$	367 $^{+55}_{-55}$	1204	
085801.1-004103	11717	134.5038	-0.6842	12.4	2.479	0.245	2.479	1.02 $^{+0.69}_{-0.60}$	11.6 $^{+1.58}_{-1.50}$	11.6 $^{+1.58}_{-1.50}$	2.85 $^{+0.22}_{-0.22}$	2.89 $^{+0.22}_{-0.22}$	9.2 $^{+3.38}_{-3.38}$	4.45 $^{+1.66}_{-1.66}$	1203	
085805.0+010906	4070	134.5209	+1.1517	90.8	0.071	5.196	2.59 $^{+1.23}_{-1.20}$	2.74 $^{+1.30}_{-1.30}$	6.9 $^{+1.43}_{-1.43}$	1.31 $^{+0.28}_{-0.28}$	3.4 $^{+1.18}_{-1.18}$	1.79 $^{+0.36}_{-0.36}$	2.13 $^{+0.08}_{-0.08}$	4.83 $^{+0.33}_{-0.33}$	1206	
085830.0-010656	4297	134.6251	-1.1157	19.5	70.5	0.224	2.902	5.1 $^{+0.74}_{-0.74}$	9.1 $^{+1.01}_{-0.98}$	31.2 $^{+2.8}_{-2.8}$	4.97 $^{+0.36}_{-0.36}$	24 $^{+6.65}_{-6.65}$	7.3 $^{+0.94}_{-0.94}$	31 $^{+20}_{-10}$	31 $^{+20}_{-10}$	1912
085837.9+012657	8857	134.6581	+1.4494	7.8	18.9	0.750	1.403	2.8 $^{+2.5}_{-2.5}$	<47	<140	9.2 $^{+1.4}_{-1.4}$	2.7 $^{+0.73}_{-0.73}$	7.5 $^{+0.65}_{-0.65}$	24 $^{+12}_{-12}$	31 $^{+10}_{-10}$	1198
085841.8-020541	2367	134.6744	-2.0948	15.5	42.0	0.575	1.555	1.47 $^{+0.67}_{-0.67}$	32.5 $^{+7.1}_{-7.1}$	73 $^{+16}_{-14}$	7.4 $^{+1.6}_{-1.4}$	11.0 $^{+0.56}_{-0.56}$	22.9 $^{+6.7}_{-6.7}$	53 $^{+16}_{-16}$	2301	
085849.8+022800	715	134.7076	+2.4668	92.3	304.5	0.215	3.648	1.76 $^{+0.77}_{-0.77}$	29.3 $^{+8.9}_{-8.9}$	67.5 $^{+1.92}_{-1.92}$	9.8 $^{+1.8}_{-1.8}$	17.2 $^{+3.4}_{-2.9}$	1.65 $^{+0.30}_{-0.30}$	16.9 $^{+5.6}_{-5.6}$	38.4 $^{+5.9}_{-5.9}$	1207
085901.1-012025	3527	134.7547	-1.3406	30.1	1.301	0.239	10.9 $^{+0.45}_{-0.45}$	147 $^{+4.80}_{-4.80}$	720 $^{+30}_{-30}$	19.3 $^{+3.4}_{-3.4}$	<50	17.3 $^{+0.71}_{-0.71}$	1.22 $^{+0.69}_{-0.69}$	760 $^{+20}_{-20}$	2238	
085901.5+010649	2757	134.7564	+1.1137	33.6	97.4	0.162	3.365	2.79 $^{+5.53}_{-5.53}$	5.55 $^{+0.92}_{-0.92}$	15.4 $^{+2.5}_{-2.5}$	2.36 $^{+0.71}_{-0.71}$	7.0 $^{+2.4}_{-2.4}$	3.4 $^{+0.92}_{-0.92}$	11.2 $^{+2.6}_{-2.6}$	1208	
085907.3-005056	16320	134.7808	-0.8489	7.3	11.6	0.623	1.689	11.5 $^{+0.76}_{-0.76}$	26.3 $^{+2.95}_{-2.95}$	144 $^{+2.85}_{-2.85}$	9.0 $^{+0.49}_{-0.49}$	<340	10.2 $^{+1.57}_{-1.57}$	25.5 $^{+6.6}_{-6.6}$	130 $^{+32}_{-32}$	1989
085913.1+031334	485	134.8048	+3.2263	15.9	16.8	0.189	2.980	2.34 $^{+2.5}_{-2.5}$	13.1 $^{+2.8}_{-2.8}$	34.1 $^{+1.51}_{-1.51}$	3.79 $^{+0.74}_{-0.74}$	9.2 $^{+1.21}_{-1.21}$	1.78 $^{+0.84}_{-0.84}$	15.6 $^{+4.9}_{-4.9}$	1210	
085931.9+030839	360	134.8830	+3.1443	175.1	617.4	0.196	4.648	2.50 $^{+2.33}_{-2.33}$	41.3 $^{+2.33}_{-2.33}$	106.0 $^{+0.66}_{-0.66}$	14.4 $^{+0.66}_{-0.66}$	36.0 $^{+3.9}_{-3.9}$	24.8 $^{+2.10}_{-2.10}$	65.1 $^{+9.2}_{-9.2}$	1211	
085939.1-004932	6894	134.9133	-0.8258	10.9	8.2	0.812	1.369	1.24 $^{+0.36}_{-0.36}$	63.3 $^{+3.8}_{-3.8}$	138 $^{+6.6}_{-6.6}$	11.8 $^{+1.1}_{-1.1}$	14.3 $^{+0.64}_{-0.64}$	1.22 $^{+0.61}_{-0.61}$	124 $^{+4.4}_{-4.4}$	2238	
085948.9+041120	1350	134.9539	+4.1889	22.6	43.0	0.208	3.177	1.69 $^{+0.45}_{-0.45}$	31.6 $^{+4.48}_{-4.48}$	4.84 $^{+0.80}_{-0.80}$	4.8 $^{+2.6}_{-2.6}$	7.8 $^{+1.7}_{-1.7}$	1.58 $^{+0.45}_{-0.45}$	17.8 $^{+3.9}_{-3.9}$	1212	
085950.1-001221	4539	134.9589	-0.2058	16.9	35.1	0.427	0.494	5.1 $^{+0.76}_{-0.76}$	11.8 $^{+3.0}_{-3.0}$	41 $^{+2.2}_{-2.2}$	0.73 $^{+0.63}_{-0.63}$	<15	13.7 $^{+0.82}_{-0.82}$	61 $^{+33}_{-33}$	1306	
085954.2-013308	13823	134.9738	-1.5524	6.5	16.4	0.577	1.464	10.2 $^{+2.61}_{-2.61}$	15.6 $^{+0.66}_{-0.66}$	76 $^{+3.8}_{-3.8}$	5.4 $^{+0.54}_{-0.54}$	<60	8.8 $^{+1.94}_{-1.94}$	<12	2033	
090004.3+033324	7945	135.0183	+3.5568	11.8	30.8	0.698	1.570	1.65 $^{+0.76}_{-0.76}$	41.3 $^{+2.33}_{-2.33}$	106.0 $^{+0.66}_{-0.66}$	14.4 $^{+0.66}_{-0.66}$	36.0 $^{+3.9}_{-3.9}$	37.9 $^{+1.52}_{-1.52}$	151 $^{+114}_{-114}$	1203	
090010.4+026361	10878	135.0435	+2.6086	12.9	23.6	0.200	2.781	2.29 $^{+2.92}_{-2.92}$	11.7 $^{+3.8}_{-3.8}$	4.59 $^{+0.93}_{-0.93}$	2.69 $^{+0.78}_{-0.78}$	2.69 $^{+0.78}_{-0.78}$	3.1 $^{+2.57}_{-2.57}$	10.5 $^{+5.7}_{-5.7}$	1211	
090020.8-002602	1315	135.0867	-0.4340	17.9	184.8	0.490	0.991	2.96 $^{+3.38}_{-3.38}$	<41	<120	<12	<50	<25	<89	1476	
090033.7+033932	2407	135.1221	+3.9591	25.2	19.6	0.809	1.690	3.5 $^{+0.74}_{-0.74}$	73 $^{+29}_{-29}$	225 $^{+9.9}_{-9.9}$	17.3 $^{+4.9}_{-4.9}$	59 $^{+4.3}_{-4.3}$	3.0 $^{+0.88}_{-0.88}$	68 $^{+27}_{-27}$	198 $^{+78}_{-78}$	1207
090034.1-010649	1652	135.1422	-1.1137	15.4	29.8	0.273	2.651	2.94 $^{+1.90}_{-1.90}$	11.1 $^{+2.8}_{-2.8}$	30.2 $^{+8.7}_{-8.7}$	5.94 $^{+0.85}_{-0.85}$	17.4 $^{+2.12}_{-2.12}$	9.1 $^{+1.52}_{-1.52}$	26.0 $^{+9.9}_{-9.9}$	3253	
090044.6-011104	8508	135.1862	-1.1845	8.1	6.3	0.430	1.825	16.5 $^{+0.88}_{-0.88}$	3.0 $^{+1.32}_{-1.32}$	19.4 $^{+1.67}_{-1.67}$	16.4 $^{+0.95}_{-0.95}$	3.1 $^{+0.54}_{-0.54}$	55.8 $^{+24}_{-24}$	15.1 $^{+114}_{-114}$	1203	
090051.6-003457	9834	135.2152	-0.5826	6.0	13.7	0.350	1.787	3.2 $^{+0.41}_{-0.41}$	7.5 $^{+1.3}_{-1.3}$	22.3 $^{+3.6}_{-3.6}$	3.53 $^{+0.89}_{-0.89}$	11.4 $^{+1.55}_{-1.55}$	1.4 $^{+0.57}_{-0.57}$	20.5 $^{+13.9}_{-13.9}$	1585	
090053.0-002837	9310	135.2212	-0.4777	15.8	27.0	0.295	2.190	1.21 $^{+0.19}_{-0.19}$	7.2 $^{+1.9}_{-1.9}$	15.0 $^{+0.94}_{-0.94}$	3.97 $^{+0.94}_{-0.94}$	3.6 $^{+0.86}_{-0.86}$	11.0 $^{+3.57}_{-3.57}$	11.0 $^{+3.57}_{-3.57}$	1571	
090059.3+035925	983	135.2471	+3.9905	43.2	230.7	0.412	2.490	11.0 $^{+0.90}_{-0.90}$	27.5 $^{+1.91}_{-1.91}$	49.8 $^{+8.8}_{-8.8}$	25.7 $^{+10.0}_{-10.0}$	11.9 $^{+2.6}_{-2.6}$	12.6 $^{+5.1}_{-5.1}$	130 $^{+85}_{-85}$	1202	
090104.4+011643	3171	135.2686	+1.2788	38.0	62.8	0.251	3.247	2.75 $^{+1.91}_{-1.91}$	19.2 $^{+2.17}_{-2.17}$	51.1 $^{+1.12}_{-1.12}$	8.2 $^{+1.2}_{-1.2}$	5.94 $^{+0.82}_{-0.82}$	2.27 $^{+0.59}_{-0.59}$	14.3 $^{+1.58}_{-1.58}$	1230	
090105.2-012525	11836	135.2718	-1.4237	17.8	29.4	0.405	2.178	8.2 $^{+0.89}_{-0.89}$	18.0 $^{+2.3}_{-2.3}$	79 $^{+5}_{-5}$	9.0 $^{+1.3}_{-1.3}$	<300	7.6 $^{+3.19}_{-3.19}$	68 $^{+19}_{-19}$	2274	
090115.3+005040	8881	135.3140	+0.8445	10.1	28.9	0.312	2.077	2.39 $^{+0.02}_{-0.02}$	3.1 $^{+1.0}_{-1.0}$	3.12 $^{+0.21}_{-0.21}$	39.4 $^{+4.5}_{-4.5}$	13.8 $^{+6.5}_{-6.5}$	37.7 $^{+11.6}_{-11.6}$	13.1 $^{+2.7}_{-2.7}$	1371	
090119.0+032024	70117	135.3294	+3.0345	24.7	22.7	0.193	2.660	4.3 $^{+0.52}_{-0.52}$	<9.4	<33	<23	4.1 $^{+1.53}_{-1.53}$	<8.0	<30	1203	
090121.9-003709	16040	135.3414	-0.6194	9.8	24.8	0.555	1.778	15.5 $^{+0.76}_{-0.76}$	15.5 $^{+0.76}_{-0.76}$	36.8 $^{+8.3}_{-8.3}$	9.7 $^{+2.28}_{-2.28}$	9.7 $^{+2.28}_{-2.28}$	<350	<350	1611	
090129.1-013853	1104	135.3715	-1.6483	86.6	274.4	0.311	3.794	6.1 $^{+0.98}_{-0.98}$	167 $^{+1.43}_{-1.43}$	63.0 $^{+20}_{-20}$	44.9 $^{+5.2}_{-5.2}$	271 $^{+20}_{-20}$	8.3 $^{+7.92}_{-7.92}$	135.0 $^{+8.80}_{-8.80}$	967	
090131.1+030056	152	135.3800	+3.0157	37.3	1266.7	0.193	5.184	4.12 $^{+1.02}_{-1.02}$	71.3 $^{+2.05}_{-2.05}$	219 $^{+28}_{-28}$	23.1 $^{+4.8}_{-4.8}$	95 $^{+27}_{-27}$	4.20 $^{+3.88}_{-3.88}$	45.8 $^{+5.4}_{-5.4}$	145 $^{+26}_{-26}$	1210
090133.2+021651	4181	135.3886	+2.2809	28.2	31.2	0.354	2.168	3.1 $^{+0.98}_{-0.98}$	56 $^{+18}_{-18}$	56 $^{+18}_{-18}$	4.7 $^{+1.5}_{-1.5}$	24.6 $^{+3.0}_{-3.0}$	16.3 $^{+2.7}_{-2.7}$	53 $^{+13}_{-13}$	1210	
090153.9-012209	10870	135.3898	-1.0946	11.8	28.3	0.270	2.016	2.42 $^{+0.02}_{-0.02}$	3.80 $^{+0.24}_{-0.24}$	10.2 $^{+1.39}_{-1.39}$	1.92 $^{+0.39}_{-0.39}$	4.7 $^{+0.75}_{-0.75}$	2.39 $^{+2.36}_{-2.36}$	13.6 $^{+2.9}_{-2.9}$	2016	
090200.5+023359	3800	135.5024	+2.3943	6.4	11.0	0.188	2.730	3.222	13.6 $^{+1.36}_{-1.36}$	<64	<470	<45	<10	27.5 $^{+2.5}_{-2.5}$	1211	
090210.9-012132	2412	135.5420	-4.6767	20.4	43.8	0.295	1.912	3.1 $^{+0.80}_{-0.80}$	13.8 $^{+2.29}_{-2.29}$	389 $^{+8.4}_{-8.4}$	<4.3	<60	<23	1205		
090223.3+015205	6840	135.5974	+1.8682	6.7	43.2	0.561	1.657	1.61 $^{+0.45}_{-0.45}$	13.8 $^{+2.38}_{-2.38}$	69 $^{+20}_{-20}$	5.0 $^{+0.17}_{-0.17}$	<60	<11	1376		
090224																

Table 4: continued.

Cluster (eFEDS I+)	ID_SRC	RA (deg)	Dec (deg)	\mathcal{L}_{ext}	\mathcal{L}_{ext} (deg)	R_{500} (arcmin)	T (keV)	L_X (10^{42} erg s $^{-1}$)	L_{bol} (10^{42} erg s $^{-1}$)	M_{gas} (10^{12} M $_{\odot}$)	Y_X (10^{12} M $_{\odot}$ keV)	T_{ex} (keV)	$L_{\text{bol,ex}}$ (10^{42} erg s $^{-1}$)	t_{exp} (s)			
090409.7+003831	9877	136.0404	+0.6421	12.2	18.6	0.311	2.644	$2.79^{+0.93}_{-0.87}$	$13.1^{+2.0}_{-1.9}$	$35.5^{+9.8}_{-8.7}$	$7.2^{+1.2}_{-1.1}$	$20.5^{+14.6}_{-6.9}$	$2.2^{+2.6}_{-1.3}$	$10.7^{+1.8}_{-1.8}$	$26.0^{+10.5}_{-5.9}$	1400	
090417.0+040439	13330	136.0712	+4.0776	10.9	19.8	0.536	1.819	$12.7^{+0.87}_{-0.81}$	$43.8^{+6.3}_{-5.3}$	$23.7^{+1.5}_{-1.4}$	$13.6^{+2.6}_{-2.6}$	< 510	$14.3^{+12.3}_{-8.2}$	$38.9^{+5.2}_{-3.2}$	226^{+116}_{-78}	1341	
090418.6+020642	3590	136.0778	+2.1117	32.9	78.5	0.808	1.611	$3.8^{+1.3}_{-1.2}$	$124^{+8.9}_{-8.0}$	$37.5^{+1.5}_{-1.4}$	$20.0^{+2.6}_{-2.6}$	77^{+38}_{-32}	278^{+57}_{-57}	95^{+19}_{-19}	278^{+57}_{-57}	1595	
090419.1-010436	12660	136.0796	-1.0767	13.6	23.6	0.306	2.266	$2.2^{+1.7}_{-1.7}$	$22.0^{+1.6}_{-1.6}$	$4.1^{+1.0}_{-1.0}$	< 47	$3.2^{+0.2}_{-0.2}$	$6.6^{+2.0}_{-2.0}$	$19.8^{+18.0}_{-7.4}$	1537		
090430.7+0242648	1075	136.1282	+4.4468	37.7	209.8	0.457	2.308	$5.9^{+1.0}_{-0.9}$	$59.0^{+2.0}_{-2.0}$	$21.7^{+1.7}_{-1.7}$	$11.7^{+2.3}_{-2.3}$	$66^{+11.2}_{-20}$	$7.1^{+1.8}_{-1.8}$	$23.6^{+5.4}_{-5.4}$	98^{+65}_{-65}	1192	
090452.4+033326	2931	136.2187	+3.5574	18.8	66.3	0.808	1.677	$4.2^{+1.6}_{-1.6}$	$159^{+2.2}_{-2.2}$	$522^{+1.5}_{-1.5}$	$26.0^{+3.9}_{-3.9}$	$11.0^{+2.0}_{-2.0}$	$7.1^{+1.8}_{-1.8}$	428^{+81}_{-81}	$131^{+3.7}_{-3.7}$	1490	
090540.0+043440	354	136.4171	+4.5780	231.4	678.2	0.236	4.608	$3.73^{+0.79}_{-0.77}$	$93.3^{+3.1}_{-3.1}$	$274^{+2.4}_{-2.4}$	$25.9^{+2.4}_{-2.4}$	$139^{+17.2}_{-17.2}$	$95^{+12.3}_{-12.3}$	$3.46^{+1.0}_{-1.0}$	$58.8^{+4.2}_{-3.8}$	$171^{+1.3}_{-1.3}$	1048
090540.7+013219	3585	136.4199	+1.5388	28.1	79.6	0.644	1.973	$6.2^{+0.9}_{-0.9}$	$96^{+1.7}_{-1.7}$	$366^{+1.8}_{-1.8}$	$22.9^{+3.5}_{-3.5}$	< 47	$5.9^{+1.7}_{-1.7}$	76^{+17}_{-17}	285^{+193}_{-193}	1273	
090553.5+002244	5170	136.4732	+0.3791	10.8	69.4	0.367	2.168	$14.6^{+1.8}_{-1.8}$	$58^{+1.6}_{-1.6}$	$5.7^{+1.0}_{-1.0}$	< 240	$18^{+1.6}_{-1.6}$	$8.9^{+1.6}_{-1.6}$	$5.9^{+1.6}_{-1.6}$	1517		
090600.3-002521	9359	136.5016	-0.4226	18.7	0.299	0.299	2.507	$2.25^{+0.86}_{-0.86}$	$29.6^{+6.2}_{-6.2}$	$4.4^{+1.4}_{-1.4}$	$1.8^{+1.6}_{-1.6}$	$1.82^{+0.61}_{-0.61}$	$18.8^{+5.4}_{-5.4}$	$1.82^{+0.61}_{-0.61}$	1212		
090601.0+000055	3259	136.5043	+0.0154	18.6	92.2	0.200	2.876	$2.63^{+0.94}_{-0.94}$	$12.5^{+2.0}_{-2.0}$	$32.9^{+6.5}_{-6.5}$	$4.83^{+0.82}_{-0.82}$	$12.9^{+6.6}_{-6.6}$	$2.13^{+0.99}_{-0.99}$	$9.9^{+1.4}_{-1.4}$	$24.6^{+1.7}_{-1.7}$	1208	
090609.4+042924	11420	136.5392	+4.4901	7.8	19.4	0.406	2.010	$4.9^{+1.0}_{-1.0}$	$17.4^{+1.9}_{-1.9}$	$7.1^{+1.4}_{-1.4}$	60^{+16}_{-16}	$7.1^{+1.5}_{-1.5}$	$14.3^{+3.5}_{-3.5}$	$3.8^{+1.7}_{-1.7}$	44^{+18}_{-18}	1286	
090614.6-010819	5854	136.5612	-1.1389	16.9	15.5	0.894	1.602	$14.8^{+1.7}_{-1.7}$	80^{+24}_{-24}	490^{+20}_{-20}	< 680	$8.5^{+1.7}_{-1.7}$	< 110	< 600	1521		
090627.5+035846	10162	136.6148	+3.9795	7.4	24.6	0.463	2.032	$3.1^{+1.6}_{-1.6}$	$58^{+1.7}_{-1.7}$	$7.6^{+2.2}_{-2.2}$	$24.1^{+2.9}_{-2.9}$	$7.2^{+2.4}_{-2.4}$	$19.5^{+5.3}_{-5.3}$	$16.8^{+2.4}_{-2.4}$	1634		
090628.9-012938	2424	136.6207	-1.9441	46.1	119.0	0.431	2.235	$3.10^{+1.4}_{-1.4}$	$40.2^{+1.7}_{-1.7}$	$125^{+3.2}_{-3.2}$	$14.0^{+1.8}_{-1.8}$	$4.4^{+1.7}_{-1.7}$	$9.8^{+1.8}_{-1.8}$	$9.8^{+1.8}_{-1.8}$	2120		
090634.9+045033	8384	136.6454	+4.8427	10.6	42.7	0.884	1.605	$4.4^{+0.78}_{-0.78}$	$16.3^{+1.6}_{-1.6}$	$163^{+1.5}_{-1.5}$	$24.6^{+5.6}_{-5.6}$	$10.8^{+2.0}_{-2.0}$	$12.3^{+3.8}_{-3.8}$	420^{+110}_{-110}	695		
090636.9+010832	7086	136.6542	+1.1479	29.6	53.7	0.786	1.723	$7.1^{+1.3}_{-1.3}$	$91^{+1.3}_{-1.3}$	$370^{+1.3}_{-1.3}$	$20.9^{+9.6}_{-9.6}$	< 660	$5.0^{+2.6}_{-2.6}$	$5.0^{+2.6}_{-2.6}$	271^{+189}_{-189}	1214	
090644.8+011124	5858	136.6867	+1.1902	9.8	60.3	0.441	1.919	$4.6^{+1.4}_{-1.4}$	$17.3^{+1.8}_{-1.8}$	$58^{+1.6}_{-1.6}$	< 8.8	< 66	$9.4^{+1.6}_{-1.6}$	$9.4^{+1.6}_{-1.6}$	141^{+13}_{-13}	1209	
090656.3+044717	12153	136.7347	+4.7882	29.0	32.2	0.120	4.349	$1.70^{+2.1}_{-2.1}$	$8.1^{+0.95}_{-0.95}$	$18.6^{+2.6}_{-2.6}$	$4.23^{+0.75}_{-0.75}$	$4.23^{+0.75}_{-0.75}$	$1.64^{+0.47}_{-0.47}$	$19.5^{+5.3}_{-5.3}$	$7.38^{+0.81}_{-0.81}$	864	
090700.7+011032	9463	136.7531	+1.1737	10.3	23.1	0.799	1.391	$4.6^{+1.5}_{-1.5}$	$13.7^{+1.5}_{-1.5}$	$137^{+1.5}_{-1.5}$	< 16	< 180	$1.3^{+0.8}_{-0.8}$	$1.3^{+0.8}_{-0.8}$	< 250	1216	
090703.9+010756	13484	136.7827	+3.8829	23.3	50.3	0.729	1.691	$13.0^{+1.25}_{-1.25}$	$7.1^{+1.4}_{-1.4}$	400^{+210}_{-210}	$17.5^{+3.0}_{-3.0}$	700	$11.5^{+5.7}_{-5.7}$	58^{+14}_{-14}	300^{+100}_{-100}	1464	
090718.6+035258	6439	136.8275	+2.7791	7.5	21.1	0.618	1.507	$2.31^{+0.84}_{-0.84}$	$2.38^{+1.75}_{-1.75}$	$15.7^{+1.7}_{-1.7}$	$39.1^{+1.3}_{-1.3}$	$6.84^{+0.99}_{-0.99}$	$16.0^{+6.7}_{-6.7}$	$11.9^{+1.7}_{-1.7}$	$30.5^{+7.0}_{-7.0}$	1685	
090723.8-012110	2680	136.8494	-1.2029	32.5	107.9	0.251	2.855	$2.15^{+0.48}_{-0.48}$	< 72	< 200	< 11	< 45	< 47	< 150	2000	2000	
090734.3-012744	13028	136.8930	-1.4625	10.2	20.0	0.922	2.034	$2.15^{+0.97}_{-0.97}$	$4.46^{+0.90}_{-0.90}$	$8.6^{+2.0}_{-2.0}$	$1.81^{+0.52}_{-0.52}$	$1.76^{+0.59}_{-0.59}$	$1.76^{+0.59}_{-0.59}$	$1.3^{+0.53}_{-0.53}$	$2.97^{+1.07}_{-1.07}$	1207	
090739.7-010633	10976	136.9157	+1.094	6.5	23.1	0.307	2.121	$7.2^{+2.62}_{-2.62}$	< 4.4	< 21	< 17	< 19	< 9.1	< 9.1	1212		
090750.1+025006	4691	136.9591	+2.8851	22.6	54.0	0.468	1.738	$6.6^{+1.05}_{-1.05}$	$7.0^{+1.06}_{-1.06}$	$273^{+1.06}_{-1.06}$	$16.4^{+2.0}_{-2.0}$	$16.4^{+2.0}_{-2.0}$	$1.7^{+0.53}_{-0.53}$	$8.7^{+1.8}_{-1.8}$	$55.5^{+8.9}_{-8.9}$	1205	
090751.9+024647	13368	136.9606	+2.7791	7.5	21.1	0.618	1.507	$3.1^{+1.0}_{-1.0}$	$13.0^{+1.25}_{-1.25}$	$25.9^{+1.40}_{-1.40}$	$89^{+1.38}_{-1.38}$	$29^{+5.6}_{-5.6}$	$2.00^{+3.32}_{-0.51}$	$25.2^{+23.3}_{-23.3}$	66^{+58}_{-58}	1212	
090752.9+013407	2074	136.9705	+1.5687	9.4	17.9	0.163	3.444	$2.38^{+1.75}_{-1.75}$	$6.4^{+1.4}_{-1.4}$	$16.2^{+4.4}_{-4.4}$	$3.46^{+1.39}_{-1.39}$	$3.0^{+1.38}_{-1.38}$	$2.37^{+0.49}_{-0.49}$	$14.1^{+1.8}_{-1.8}$	$14.1^{+1.8}_{-1.8}$	1215	
090754.5+005738	5219	136.9772	+0.9607	16.6	58.4	0.738	1.650	$10.4^{+1.58}_{-1.58}$	$9.1^{+1.6}_{-1.6}$	$460^{+1.93}_{-1.93}$	$19.2^{+1.55}_{-1.55}$	$19.2^{+1.55}_{-1.55}$	$7.4^{+1.53}_{-1.53}$	$3.25^{+2.17}_{-2.17}$	76^{+15}_{-15}	1210	
090757.5+025427	9569	136.9900	+2.9077	9.2	32.3	0.798	1.436	$7.0^{+0.50}_{-0.50}$	$7.0^{+0.50}_{-0.50}$	$31.9^{+1.6}_{-1.6}$	$14.7^{+2.8}_{-2.8}$	< 360	$6.6^{+1.5}_{-1.5}$	213^{+89}_{-89}	213^{+89}_{-89}	1208	
090803.8+020045	2234	137.0162	+2.0127	15.4	21.1	0.618	2.118	$7.1^{+1.35}_{-1.35}$	$47.9^{+1.56}_{-1.56}$	$198^{+1.11}_{-1.11}$	$16.4^{+2.5}_{-2.5}$	$16.4^{+2.5}_{-2.5}$	$2.8^{+1.8}_{-1.8}$	$28.6^{+8.8}_{-8.8}$	112^{+38}_{-38}	1209	
090805.9+011952	7084	137.0250	+1.3314	10.6	34.9	0.659	1.593	$8.9^{+1.04}_{-1.04}$	$44.1^{+0.63}_{-0.63}$	200^{+10}_{-10}	$10.1^{+2.3}_{-2.3}$	< 300	$3.0^{+0.51}_{-0.51}$	$32.4^{+7.3}_{-7.3}$	$124^{+7.3}_{-7.3}$	1214	
090806.4+026113	12592	137.0270	+3.4370	7.1	18.6	0.740	1.468	$3.0^{+0.56}_{-0.56}$	$37.7^{+8.5}_{-8.5}$	$116^{+5.9}_{-5.9}$	$10.1^{+2.5}_{-2.5}$	$10.1^{+2.5}_{-2.5}$	$3.0^{+0.87}_{-0.87}$	89^{+42}_{-42}	1214		
0908081.9+025151	6554	137.0289	+4.3977	33.2	56.7	0.205	3.255	$2.91^{+0.74}_{-0.74}$	$11.8^{+1.5}_{-1.5}$	$32.4^{+0.96}_{-0.96}$	$6.3^{+1.6}_{-1.6}$	$3.0^{+0.93}_{-0.93}$	$10.1^{+1.4}_{-1.4}$	$27.3^{+2.9}_{-2.9}$	1337		
090811.6-014811	3984	137.0486	-1.8032	13.4	72.5	0.040	5.725	$0.367^{+0.257}_{-0.257}$	$0.135^{+0.039}_{-0.039}$	$0.333^{+0.15}_{-0.15}$	$0.054^{+0.060}_{-0.060}$	$0.0229^{+0.0215}_{-0.0215}$	$0.319^{+0.038}_{-0.038}$	$0.120^{+0.032}_{-0.032}$	1959		
090816.3+034116	4974	137.0681	+3.5713	9.9	22.8	0.137	2.828	$4.5^{+1.04}_{-1.04}$	$2.18^{+0.78}_{-0.78}$	$22.3^{+1.5}_{-1.5}$	$4.02^{+0.78}_{-0.78}$	$2.44^{+0.55}_{-0.55}$	$5.3^{+1.5}_{-1.5}$	$6.1^{+1.6}_{-1.6}$	2073		
090817.2-010334	15548	137.0717	-1.5096	14.1	18.2	0.331	2.042	$10.7^{+1.25}_{-1.25}$	$7.3^{+1.4}_{-1.4}$	$201^{+1.25}_{-1.25}$	35^{+14}_{-14}	$4.1^{+0.93}_{-0.93}$	$6.1^{+0.88}_{-0.88}$	421^{+54}_{-54}	1241		

Table 4: continued.

Cluster	ID_SRC	RA (deg)	Dec (deg)	\mathcal{L}_{ext}	\mathcal{L}_{ext}	R_{500} (arcmin)	T (keV)	L_X (10^{42} erg s $^{-1}$)	L_{bol} (10^{42} erg s $^{-1}$)	M_{gas} (10^{12} M $_{\odot}$)	Y_X (10^{42} M $_{\odot}$ keV)	T_{ex} (keV)	$L_{\text{bol,ex}}$ (10^{42} erg s $^{-1}$)	t_{exp} (s)
(eFEDS I+)														
091135.9+034626	3774	137.8997	+3.7741	12.7	72.9	0.927	1.502	$1.98^{+1.21}_{-0.37}$	201^{+41}_{-41}	499^{+84}_{-84}	54^{+26}_{-13}	$1.75^{+0.92}_{-0.74}$	179^{+57}_{-57}	430 ⁺¹²⁰ ₋₁₀₀
091139.3-014444	5511	137.9141	-1.6958	23.8	53.7	0.589	1.881	$3.00^{+2.37}_{-0.35}$	$52.2^{+9.7}_{-9.7}$	146^{+44}_{-44}	$13.0^{+2.4}_{-2.4}$	$39^{+2.8}_{-2.8}$	$2.38^{+0.46}_{-0.46}$	98 ⁺²³ ₋₂₃
091159.7+031036	9374	137.9988	+3.1768	10.7	29.1	0.243	2.370	$7.7^{+1.92}_{-1.92}$	$3.5^{+2.5}_{-1.7}$	$3.99^{+0.88}_{-0.88}$	<130	$7.0^{+0.57}_{-0.57}$	$27.8^{+2.3}_{-2.3}$	1531
091213.4-021621	7639	138.0539	-2.2726	10.5	9.2	0.160	4.087	$2.60^{+0.99}_{-0.99}$	<4.5	<4.5	<13	$3.03^{+0.87}_{-0.87}$	<17	1193
091214.1+022443	18040	138.0589	+2.4121	6.8	17.1	0.181	2.430	$1.07^{+0.34}_{-0.34}$	<4.0	<8.2	<2.0	$1.13^{+0.71}_{-0.71}$	<3.4	533
091215.3-021743	626	138.0641	-2.2956	120.3	435.9	0.159	5.791	$2.10^{+0.34}_{-0.34}$	$65.5^{+5.5}_{-5.5}$	159^{+15}_{-15}	$19.7^{+1.5}_{-1.5}$	$41.5^{+1.4}_{-1.4}$	$1.92^{+0.77}_{-0.77}$	1102
091248.2+022446	11837	138.2011	+0.4130	7.1	17.4	0.308	2.602	$3.2^{+3.97}_{-1.2}$	$12.2^{+3.1}_{-3.1}$	$35.2^{+1.8}_{-1.8}$	$7.1^{+1.6}_{-1.6}$	$22.3^{+2.6}_{-2.6}$	$2.86^{+0.73}_{-0.73}$	29.7 ⁺¹⁰ ₋₈
091254.4+032028	1415	138.2270	+3.3444	48.5	99.3	0.619	2.191	$3.45^{+1.48}_{-1.48}$	$136^{+1.1}_{-1.1}$	395^{+82}_{-82}	$23.9^{+4.5}_{-4.5}$	83^{+32}_{-32}	$3.2^{+1.8}_{-1.8}$	1211
091300.9-013152	7531	138.2538	-1.5311	14.0	33.4	0.592	1.715	$1.04^{+0.80}_{-0.80}$	$41.6^{+0.83}_{-0.83}$	$129^{+7.5}_{-7.5}$	$10.1^{+0.33}_{-0.33}$	$80^{+1.5}_{-1.5}$	$30^{+0.5}_{-0.5}$	1216
091302.1+035000	1277	138.2590	+3.8336	11.4	18.7	0.455	2.168	$5.7^{+0.9}_{-0.9}$	$64.5^{+8.9}_{-8.9}$	234^{+17}_{-17}	$18.3^{+2.8}_{-2.8}$	101^{+207}_{-207}	$3.7^{+1.9}_{-1.9}$	1218
091305.9+030521	3797	138.2747	+3.8394	15.7	25.6	0.456	2.352	$3.26^{+2.88}_{-2.88}$	$70.4^{+8.0}_{-8.0}$	203^{+54}_{-54}	$20.8^{+2.4}_{-2.4}$	68^{+50}_{-50}	<1.8	1215
091315.0+034850	593	138.3125	+3.8139	88.3	393.5	0.455	2.666	$4.8^{+2.74}_{-2.74}$	$133^{+1.7}_{-1.7}$	439^{+39}_{-39}	$30.7^{+3.9}_{-3.9}$	145^{+75}_{-75}	$5.7^{+6.3}_{-6.3}$	1213
091320.3+032834	2977	138.3348	+3.4763	9.3	84.6	0.399	2.082	$2.74^{+1.75}_{-1.75}$	$24.3^{+4.8}_{-4.8}$	66^{+13}_{-13}	$14.9^{+2.0}_{-2.0}$	$12.0^{+5.3}_{-5.3}$	$2.39^{+1.32}_{-1.32}$	1218
091322.9+046167	9801	138.3454	+4.1050	9.6	9.6	0.088	3.752	$0.868^{+0.880}_{-0.880}$	$1.74^{+0.75}_{-0.75}$	$8.66^{+0.78}_{-0.78}$	$0.74^{+0.49}_{-0.49}$	$0.74^{+0.68}_{-0.68}$	$1.60^{+0.39}_{-0.39}$	1220
091331.0+024513	3488	138.3792	+2.7539	15.4	61.0	0.156	2.953	$1.03^{+0.34}_{-0.34}$	$6.25^{+0.93}_{-0.93}$	$0.25^{+0.15}_{-0.15}$	$0.197^{+0.10}_{-0.10}$	$0.84^{+0.09}_{-0.09}$	$2.99^{+0.70}_{-0.70}$	1214
091336.6+031723	5541	138.4040	+2.7899	54.9	82.7	0.142	4.335	$1.74^{+0.98}_{-0.98}$	$7.09^{+0.49}_{-0.49}$	$7.09^{+0.49}_{-0.49}$	$4.32^{+0.11}_{-0.11}$	<0.88	<1.8	1202
091351.1-004507	1319	138.4632	-0.7520	64.6	113.1	0.294	3.285	$2.40^{+0.93}_{-0.93}$	$44.2^{+2.2}_{-2.2}$	$111^{+1.6}_{-1.6}$	$15.1^{+1.5}_{-1.5}$	$34.9^{+7.0}_{-7.0}$	$2.36^{+0.38}_{-0.38}$	1218
091354.7+025323	16902	138.4782	+2.8898	6.3	15.4	0.423	1.912	$3.8^{+0.93}_{-0.93}$	$11.2^{+1.4}_{-1.4}$	36^{+26}_{-26}	$5.4^{+1.8}_{-1.8}$	$21.0^{+5.2}_{-5.2}$	$8.6^{+3.4}_{-3.4}$	1217
091358.1+025707	940	138.4924	+2.9521	17.2	21.8	0.417	2.256	$9.6^{+1.43}_{-1.43}$	$7.4^{+0.60}_{-0.60}$	82^{+16}_{-16}	$8.1^{+1.3}_{-1.3}$	<310	$14.2^{+2.4}_{-2.4}$	1216
091402.7-010208	5561	138.5116	-1.0358	9.7	48.7	0.516	1.858	$1.02^{+0.30}_{-0.30}$	$32.3^{+3.7}_{-3.7}$	$9.3^{+2.3}_{-2.3}$	$1.2^{+0.2}_{-0.2}$	$25.2^{+3.75}_{-3.75}$	$2.39^{+0.86}_{-0.86}$	1213
091403.3+013846	1465	138.5140	+1.6464	42.7	185.7	0.168	4.597	$6.0^{+0.83}_{-0.83}$	$14.5^{+1.5}_{-1.5}$	53^{+24}_{-24}	$8.4^{+2.4}_{-2.4}$	$50^{+1.6}_{-1.6}$	$9.1^{+1.6}_{-1.6}$	1210
091412.6+001836	1844	138.5528	+0.3158	55.0	87.3	0.165	3.985	$2.84^{+2.02}_{-2.02}$	$13.0^{+1.8}_{-1.8}$	$35.2^{+7.7}_{-7.7}$	$6.1^{+1.6}_{-1.6}$	$17.9^{+10.5}_{-10.5}$	$9.8^{+1.9}_{-1.9}$	1217
091414.9+022709	1424	138.5623	+2.4527	10.2	22.6	0.348	2.315	$2.39^{+1.57}_{-1.57}$	$12.1^{+1.4}_{-1.4}$	32^{+17}_{-17}	$8.1^{+1.1}_{-1.1}$	<24	<15	1214
091417.7+031159	396	138.5740	+3.1998	16.7	26.9	0.231	3.183	$1.02^{+0.50}_{-0.50}$	$10.7^{+3.3}_{-3.3}$	21.1^{+10}_{-10}	$6.7^{+1.4}_{-1.4}$	<6.7	<9.7	1219
091443.9+022833	7735	138.5999	+2.4759	14.3	32.7	0.319	2.356	$2.40^{+0.88}_{-0.88}$	$25.0^{+1.6}_{-1.6}$	64^{+14}_{-14}	$9.2^{+1.7}_{-1.7}$	$22.3^{+3.75}_{-3.75}$	$23.8^{+4.3}_{-4.3}$	1219
091443.1-0010910	4637	138.6318	+1.1528	10.9	55.2	0.543	1.751	$2.30^{+0.93}_{-0.93}$	$10.9^{+1.3}_{-1.3}$	79^{+28}_{-28}	$8.4^{+2.4}_{-2.4}$	$50^{+1.6}_{-1.6}$	<120	1214
091443.8+022718	3159	138.6411	+2.4550	38.1	99.6	0.316	2.657	$3.77^{+1.54}_{-1.54}$	74^{+21}_{-21}	$9.2^{+2.1}_{-2.1}$	33^{+50}_{-50}	$2.58^{+1.24}_{-1.24}$	$18.3^{+5.3}_{-5.3}$	1212
091443.5-014416	6130	138.6648	-1.7380	11.3	39.7	0.484	1.765	$3.7^{+1.53}_{-1.53}$	$35.2^{+6.3}_{-6.3}$	107^{+33}_{-33}	$9.8^{+1.4}_{-1.4}$	36^{+15}_{-15}	$30.2^{+8.9}_{-8.9}$	1211
091445.7+032755	8636	138.6906	+3.4655	8.7	17.7	0.122	4.059	$1.94^{+0.39}_{-0.39}$	$1.94^{+0.36}_{-0.36}$	$8.2^{+8.6}_{-8.6}$	$1.52^{+0.40}_{-0.40}$	<68	$1.38^{+0.38}_{-0.38}$	1214
091445.8+046261	13299	138.6909	+4.4394	14.8	17.7	0.348	2.375	$1.45^{+0.63}_{-0.63}$	$144^{+1.5}_{-1.5}$	325^{+64}_{-64}	$19.0^{+0.44}_{-0.44}$	$19.0^{+1.2}_{-1.2}$	$11.0^{+0.51}_{-0.51}$	1221
091446.1+001047	1917	138.6925	+0.1799	25.2	156.6	0.533	2.104	$2.37^{+0.54}_{-0.54}$	87^{+10}_{-10}	$26.2^{+4.0}_{-4.0}$	$27.8^{+1.6}_{-1.6}$	$27.8^{+1.6}_{-1.6}$	$15.5^{+3.3}_{-3.3}$	1219
091450.6-022606	2154	138.7110	-2.4351	44.3	121.9	0.504	2.045	$4.0^{+4.37}_{-4.37}$	$40.4^{+3.7}_{-3.7}$	341^{+75}_{-75}	$15.0^{+1.7}_{-1.7}$	$15.0^{+1.7}_{-1.7}$	16.84	1569
091453.6+041613	372	138.7235	+4.2704	123.9	398.6	0.143	5.827	$2.77^{+1.68}_{-1.68}$	$25.5^{+5.8}_{-5.8}$	$67.5^{+9.7}_{-9.7}$	$11.3^{+2.4}_{-2.4}$	$24.8^{+0.65}_{-0.65}$	$15.8^{+5.3}_{-5.3}$	1216
091509.5+051521	6244	138.7897	+5.2560	48.0	70.0	0.249	3.720	$2.47^{+0.91}_{-0.91}$	$50.4^{+6.2}_{-6.2}$	129^{+37}_{-37}	$19.6^{+1.7}_{-1.7}$	$3.35^{+0.41}_{-0.41}$	$41.8^{+4.9}_{-4.9}$	577
091512.2+043506	4253	138.8012	+4.5851	11.6	59.8	0.361	2.138	$2.41^{+0.44}_{-0.44}$	$11.6^{+2.5}_{-2.5}$	29.8^{+15}_{-15}	$4.5^{+1.7}_{-1.7}$	$1.96^{+0.76}_{-0.76}$	<9.1	<22
091517.4-005909	13537	138.8229	-0.9860	6.2	24.8	0.405	1.822	$3.77^{+1.26}_{-1.26}$	87^{+10}_{-10}	$42.4^{+5.4}_{-5.4}$	$6.9^{+1.5}_{-1.5}$	$3.4^{+0.39}_{-0.39}$	$11.8^{+4.3}_{-4.3}$	1220
091520.5+05203	14354	138.8357	+4.8676	10.5	11.8	0.149	3.013	$3.3^{+1.08}_{-1.08}$	$1.41^{+0.57}_{-0.57}$	$4.4^{+1.7}_{-1.7}$	$0.96^{+0.45}_{-0.45}$	<24	$3.4^{+6.2}_{-6.2}$	1233
091522.5+0421201	14525	138.8438	+4.2003	7.6	10.2	0.1932	3.74	$3.7^{+1.3}_{-1.3}$	$17.3^{+0.43}_{-0.43}$	53^{+25}_{-25}	$7.2^{+0.39}_{-0.39}$	$3.4^{+1.7}_{-1.7}$	$13.4^{+0.47}_{-0.47}$	1219
091543.5-004944	10164	138.9316	-0.8291	6.3	23.7	0.296	1.948	$11.4^{+1.90}_{-1.90}$	$3.28^{+0.89}_{-0.89}$	$16.4^{+1.18}_{-1.18}$	$10.9^{+0.79}_{-0.79}$	$3.28^{+0.44}_{-0.44}$	$1.10^{+0.62}_{-0.62}$	1260
091553.1+040545	12204	138.9715	+4.0961	6.4	23.4	0.567	1.560	$8.0^{+1.29}_{-1.29}$	$12.6^{+0.96}_{-0.96}$	55^{+40}_{-40}	$4.5^{+1.7}_{-1.7}$	$22.5^{+4.7}_{-4.7}$	$1.10^{+0.52}_{-0.52}$	1215
091555.6-013248	888	138.9820	-1.5468	86.6	275.5	0.490	2.957	$7.3^{+2.51}_{-2.51}$	151^{+14}_{-14}	$42.4^{+3.54}_{-3.54}$	$42.4^{+3.54}_{-3.54}$	$31.0^{+5.30}_{-5.30}$	$11.1^{+3.4}_{-3.4}$	1215
091601.8+00831	9930	139.1704	+4.1095	12.9	32.0	0.563	1.760	$3.7^{+1.4}_{-1.4}$	144^{+10}_{-10}	144^{+10}_{-10}	144^{+10}_{-10}	$3.4^{+6.2}_{-6.2}$	$12.8^{+8.0}_{-8.0}$	1222
091609.4+035119	8107	139.0393	+1.9255	36.7	41.8	0.259	2.957	$18.1^{+1.45}_{-1.45}$	$28.1^{+2.47}_{-2.47}$	102^{+63}_{-63}	7.2			

Table 4: continued.

Cluster (eFEDS I+)	ID_SRC	RA (deg)	Dec (deg)	\mathcal{L}_{ext}	\mathcal{L}_{ext} (deg)	R_{500} (arcmin)	T (keV)	L_X (10^{42} erg s $^{-1}$)	L_{bol} (10^{42} erg s $^{-1}$)	M_{gas} (10^{12} M $_{\odot}$)	Y_X (10^{12} M $_{\odot}$ keV)	T_{ex} (keV)	$L_{\text{bol,ex}}$ (10^{42} erg s $^{-1}$)	t_{exp} (s)	
091849.0+021204	994	139.7042	+2.2013	94.8	245.3	0.283	3.428	$75.4^{+5.8}_{-4.5}$	$242^{+2.8}_{-2.5}$	$109^{+6.6}_{-5.4}$	$4.7^{+3.1}_{-2.4}$	$62.4^{+4.7}_{-4.6}$	208^{+59}_{-50}	1220	
091850.7+030942	19979	139.7113	+3.1619	12.8	14.7	0.838	1.462	$5.1^{+2.7}_{-1.3}$	$15.2^{+3.8}_{-2.8}$	75^{+12}_{-12}	$5.3^{+5.4}_{-5.2}$	$63^{+2.7}_{-2.7}$	229^{+104}_{-96}	1220	
091851.7+021432	4105	139.7155	+2.2423	10.0	19.0	0.283	2.389	$5.5^{+2.5}_{-2.5}$	<24	48^{+36}_{-36}	$6.1^{+2.8}_{-2.8}$	$5.9^{+7.0}_{-7.0}$	<22	<100	1220
091855.8+004916	12125	139.7221	+0.8211	12.1	19.4	0.845	1.388	$2.8^{+3.4}_{-2.4}$	76^{+24}_{-24}	219^{+59}_{-59}	$13.8^{+2.9}_{-2.9}$	$2.8^{+2.2}_{-2.2}$	179^{+70}_{-70}	1495	
091858.0+024946	7194	139.7418	+2.8295	26.3	46.3	0.199	3.204	$1.71^{+1.88}_{-1.28}$	$10.6^{+2.0}_{-2.0}$	$24.8^{+5.6}_{-5.6}$	$5.24^{+0.90}_{-0.90}$	$9.2^{+4.8}_{-4.8}$	$21.2^{+4.8}_{-4.8}$	1223	
091900.0+035311	5545	139.7503	+3.8864	25.3	53.8	0.403	2.258	$2.11^{+0.78}_{-0.78}$	$39.9^{+3.8}_{-3.8}$	98^{+13}_{-13}	$12.9^{+1.7}_{-1.7}$	$27.9^{+5.6}_{-5.6}$	$8.9^{+1.8}_{-1.8}$	1221	
091925.6-010430	4254	139.8567	-1.0752	9.2	55.6	0.513	1.734	$7.7^{+3.5}_{-3.5}$	$28.3^{+2.9}_{-2.9}$	124^{+73}_{-73}	<12	$1.14^{+0.89}_{-0.89}$	$1.42^{+0.65}_{-0.65}$	<32	1433
091934.6+033941	1892	139.8943	+3.6615	20.8	126.9	0.223	2.788	$1.26^{+3.15}_{-2.18}$	$7.8^{+1.6}_{-1.6}$	$16.4^{+3.4}_{-3.4}$	$0.41^{+0.34}_{-0.34}$	$2.6^{+1.5}_{-1.5}$	<4.3	<8.6	1224
091936.6+042553	11376	139.9028	+4.4314	9.3	21.3	0.179	2.567	$1.57^{+1.51}_{-1.51}$	$1.13^{+0.64}_{-0.64}$	$2.6^{+1.0}_{-1.0}$	$0.41^{+0.34}_{-0.34}$	$1.79^{+0.55}_{-0.55}$	<2.8	<3.4	1313
091957.7+035012	4131	139.9908	+3.8369	38.5	74.3	0.525	2.211	$2.01^{+0.53}_{-0.53}$	$75.2^{+0.8}_{-0.8}$	$18.2^{+0.24}_{-0.24}$	$0.102^{+0.06}_{-0.06}$	$38^{+2.3}_{-2.3}$	$2.32^{+0.62}_{-0.62}$	145^{+39}_{-39}	1221
092002.1+010219	150	140.0090	+1.0389	179.6	1049.6	0.017	15.354	$0.86^{+0.51}_{-0.51}$	$0.295^{+0.05}_{-0.05}$	$0.69^{+0.26}_{-0.26}$	$0.102^{+0.06}_{-0.06}$	$0.85^{+0.55}_{-0.55}$	$1.03^{+0.61}_{-0.61}$	<0.75	1572
092004.3+010023	11754	140.0183	+1.0066	20.0	35.9	0.033	7.193	$0.779^{+0.08}_{-0.08}$	<0.17	<0.31	$0.0145^{+0.003}_{-0.003}$	$0.0114^{+0.0083}_{-0.0056}$	<0.06	1570	
092022.0+031016	6534	140.0918	+3.0186	6.6	14.1	0.481	1.608	$2.8^{+1.12}_{-1.12}$	$9.0^{+4.4}_{-4.4}$	<97	<9.6	<39	$3.0^{+1.15}_{-1.15}$	<27	1304
092022.8+050112	5320	140.0934	+4.8369	12.0	60.2	0.270	2.774	$4.2^{+0.9}_{-0.9}$	$23.7^{+4.1}_{-4.1}$	76^{+51}_{-51}	$8.7^{+1.7}_{-1.7}$	$4.1^{+0.54}_{-0.54}$	$16.7^{+4.9}_{-4.9}$	55^{+13}_{-13}	695
092023.2+013444	222	140.0967	+1.5789	88.4	719.6	0.708	2.178	$3.20^{+0.70}_{-0.70}$	$3.15^{+0.80}_{-0.80}$	869^{+86}_{-86}	$36.5^{+5.5}_{-5.5}$	$11.6^{+3.1}_{-3.1}$	$2.87^{+0.79}_{-0.79}$	157^{+35}_{-35}	1547
092031.3+024710	18068	140.1306	+2.7863	11.6	11.7	0.278	2.406	$2.36^{+0.58}_{-0.58}$	$4.0^{+2.6}_{-2.6}$	$10.6^{+0.8}_{-0.8}$	$2.25^{+1.40}_{-1.40}$	$5.6^{+2.9}_{-2.9}$	$2.17^{+2.55}_{-2.55}$	$6.6^{+7.7}_{-7.7}$	1377
092031.8+040621	4115	140.1329	+4.1059	12.5	53.2	0.575	1.755	$7.7^{+1.21}_{-1.21}$	$1.26^{+0.20}_{-0.20}$	$6.0^{+0.77}_{-0.77}$	$3.28^{+0.52}_{-0.52}$	<4.0	$4.18^{+0.09}_{-0.09}$	$4.64^{+0.70}_{-0.70}$	1224
092037.0-011506	5739	140.1545	-1.2519	34.3	63.0	0.154	3.760	$1.26^{+0.20}_{-0.20}$	$1.26^{+0.18}_{-0.18}$	$6.1^{+0.77}_{-0.77}$	$30.6^{+1.71}_{-1.71}$	$30.6^{+1.71}_{-1.71}$	$3.25^{+0.88}_{-0.88}$	$9.2^{+1.4}_{-1.4}$	1354
092037.9+033528	6467	140.1580	+3.5913	6.8	44.8	0.362	1.984	$3.3^{+0.13}_{-0.13}$	$8.1^{+0.67}_{-0.67}$	23^{+18}_{-18}	<6.0	<28	$5.1^{+0.63}_{-0.63}$	<11	1247
092039.1+004725	6669	140.1632	+0.7904	8.8	45.1	0.472	1.766	$9.6^{+0.62}_{-0.62}$	$10.0^{+0.36}_{-0.36}$	$6.8^{+1.4}_{-1.4}$	<100	$10.4^{+0.33}_{-0.33}$	$14.5^{+4.0}_{-4.0}$	67^{+44}_{-44}	1496
092041.1+041117	10334	140.1716	+4.1883	10.8	23.6	0.580	1.632	$2.53^{+0.53}_{-0.53}$	$2.53^{+0.53}_{-0.53}$	$5.5^{+2.2}_{-2.2}$	$5.7^{+2.1}_{-2.1}$	$13.8^{+9.6}_{-9.6}$	$12.6^{+5.6}_{-5.6}$	<12	1329
092046.2+022849	1915	140.1926	+0.4803	40.0	69.6	0.413	2.716	$2.54^{+0.74}_{-0.74}$	$19.4^{+5.8}_{-5.8}$	193^{+27}_{-27}	$12.7^{+1.8}_{-1.8}$	$22.5^{+3.4}_{-3.4}$	$2.68^{+1.17}_{-1.17}$	$57.3^{+9.9}_{-9.9}$	1422
092049.5+024513	489	140.2063	+2.7538	142.1	514.2	0.284	3.708	$3.16^{+0.88}_{-0.88}$	105.0^{+50}_{-50}	290^{+24}_{-24}	$30.6^{+1.71}_{-1.71}$	$30.6^{+1.71}_{-1.71}$	$3.25^{+0.88}_{-0.88}$	$9.2^{+1.4}_{-1.4}$	1357
092053.4+021125	18194	140.2228	+2.1905	12.8	17.4	0.280	2.488	$2.10^{+0.54}_{-0.54}$	$19.4^{+2.3}_{-2.3}$	$19.4^{+2.3}_{-2.3}$	$4.68^{+1.31}_{-1.31}$	$10.3^{+1.7}_{-1.7}$	$1.97^{+0.62}_{-0.62}$	$16.6^{+6.7}_{-6.7}$	1540
092105.0+004452	6459	140.2710	+0.7480	7.3	33.9	0.159	2.780	$11.5^{+0.62}_{-0.62}$	$11.5^{+0.62}_{-0.62}$	$6.7^{+1.3}_{-1.3}$	$4.1^{+0.34}_{-0.34}$	$10.4^{+0.34}_{-0.34}$	$12.6^{+5.9}_{-5.9}$	$12.6^{+5.9}_{-5.9}$	1419
092121.2+031726	100	140.3395	+3.2906	478.6	1729.7	0.333	4.068	$5.1^{+0.68}_{-0.68}$	$25.0^{+1.00}_{-1.00}$	887^{+80}_{-80}	$53.1^{+2.2}_{-2.2}$	$29.2^{+0.64}_{-0.64}$	$29.2^{+0.64}_{-0.64}$	163^{+40}_{-40}	1437
092133.2+034341	9512	140.3885	+4.5754	14.1	24.9	0.417	1.716	$2.54^{+0.74}_{-0.74}$	$19.4^{+5.8}_{-5.8}$	47^{+13}_{-13}	$6.8^{+1.4}_{-1.4}$	$57.2^{+6.7}_{-6.7}$	$4.50^{+0.63}_{-0.63}$	$13.3^{+4.4}_{-4.4}$	1066
092134.4+015832	810	140.3936	+1.9757	56.1	133.2	0.290	3.175	$3.7^{+0.45}_{-0.45}$	$30.6^{+1.72}_{-1.72}$	94^{+49}_{-49}	$12.3^{+1.5}_{-1.5}$	$44^{+5.6}_{-5.6}$	$6.1^{+1.45}_{-1.45}$	$21.2^{+5.7}_{-5.7}$	1439
092135.4+005128	7447	140.3977	+0.8580	7.4	35.0	0.488	1.780	$2.62^{+0.68}_{-0.68}$	$2.62^{+0.68}_{-0.68}$	$7.7^{+2.5}_{-2.5}$	$4.68^{+1.31}_{-1.31}$	$10.3^{+1.7}_{-1.7}$	$1.97^{+0.62}_{-0.62}$	$16.6^{+6.7}_{-6.7}$	1355
092136.4-001449	4168	140.4020	-0.2471	37.9	80.2	0.313	2.780	$4.0^{+0.52}_{-0.52}$	$8.2^{+0.89}_{-0.89}$	82^{+30}_{-30}	$1.68^{+0.38}_{-0.38}$	$10.4^{+0.38}_{-0.38}$	$20.3^{+4.0}_{-4.0}$	75^{+53}_{-53}	1184
092202.2+034520	5347	140.5095	+3.7557	43.4	66.6	0.270	3.155	$4.49^{+0.73}_{-0.73}$	$14.3^{+1.4}_{-1.4}$	$44.9^{+1.4}_{-1.4}$	$15.5^{+1.5}_{-1.5}$	$15.5^{+1.5}_{-1.5}$	$4.35^{+0.63}_{-0.63}$	140	
092209.3+034628	367	140.5391	+3.7741	369.0	783.1	0.270	4.315	$4.83^{+0.90}_{-0.90}$	$19.4^{+5.8}_{-5.8}$	$31.7^{+1.7}_{-1.7}$	$30.4^{+1.7}_{-1.7}$	$3.1^{+1.44}_{-1.44}$	$4.50^{+0.63}_{-0.63}$	$13.3^{+4.4}_{-4.4}$	1066
092212.0-002731	857	140.5503	-0.4586	165.1	361.5	0.321	3.647	$5.1^{+0.87}_{-0.87}$	$3.74^{+0.45}_{-0.45}$	390^{+51}_{-51}	$36.6^{+5.5}_{-5.5}$	$12.3^{+1.5}_{-1.5}$	$4.8^{+1.4}_{-1.4}$	$7.9^{+1.8}_{-1.8}$	1537
092220.4+034806	4014	140.5852	+3.8017	24.1	48.9	0.267	0.719	$1.51^{+0.75}_{-0.75}$	$1.51^{+0.75}_{-0.75}$	$8.6^{+2.1}_{-2.1}$	$19.4^{+2.1}_{-2.1}$	$1.73^{+0.78}_{-0.78}$	$1.74^{+0.73}_{-0.73}$	$18.8^{+5.3}_{-5.3}$	1494
092235.8-002443	3133	140.6494	-0.4120	30.2	49.4	0.055	6.929	$2.64^{+0.38}_{-0.38}$	$1.24^{+0.38}_{-0.38}$	$3.21^{+0.08}_{-0.08}$	$0.57^{+0.13}_{-0.13}$	$1.54^{+0.38}_{-0.38}$	$0.53^{+0.36}_{-0.36}$	$1.44^{+0.36}_{-0.36}$	1124
092241.9+023719	1535	140.6749	+2.1222	32.5	52.2	0.198	3.310	$1.38^{+0.27}_{-0.27}$	$8.9^{+1.4}_{-1.4}$	$39.7^{+1.76}_{-1.76}$	$3.97^{+0.43}_{-0.43}$	$1.57^{+0.16}_{-0.16}$	$3.97^{+0.16}_{-0.16}$	$1.29^{+0.07}_{-0.07}$	1440
092246.2+034251	2216	140.6928	+3.7143	27.5	65.5	0.269	2.759	$2.06^{+0.55}_{-0.55}$	$19.0^{+6.5}_{-6.5}$	$46.0^{+6.3}_{-6.3}$	$6.59^{+1.75}_{-1.75}$	$13.7^{+3.3}_{-3.3}$	$4.50^{+0.63}_{-0.63}$	$21.7^{+6.2}_{-6.2}$	1469
092246.4+024242	5348	140.6936	+4.4067	12.5	55.0	0.346	2.180	$1.80^{+0.34}_{-0.34}$	$1.80^{+0.34}_{-0.34}$	$5.8^{+0.67}_{-0.67}$	$10.5^{+3.3}_{-3.3}$	$10.5^{+3.3}_{-3.3}$	$3.0^{+1.88}_{-1.88}$	$11.9^{+3.4}_{-3.4}$	1377
092258.2+032041	4833	140.7426	+3.3449	14.4	51.1	0.575	1.762	$3.5^{+0.5}_{-0.5}$	$3.44^{+0.36}_{-0.36}$	$10.2^{+0.99}_{-0.99}$	$8.2^{+0.99}_{-0.99}$	$1.74^{+0.73}_{-0.73}$	28^{+27}_{-27}	$18.8^{+5.3}_{-5.3}$	1543
092302.6+034002	9076	140.7611	+3.6673	7.9	13.7	0.269	2.211	<math							

Table 4: continued.

Cluster	ID_SRC	RA (deg)	Dec (deg)	\mathcal{L}_{ext}	\mathcal{L}_{ext}	R_{500} (arcmin)	T (keV)	L_X (10^{42} erg s $^{-1}$)	L_{bol} (10^{42} erg s $^{-1}$)	M_{gas} (10^{12} M $_{\odot}$)	Y_X (10^{12} M $_{\odot}$ keV)	T_{ex} (keV)	$L_{\text{bol,ex}}$ (10^{42} erg s $^{-1}$)	t_{exp} (s)			
09253.6-014205	1483	141.3903	-1.7016	51.0	150.6	0.229	0.815	$2.97^{+2.41}_{-0.83}$	$7.65^{+1.23}_{-0.83}$	$21.2^{+7.4}_{-3.3}$	$0.73^{+0.27}_{-0.19}$	$2.31^{+2.39}_{-0.80}$	$6.86^{+10}_{-6.5}$	18.3 $^{+4.9}_{-2.8}$	2065		
092546.3-014347	566	141.4432	-1.7298	197.1	480.2	0.228	3.813	$2.88^{+0.84}_{-0.84}$	$33.4^{+2.38}_{-2.38}$	$89.8^{+10.2}_{-9.0}$	$12.3^{+1.9}_{-1.5}$	$36.0^{+0.92}_{-0.82}$	$2.87^{+0.52}_{-0.52}$	$23.3^{+0.38}_{-0.38}$	62.5 $^{+2.9}_{-8.4}$	2008	
092548.9-011725	5488	141.4539	-1.2903	12.0	18.4	0.337	2.390	$2.25^{+0.34}_{-0.34}$	$23.8^{+2.34}_{-2.34}$	$59.6^{+0.1}_{-0.1}$	$9.6^{+1.5}_{-1.4}$	$22.3^{+0.4}_{-0.4}$	$2.37^{+0.38}_{-0.38}$	$20.6^{+2.4}_{-2.4}$	52.3 $^{+3.9}_{-9.7}$	1718	
092553.3+015519	991	141.4724	+1.9220	11.3	33.3	0.231	3.126	$2.58^{+0.34}_{-0.34}$	$33.2^{+2.34}_{-2.34}$	< 106	< 18	< 18	< 3.0	< 3.0	< 9.8	1129	
092555.6+004311	6732	141.4820	+0.7199	64.5	88.9	0.255	3.279	$4.2^{+0.82}_{-0.82}$	$106^{+4.9}_{-4.9}$	$14.5^{+2.1}_{-1.9}$	$61^{+7.5}_{-7.5}$	$4.5^{+1.4}_{-1.4}$	$29.7^{+4.6}_{-4.5}$	96^{+34}_{-17}	1184		
092619.9+021207	8160	141.5830	+2.2022	23.4	32.5	0.493	2.104	$11.1^{+1.7}_{-1.7}$	$30.5^{+2.8}_{-2.8}$	$154.7^{+0.7}_{-0.7}$	$12.0^{+2.2}_{-2.2}$	$12.0^{+2.2}_{-2.2}$	$5.9^{+0.6}_{-0.6}$	$24.7^{+2.5}_{-2.5}$	92 $^{+12}_{-12}$	1131	
092621.3-003356	4366	141.5890	-0.5657	10.1	63.4	0.340	2.118	$3.6^{+2.8}_{-2.8}$	$40^{+2.9}_{-2.7}$	$40^{+2.9}_{-2.7}$	$4.5^{+2.2}_{-2.2}$	$17.0^{+4.0}_{-4.0}$	$4.9^{+2.5}_{-2.5}$	27^{+28}_{-28}	27 $^{+28}_{-28}$	1229	
092629.3+026114	2050	141.6225	+3.4374	19.7	117.5	0.088	4.336	$1.020^{+0.60}_{-0.60}$	$2.45^{+0.36}_{-0.36}$	$4.74^{+0.73}_{-0.73}$	$1.07^{+0.25}_{-0.25}$	$1.08^{+0.25}_{-0.25}$	$1.08^{+0.25}_{-0.25}$	$1.08^{+0.25}_{-0.25}$	$1.08^{+0.25}_{-0.25}$	2.36 $^{+0.33}_{-0.33}$	1152
092631.0+014511	2967	141.6295	+1.7533	31.8	100.0	0.761	1.834	$9.2^{+0.68}_{-0.68}$	$124^{+1.43}_{-1.43}$	$580^{+1.35}_{-1.35}$	$24.8^{+1.50}_{-1.50}$	$220^{+1.37}_{-1.37}$	$220^{+1.37}_{-1.37}$	$13.4^{+0.41}_{-0.41}$	84^{+15}_{-15}	470 $^{+160}_{-160}$	1152
092639.7+040733	3560	141.6635	+4.1260	7.7	34.5	0.245	2.290	$6.2^{+3.5}_{-3.5}$	$44^{+1.20}_{-1.20}$	$11.2^{+2.3}_{-2.3}$	$3.8^{+1.0}_{-1.0}$	$14.0^{+1.0}_{-1.0}$	$16.2^{+8.9}_{-8.9}$	< 13	< 100	1184	
092644.0+040010	9238	141.6834	+0.0029	11.1	29.5	0.347	2.128	$2.59^{+3.9}_{-3.9}$	$20.0^{+2.6}_{-2.6}$	$54.0^{+1.20}_{-1.20}$	$7.6^{+1.5}_{-1.5}$	$20.4^{+2.05}_{-2.05}$	$3.6^{+1.7}_{-1.7}$	$17.0^{+4.0}_{-4.0}$	52^{+31}_{-31}	1171	
092647.5+050032	137	141.6980	+5.0091	505.4	1395.7	0.455	3.422	$6.5^{+1.6}_{-1.6}$	$31.9^{+0.80}_{-0.80}$	$122.0^{+0.90}_{-0.90}$	$61.3^{+5.7}_{-5.7}$	$400^{+1.20}_{-1.20}$	$7.3^{+2.0}_{-2.0}$	205^{+210}_{-210}	840^{+140}_{-140}	1330	
092647.5+030946	12965	141.6981	+3.1630	16.2	16.0	0.226	2.851	$3.2^{+1.6}_{-1.6}$	$5.0^{+1.5}_{-1.5}$	$14.7^{+1.5}_{-1.5}$	$3.16^{+0.89}_{-0.89}$	$10.0^{+1.37}_{-1.37}$	$10.0^{+1.37}_{-1.37}$	3.2^{+29}_{-29}	$11.0^{+8.5}_{-8.5}$	1135	
092740.1+002922	6875	141.7002	+5.0234	16.0	26.5	0.454	2.542	$6.2^{+3.0}_{-3.0}$	$44.2^{+1.44}_{-1.44}$	$11.5^{+1.5}_{-1.5}$	$27.8^{+1.48}_{-1.48}$	$5.4^{+1.5}_{-1.5}$	174^{+46}_{-46}	88^{+15}_{-15}	312 $^{+97}_{-97}$	1152	
092745.0+035755	671	141.7106	+3.9654	33.0	304.8	0.377	2.594	$2.27^{+0.52}_{-0.52}$	$45.1^{+1.01}_{-1.01}$	$11.1^{+2.5}_{-2.5}$	$11.1^{+2.5}_{-2.5}$	$11.1^{+2.5}_{-2.5}$	$16.8^{+3.4}_{-3.4}$	$14.7^{+9.1}_{-9.1}$	39^{+26}_{-26}	1166	
092747.1+011735	10285	141.7981	+1.2933	7.5	25.8	0.613	1.558	$12.5^{+0.43}_{-0.43}$	$33.4^{+1.50}_{-1.50}$	$19.0^{+1.02}_{-1.02}$	$10.1^{+1.9}_{-1.9}$	$10.1^{+1.9}_{-1.9}$	< 400	$11.1^{+0.58}_{-0.58}$	149^{+95}_{-95}	1209	
092747.5+014423	266	141.8974	+1.7399	32.9	43.2	0.149	4.171	$4.7^{+0.70}_{-0.70}$	$8.2^{+1.70}_{-1.70}$	$27.0^{+2.5}_{-2.5}$	$4.42^{+0.44}_{-0.44}$	$20.6^{+4.04}_{-4.04}$	$4.8^{+0.57}_{-0.57}$	$20.8^{+5.6}_{-5.6}$	1205	1205	
092737.7+020607	1924	141.9074	+2.1021	106.4	191.5	0.419	2.793	$3.7^{+2.7}_{-2.7}$	$90.2^{+0.81}_{-0.81}$	$266^{+1.56}_{-1.56}$	$27.5^{+2.5}_{-2.5}$	$101^{+3.3}_{-33}$	$3.7^{+2.4}_{-2.4}$	$74.7^{+6.6}_{-6.6}$	22^{+34}_{-34}	1191	
092739.7-010427	2636	141.9158	-1.0743	34.8	47.3	0.329	2.747	$18.0^{+0.92}_{-0.92}$	$34.0^{+0.88}_{-0.88}$	$242^{+0.80}_{-0.80}$	$15.4^{+2.5}_{-2.5}$	$15.0^{+1.4}_{-1.4}$	$15.0^{+1.4}_{-1.4}$	$15.0^{+1.4}_{-1.4}$	$15.0^{+1.4}_{-1.4}$	1232	
092740.1-002922	3454	141.9171	-0.4897	11.4	77.7	0.138	3.308	$1.38^{+0.56}_{-0.56}$	$7.8^{+1.11}_{-1.11}$	$7.8^{+1.11}_{-1.11}$	$1.62^{+2.4}_{-2.4}$	$3.07^{+1.67}_{-1.67}$	$3.07^{+1.67}_{-1.67}$	$2.19^{+1.67}_{-1.67}$	$1.91^{+0.58}_{-0.58}$	1230	
092740.1+042038	4999	141.9173	+4.3440	6.2	21.4	0.275	2.929	$1.82^{+0.70}_{-0.70}$	$1.2^{+0.33}_{-0.33}$	$63^{+3.4}_{-3.4}$	$5.9^{+1.3}_{-1.3}$	$5.9^{+1.3}_{-1.3}$	$5.9^{+1.3}_{-1.3}$	$8.3^{+3.5}_{-3.5}$	$11.0^{+6.5}_{-6.5}$	1151	
092740.7-015320	7063	141.9196	-1.8889	16.1	41.4	0.332	2.362	$10.4^{+0.33}_{-0.33}$	$12.5^{+2.3}_{-2.3}$	$34.0^{+0.88}_{-0.88}$	$14.1^{+1.3}_{-1.3}$	$14.1^{+1.3}_{-1.3}$	$14.1^{+1.3}_{-1.3}$	4.3^{+29}_{-29}	4.3^{+29}_{-29}	1443	
092744.6+045630	17315	141.9360	+4.9418	11.3	9.6	0.355	2.192	$1.32^{+0.64}_{-0.64}$	$6.3^{+1.28}_{-1.28}$	$32.6^{+0.84}_{-0.84}$	$11.4^{+1.4}_{-1.4}$	$5.3^{+1.4}_{-1.4}$	$5.3^{+1.4}_{-1.4}$	8.7^{+18}_{-18}	1281	1281	
092755.9+000439	10316	141.9829	+0.0778	10.9	21.9	0.983	1.384	$1.53^{+0.38}_{-0.38}$	$1.53^{+0.38}_{-0.38}$	$126^{+4.8}_{-4.8}$	$30.0^{+1.49}_{-1.49}$	$17.6^{+4.4}_{-4.4}$	$17.6^{+4.4}_{-4.4}$	$26.8^{+18.9}_{-18.9}$	23^{+106}_{-106}	1229	
092803.4+010953	1527	142.0142	+1.1648	13.0	163.7	0.552	1.987	$2.21^{+0.83}_{-0.83}$	$2.21^{+0.83}_{-0.83}$	$191^{+1.42}_{-1.42}$	$19.1^{+1.42}_{-1.42}$	$13.2^{+3.0}_{-3.0}$	$31.6^{+6.3}_{-6.3}$	35^{+35}_{-35}	101^{+56}_{-56}	1228	
092807.5-001353	13561	142.0314	-0.2316	9.5	25.9	0.771	1.390	$1.24^{+0.36}_{-0.36}$	$1.24^{+0.36}_{-0.36}$	$104^{+1.47}_{-1.47}$	$104^{+1.47}_{-1.47}$	$104^{+1.47}_{-1.47}$	$15.4^{+1.64}_{-1.64}$	$15.4^{+1.64}_{-1.64}$	$15.4^{+1.64}_{-1.64}$	$15.4^{+1.64}_{-1.64}$	1228
092807.7-012704	6687	142.0323	-1.4512	6.8	28.9	1.304	1.145	$10.4^{+0.34}_{-0.34}$	$10.4^{+0.34}_{-0.34}$	< 150	< 810	< 810	< 310	< 310	< 500	1543	
092813.0-004508	13305	142.0544	-0.7524	7.8	16.9	0.318	1.942	$3.1^{+0.61}_{-0.61}$	$13.6^{+2.4}_{-2.4}$	$3.1^{+0.61}_{-0.61}$	< 2.3	< 2.3	< 8.5	< 8.5	< 8.5	1135	
092821.1+041941	7167	142.0880	+4.3283	8.3	20.4	0.157	2.929	$3.26^{+0.52}_{-0.52}$	$3.26^{+0.52}_{-0.52}$	< 3.5	< 10	< 10	< 3.1	< 3.1	< 3.1	1228	
092821.2+042149	666	142.0884	+4.3637	113.0	323.5	0.235	3.863	$2.21^{+0.83}_{-0.83}$	$4.3^{+3.6}_{-3.6}$	$106.0^{+0.0}_{-0.0}$	$106.0^{+0.0}_{-0.0}$	$14.4^{+1.66}_{-1.66}$	$14.4^{+1.66}_{-1.66}$	$14.4^{+1.66}_{-1.66}$	$14.4^{+1.66}_{-1.66}$	1136	
092828.3-000955	845	142.1180	-0.1653	7.1	22.9	0.509	1.703	$16.4^{+0.36}_{-0.36}$	$16.4^{+0.36}_{-0.36}$	$23.9^{+1.72}_{-1.72}$	$14.9^{+0.94}_{-0.94}$	$8.7^{+2.5}_{-2.5}$	< 340	< 340	< 340	1229	
092832.4+041517	4192	142.1354	+4.2585	16.4	55.8	0.440	2.053	$17.9^{+0.65}_{-0.65}$	$17.9^{+0.65}_{-0.65}$	$141^{+0.77}_{-0.77}$	$8.3^{+1.21}_{-1.21}$	$8.3^{+1.21}_{-1.21}$	< 330	< 330	< 330	1136	
092844.0+005318	8858	142.1835	+0.8885	8.9	26.9	0.318	2.018	$2.38^{+0.68}_{-0.68}$	$13.1^{+0.65}_{-0.65}$	$33.5^{+0.77}_{-0.77}$	$4.97^{+0.74}_{-0.74}$	$11.9^{+8.5}_{-8.5}$	$11.9^{+8.5}_{-8.5}$	$22.0^{+4.09}_{-4.09}$	$22.0^{+4.09}_{-4.09}$	1228	
092846.5+000536	10287	142.1940	+0.0157	19.8	38.4	0.344	2.650	$1.45^{+0.88}_{-0.88}$	$25.6^{+0.86}_{-0.86}$	$56^{+1.6}_{-1.6}$	$11.0^{+0.99}_{-0.99}$	$16.5^{+1.72}_{-1.72}$	$2.6^{+0.75}_{-0.75}$	$2.6^{+0.75}_{-0.75}$	$2.6^{+0.75}_{-0.75}$	1226	
092859.0+045322	4029	142.2462	+4.0923	52.6	113.0	0.259	3.325	$4.0^{+0.84}_{-0.84}$	$24.8^{+0.84}_{-0.84}$	$24.8^{+0.84}_{-0.84}$	76^{+27}_{-27}	$11.8^{+1.88}_{-1.88}$	48^{+44}_{-44}	$4.7^{+1.73}_{-1.73}$	$20.0^{+4.73}_{-4.73}$	1152	
092900.0-003920	5593	142.2502	-0.6557	6.1	44.5	0.503	1.722	$12.1^{+0.53}_{-0.53}$	$20.0^{+0.70}_{-0.70}$	$20.0^{+0.70}_{-0.70}$	$113^{+0.70}_{-0.70}$	$7.1^{+1.52}_{-1.52}$	< 290	< 290	< 290 </		

Table 4: continued.

Cluster (eFEDS I+)	ID_SRC	RA (deg)	Dec (deg)	\mathcal{L}_{ext}	\mathcal{L}_{det}	R_{500} (arcmin)	T (keV)	L_X (10^{42} erg s $^{-1}$)	L_{bol} (10^{42} erg s $^{-1}$)	M_{gas} (10^{12} M $_{\odot}$)	Y_X (10^{12} M $_{\odot}$ keV)	T_{ex} (keV)	$L_{\text{bol,ex}}$ (10^{42} erg s $^{-1}$)	t_{exp} (s)			
093138.7-020933	5201	142.9115	-2.1593	42.7	62.5	0.245	2.631	$1.92^{+0.86}_{-0.33}$	$7.5^{+1.3}_{-1.5}$	$18.1^{+1.1}_{-1.0}$	$7.3^{+3.9}_{-2.0}$	$2.00^{+1.18}_{-0.59}$	$5.6^{+1.3}_{-1.4}$	$13.7^{+3.9}_{-3.6}$	2462		
093141.2-004717	1705	142.9219	-0.7883	13.7	30.5	0.093	4.644	$1.02^{+0.23}_{-0.15}$	$2.51^{+0.35}_{-0.39}$	$1.27^{+0.41}_{-0.41}$	<1.3	$1.11^{+0.29}_{-0.29}$	<1.3	<2.6	1230		
093149.8-020143	6494	142.9576	-2.0289	27.5	39.9	0.134	3.094	$1.040^{+0.167}_{-0.167}$	$4.21^{+0.35}_{-0.35}$	$2.15^{+0.26}_{-0.26}$	$1.18^{+0.26}_{-0.26}$	$1.24^{+0.32}_{-0.32}$	$1.05^{+0.27}_{-0.27}$	$1.76^{+0.36}_{-0.36}$	$3.45^{+0.78}_{-0.85}$	2483	
093151.3-002212	836	142.9638	-0.3701	54.0	307.1	0.336	2.824	$2.27^{+0.67}_{-0.67}$	$48.1^{+1.42}_{-1.42}$	$119^{+1.31}_{-1.31}$	$12.2^{+1.5}_{-1.5}$	$2.02^{+0.45}_{-0.45}$	$27.8^{+3.9}_{-3.9}$	$2.6^{+0.43}_{-0.43}$	$66^{+1.1}_{-1.1}$	1236	
093207.5-021317	1674	143.0316	-2.2215	36.1	133.5	0.666	1.648	$3.00^{+0.40}_{-0.40}$	$49.0^{+0.60}_{-0.60}$	$141^{+1.52}_{-1.52}$	$10.7^{+2.3}_{-2.3}$	$3.3^{+0.28}_{-0.28}$	$32^{+0.3}_{-0.3}$	$29.7^{+4.9}_{-4.9}$	$85^{+3.7}_{-3.7}$	2463	
093222.0+012412	7346	143.0918	+1.4035	6.1	32.0	0.536	1.613	$6.9^{+1.39}_{-1.39}$	$13.6^{+1.05}_{-1.05}$	$56^{+1.39}_{-1.39}$	<6.8	<12	<20	<85	1230		
093231.0+010617	4873	143.1293	+1.1050	22.2	56.4	0.644	1.772	$2.60^{+1.77}_{-1.77}$	$72^{+1.2}_{-1.2}$	$189^{+1.4}_{-1.4}$	$13.9^{+3.3}_{-3.3}$	$36^{+2.3}_{-2.3}$	$3.0^{+1.37}_{-1.37}$	50^{+12}_{-12}	141^{+51}_{-34}	1230	
093232.8-015152	10734	143.1367	-1.8647	8.0	24.9	0.553	1.516	$5.6^{+1.08}_{-1.08}$	$14.2^{+1.2}_{-1.2}$	$52^{+2.2}_{-2.2}$	$5.3^{+1.5}_{-1.5}$	<160	$10.7^{+1.65}_{-1.65}$	$11.0^{+4.4}_{-3.3}$	<150	2134	
093253.8+025917	5631	143.2244	+2.9882	7.2	23.7	0.093	4.279	$8.9^{+1.46}_{-1.46}$	$19.4^{+0.84}_{-0.84}$	<2.8	<0.31	<3.8	$8.3^{+0.67}_{-0.67}$	<0.19	<0.91	1234	
093301.3+024301	12582	143.2558	+2.7170	10.4	16.2	0.838	1.345	$12.0^{+1.19}_{-1.19}$	$21.4^{+0.93}_{-0.93}$	108^{+84}_{-84}	<11	<260	$10.6^{+1.3}_{-1.3}$	<240	1234		
093302.7-010145	5763	143.2616	-1.0292	45.3	66.4	0.356	2.676	$3.8^{+1.53}_{-1.53}$	$28.1^{+1.2}_{-1.2}$	$87^{+4.7}_{-4.7}$	$12.0^{+2.1}_{-2.1}$	$22.4^{+5.0}_{-5.0}$	$3.6^{+8.2}_{-8.2}$	69^{+38}_{-38}	1232		
093316.6+004619	13784	143.3195	+0.7721	9.2	21.2	0.347	2.457	$5.5^{+1.53}_{-1.53}$	<8.2	<39	<6.3	<66	$8.1^{+1.56}_{-1.56}$	<3.3	<3.3	1230	
093329.3+000334	5618	143.3725	+0.0596	14.3	43.6	0.395	2.104	$3.2^{+1.55}_{-1.55}$	$21.7^{+3.9}_{-3.9}$	63^{+31}_{-31}	$7.6^{+1.5}_{-1.5}$	$24.0^{+4.7}_{-4.7}$	$5.0^{+8.6}_{-8.5}$	$16.2^{+3.7}_{-3.7}$	54^{+38}_{-38}	1230	
093332.1+020933	6577	143.3841	+2.1594	6.7	24.9	0.838	1.373	$8.8^{+1.14}_{-1.14}$	$61^{+1.1}_{-1.1}$	270^{+180}_{-180}	$10.7^{+3.4}_{-3.4}$	<350	$10.6^{+6.7}_{-6.7}$	189^{+117}_{-117}	1231		
093403.5-001422	900	143.5148	-0.2397	79.7	279.5	0.240	3.533	$2.13^{+0.62}_{-0.62}$	$31.7^{+0.77}_{-0.77}$	$78.1^{+1.0}_{-1.0}$	$11.2^{+1.5}_{-1.5}$	$24.5^{+7.2}_{-7.2}$	$2.48^{+0.78}_{-0.78}$	$20.8^{+4.5}_{-4.5}$	$54.4^{+12.9}_{-12.9}$	1226	
093431.3-002309	1641	143.6304	-0.3860	35.5	87.4	0.342	2.815	$4.7^{+1.27}_{-1.27}$	$57^{+3.6}_{-3.6}$	$187^{+1.9}_{-1.9}$	$18.1^{+2.3}_{-2.3}$	82^{+228}_{-228}	$4.7^{+7.6}_{-7.6}$	$147^{+9.6}_{-9.6}$	10.03		
093436.1+051533	9995	143.6508	+5.2594	22.6	36.6	0.341	3.141	$9.3^{+1.82}_{-1.82}$	$48.3^{+0.62}_{-0.62}$	$223^{+1.57}_{-1.57}$	$19.5^{+2.8}_{-2.8}$	640^{+160}_{-160}	$10.5^{+2.1}_{-2.1}$	$38.3^{+3.9}_{-3.9}$	183^{+73}_{-73}	336	
093456.1+031518	7091	143.7340	+3.2552	16.6	32.9	0.085	4.207	$6.61^{+0.24}_{-0.24}$	$1.31^{+0.25}_{-0.25}$	$1.645^{+0.14}_{-0.14}$	$1.31^{+0.36}_{-0.36}$	$0.206^{+0.059}_{-0.059}$	$0.116^{+0.057}_{-0.057}$	$0.59^{+0.076}_{-0.076}$	$0.250^{+0.076}_{-0.076}$	1238	
093500.7+005417	649	143.7532	+0.9048	104.4	330.3	0.361	2.973	$3.10^{+0.67}_{-0.67}$	$77.8^{+0.97}_{-0.97}$	$214^{+2.2}_{-2.2}$	$17.4^{+0.95}_{-0.95}$	54^{+18}_{-18}	$4.1^{+0.27}_{-0.27}$	$46.5^{+0.95}_{-0.95}$	145^{+17}_{-17}	1243	
093513.0+004757	213	143.8046	+0.7994	332.8	836.9	0.356	4.104	$7.3^{+1.56}_{-1.56}$	$249^{+1.4}_{-1.4}$	980^{+160}_{-160}	$62.7^{+7.7}_{-7.7}$	420^{+160}_{-160}	$5.6^{+1.6}_{-1.6}$	187^{+36}_{-36}	650^{+174}_{-174}	1233	
093520.7+003448	4394	143.8363	+0.5890	15.3	65.7	0.355	2.308	$2.15^{+1.13}_{-1.13}$	$28.8^{+1.4}_{-1.4}$	72^{+14}_{-14}	$9.8^{+1.54}_{-1.54}$	$21.6^{+1.07}_{-1.07}$	$2.43^{+1.49}_{-1.49}$	$22.7^{+7.9}_{-7.9}$	1174^{+120}_{-120}	1232	
093520.9+023234	82	143.8374	+2.5429	175.9	1645.8	0.516	2.977	$3.73^{+1.46}_{-1.46}$	$28.7^{+1.46}_{-1.46}$	1190^{+170}_{-170}	$19.5^{+2.8}_{-2.8}$	237^{+48}_{-48}	$7.0^{+1.5}_{-1.5}$	185^{+54}_{-54}	740^{+140}_{-140}	1236	
093522.2+023239	1242	143.8427	+3.3915	86.3	248.3	0.324	3.120	$2.43^{+0.67}_{-0.67}$	$49.2^{+1.71}_{-1.71}$	$125^{+1.10}_{-1.10}$	$15.4^{+0.60}_{-0.60}$	$1.5^{+0.21}_{-0.21}$	$2.71^{+0.70}_{-0.70}$	$33.4^{+1.41}_{-1.41}$	88^{+14}_{-14}	1237	
093525.6+023445	12009	143.8570	+2.5793	35.4	39.7	0.503	2.272	$2.87^{+0.62}_{-0.62}$	$58.3^{+0.65}_{-0.65}$	$156^{+1.30}_{-1.30}$	$19.7^{+3.5}_{-3.5}$	56^{+20}_{-20}	$1.7^{+0.63}_{-0.63}$	$51.7^{+10.2}_{-10.2}$	143^{+30}_{-30}	1236	
093525.9+03101	3773	143.8580	+3.8503	6.2	126.1	1.162	1.162	$2.8^{+1.96}_{-1.96}$	162^{+83}_{-83}	490^{+200}_{-200}	$16.2^{+4.4}_{-4.4}$	47^{+14}_{-14}	$1.85^{+0.97}_{-0.97}$	151^{+70}_{-70}	400^{+210}_{-210}	1241	
093531.4+022710	2609	143.8811	+2.4530	36.6	95.3	0.225	2.976	$3.05^{+1.78}_{-1.78}$	$12.7^{+1.73}_{-1.73}$	$34.6^{+1.82}_{-1.82}$	$12.7^{+1.73}_{-1.73}$	52^{+51}_{-51}	$2.40^{+1.54}_{-1.54}$	$22.7^{+4.4}_{-4.4}$	174^{+87}_{-87}	1241	
093544.2-000339	6324	143.9342	-0.0609	20.5	51.9	0.347	2.565	$5.0^{+1.37}_{-1.37}$	$37.3^{+1.46}_{-1.46}$	95^{+25}_{-25}	$10.7^{+0.84}_{-0.84}$	237^{+48}_{-48}	$5.0^{+1.48}_{-1.48}$	76^{+54}_{-54}	829^{+110}_{-110}	1236	
093546.3-001115	1761	143.9433	-0.0211	19.8	146.8	0.339	2.611	$4.7^{+1.22}_{-1.22}$	$43.8^{+1.75}_{-1.75}$	$144^{+1.59}_{-1.59}$	$12.5^{+2.3}_{-2.3}$	57^{+20}_{-20}	$5.9^{+0.63}_{-0.63}$	$26.0^{+7.5}_{-7.5}$	98^{+28}_{-28}	833	
093612.7+001650	4455	144.0529	+0.2807	17.0	58.5	0.358	2.402	$1.82^{+1.71}_{-1.71}$	$38.1^{+1.82}_{-1.82}$	92^{+14}_{-14}	$11.9^{+2.0}_{-2.0}$	$22.9^{+15.7}_{-15.7}$	52^{+17}_{-17}	$1.92^{+2.00}_{-2.00}$	$30.3^{+21.7}_{-21.7}$	75^{+20}_{-20}	802
093630.8+031838	4848	144.1287	+3.3106	11.5	57.1	0.405	2.203	$2.38^{+0.68}_{-0.68}$	<14	<38	<8.6	<30	$2.39^{+0.49}_{-0.49}$	<12	<33	1242^{+120}_{-120}	1242
093707.4+044831	11748	144.2810	+3.8089	12.6	20.7	0.279	2.503	$10.4^{+1.16}_{-1.16}$	$30.7^{+1.12}_{-1.12}$	$37.0^{+0.95}_{-0.95}$	$18.1^{+2.04}_{-2.04}$	$5.21^{+0.99}_{-0.99}$	$18.1^{+2.04}_{-2.04}$	$8.6^{+1.6}_{-1.6}$	$23.9^{+14.8}_{-14.8}$	1239	
093709.7+014143	6251	144.2908	+1.6954	27.9	50.0	0.377	2.426	$1.80^{+0.66}_{-0.66}$	$51.1^{+1.61}_{-1.61}$	$119^{+1.88}_{-1.88}$	$15.2^{+2.00}_{-2.00}$	$28.1^{+1.88}_{-1.88}$	$2.62^{+2.90}_{-2.90}$	$41.6^{+1.9}_{-1.9}$	110^{+38}_{-38}	1042^{+118}_{-118}	1042
093712.8+031651	38	144.3286	+3.2810	19.7	26.0	0.247	2.469	$3.3^{+1.29}_{-1.29}$	$12.7^{+1.54}_{-1.54}$	$37.1^{+1.44}_{-1.44}$	$0.25^{+0.25}_{-0.25}$	<7.9	$2.11^{+0.72}_{-0.72}$	<0.47	<1.3	1238	
093742.8+033841	6038	144.4285	+3.6450	19.4	48.0	0.620	1.767	$1.63^{+1.66}_{-1.66}$	69^{+15}_{-15}	159^{+33}_{-33}	$13.7^{+3.3}_{-3.3}$	$22.9^{+15.7}_{-15.7}$	52^{+17}_{-17}	$1.69^{+0.82}_{-0.82}$	118^{+38}_{-38}	1247	
093744.1+024536	3372	144.4341	+2.7600	11.8	66.6	0.024	8.111	$0.282^{+0.144}_{-0.144}$	$1.04^{+1.16}_{-1.16}$	$0.071^{+0.016}_{-0.016}$	<0.10	<0.03	$0.269^{+0.083}_{-0.083}$	<0.04	<0.19	1187	
093830.5+04523	10322	144.6272	+4.2564	20.8	37.7	0.262	2.559	$3.4^{+1.50}_{-1.50}$	$13.0^{+0.98}_{-0.98}$	$37.0^{+1.06}_{-1.06}$	$6.08^{+1.13}_{-1.13}$	$19.8^{+3.5}_{-3.5}$	$3.4^{+1.12}_{-1.12}$	$11.5^{+1.9}_{-1.9}$	$34.1^{+21.2}_{-21.2}$	1366	
093938.3+022118	1594	144.9096	+4.3717	65.2	164.9	0.369	2.717	$1.3^{+1.4}_{-1.4}$	$153^{+1.65}_{-1.65}$	$14.6^{+1.5}_{-1.5}$	57^{+17						

Table 5: X-ray best fitting parameters for [Vikhlinin et al. \(2006\)](#) model: $n_e^2(r) = n_0^2 \left(\frac{r}{r_s}\right)^{-\alpha} \left(1 + \left(\frac{r}{r_s}\right)^2\right)^{-3\beta+\alpha/2} \left(1 + \left(\frac{r}{r_s}\right)^3\right)^{-\epsilon/3}$.

Cluster (eFEDS J+)	ID_SRC	n_0 (10^{-7} cm $^{-6}$)	r_s (arcsec)	ϵ	β	α
082626.5-003429	28993	$4.0^{+36.4}_{-32.7}$	72^{+65}_{-52}	$2.5^{+1.7}_{-1.9}$	$1.56^{+0.66}_{-0.77}$	$1.09^{+1.01}_{-0.71}$
082751.7-002853	11248	$1.9^{+32.7}_{-1.6}$	72^{+67}_{-46}	$2.6^{+1.6}_{-1.7}$	$1.59^{+0.64}_{-0.77}$	$1.54^{+1.17}_{-0.98}$
082808.7-001003	4800	$0.75^{+3.53}_{-1.30}$	224^{+87}_{-82}	$1.5^{+1.8}_{-1.9}$	$1.16^{+0.90}_{-0.57}$	$1.42^{+0.34}_{-0.53}$
082820.5-000721	4169	$8.9^{+3.8}_{-3.0}$	125^{+72}_{-62}	$3.0^{+1.9}_{-1.9}$	$1.62^{+0.77}_{-0.87}$	$1.12^{+0.53}_{-0.74}$
082840.6-000500	7991	$1.7^{+1.21}_{-1.4}$	123^{+60}_{-47}	$2.6^{+1.8}_{-1.8}$	$1.39^{+0.74}_{-0.70}$	$1.38^{+0.56}_{-0.91}$
082859.9+010756	14973	$0.51^{+0.62}_{-0.52}$	296^{+115}_{-98}	$2.5^{+1.8}_{-1.9}$	$1.49^{+0.72}_{-0.80}$	$0.56^{+0.44}_{-0.37}$
082952.7+002139	7528	$7.4^{+43.9}_{-6.9}$	59^{+41}_{-23}	$2.4^{+1.8}_{-1.8}$	$1.62^{+0.80}_{-0.75}$	$1.53^{+0.37}_{-1.02}$
082955.4+004131	3810	$8.0^{+42.6}_{-4.2}$	110^{+64}_{-42}	$2.5^{+1.8}_{-1.8}$	$1.62^{+0.62}_{-0.76}$	$1.37^{+0.56}_{-0.79}$
083040.7+023219	9837	$6.2^{+5.5}_{-5.1}$	65^{+47}_{-32}	$2.6^{+1.6}_{-1.6}$	$1.63^{+0.66}_{-0.76}$	$1.34^{+0.57}_{-0.78}$
083110.5+015616	5601	$1.4^{+6.1}_{-1.1}$	173^{+93}_{-62}	$2.7^{+1.5}_{-1.6}$	$1.60^{+0.56}_{-0.60}$	$1.16^{+0.50}_{-0.69}$
083120.5+005257	9594	$3.5^{+17.6}_{-3.0}$	90^{+63}_{-30}	$2.4^{+1.9}_{-1.9}$	$1.62^{+0.67}_{-0.82}$	$1.38^{+0.66}_{-0.88}$
083120.5+030949	11134	$1.9^{+1.0}_{-1.5}$	67^{+109}_{-53}	$2.6^{+1.8}_{-1.8}$	$1.49^{+0.80}_{-0.78}$	$1.35^{+0.58}_{-0.93}$
083125.9+015533	2659	$1.9^{+6.8}_{-1.3}$	179^{+52}_{-48}	$2.6^{+1.5}_{-1.5}$	$1.16^{+0.80}_{-0.57}$	$1.42^{+0.43}_{-0.75}$
083137.9+004632	3725	$0.85^{+14.29}_{-0.64}$	111^{+52}_{-32}	$2.0^{+1.8}_{-1.8}$	$1.35^{+0.72}_{-0.76}$	$1.89^{+0.37}_{-0.44}$
083146.7-012849	4403	$1.03^{+0.81}_{-0.81}$	112^{+74}_{-56}	$2.5^{+1.4}_{-1.7}$	$1.42^{+0.73}_{-0.73}$	$1.70^{+0.44}_{-0.77}$
083149.4+005230	5463	13^{+41}_{-10}	59^{+27}_{-22}	$2.3^{+1.6}_{-1.6}$	$1.55^{+0.67}_{-0.77}$	$1.12^{+0.77}_{-0.88}$
083153.6+012530	2600	$0.74^{+4.24}_{-3.53}$	197^{+97}_{-81}	$2.2^{+1.9}_{-1.9}$	$1.37^{+0.75}_{-0.71}$	$1.56^{+0.58}_{-0.69}$
083204.4+041907	3593	$1.14^{+3.3}_{-0.69}$	318^{+97}_{-105}	$2.5^{+1.7}_{-1.7}$	$1.60^{+0.61}_{-0.75}$	$1.07^{+0.32}_{-0.44}$
083228.0-000656	7396	$1.08^{+12.05}_{-0.88}$	95^{+84}_{-57}	$2.8^{+1.5}_{-1.8}$	$1.54^{+0.66}_{-0.75}$	$1.62^{+0.23}_{-0.95}$
083238.8-003200	8565	$2.9^{+7.1}_{-4.1}$	119^{+59}_{-42}	$2.8^{+1.6}_{-1.6}$	$1.72^{+0.53}_{-0.78}$	$0.93^{+0.61}_{-0.59}$
083249.9+031737	10398	$1.06^{+24.28}_{-0.77}$	92^{+145}_{-73}	$2.5^{+1.7}_{-1.7}$	$1.48^{+0.72}_{-0.79}$	$1.21^{+1.61}_{-0.85}$
083310.2+030136	15959	$0.42^{+1.33}_{-0.88}$	310^{+180}_{-150}	$2.7^{+1.6}_{-1.6}$	$1.08^{+0.89}_{-0.75}$	$0.56^{+0.39}_{-0.36}$
083315.5+000623	6869	$0.44^{+0.30}_{-0.30}$	186^{+77}_{-77}	$2.3^{+1.7}_{-1.7}$	$1.45^{+0.72}_{-0.72}$	$1.44^{+0.30}_{-0.70}$
083321.1+012644	2879	$1.02^{+3.93}_{-0.76}$	153^{+67}_{-60}	$2.7^{+1.6}_{-1.8}$	$1.67^{+0.58}_{-0.78}$	$1.73^{+0.31}_{-0.54}$
083322.6-011128	6302	$1.5^{+6.6}_{-2.2}$	134^{+68}_{-68}	$2.6^{+1.6}_{-1.7}$	$1.64^{+0.60}_{-0.70}$	$1.21^{+1.28}_{-0.78}$
083330.4+050427	2528	$0.231^{+0.69}_{-0.087}$	234^{+85}_{-75}	$1.7^{+1.8}_{-1.2}$	$0.91^{+0.83}_{-0.42}$	$1.88^{+0.20}_{-0.24}$
083341.0-002943	6767	$8.2^{+9.9}_{-7.2}$	29^{+26}_{-15}	$1.10^{+1.10}_{-0.78}$	$0.65^{+0.30}_{-0.26}$	$1.6^{+1.2}_{-0.39}$
083345.8+004208	2984	$5.2^{+2.2}_{-2.2}$	97^{+38}_{-38}	$2.7^{+1.6}_{-1.6}$	$1.50^{+0.78}_{-0.78}$	$1.36^{+0.82}_{-0.80}$
083401.5-001337	4258	$0.27^{+0.84}_{-0.15}$	198^{+122}_{-95}	$2.4^{+1.8}_{-1.8}$	$1.55^{+0.67}_{-0.78}$	$0.83^{+0.58}_{-0.58}$
083402.5+023437	6409	$8.17^{+3.5}_{-3.5}$	67^{+37}_{-37}	$2.8^{+1.6}_{-1.6}$	$1.64^{+0.60}_{-0.69}$	$1.21^{+0.73}_{-0.78}$
083403.7+012131	4634	$3.5^{+6.9}_{-6.9}$	68^{+56}_{-42}	$2.7^{+1.6}_{-1.8}$	$1.61^{+0.61}_{-0.70}$	$2.0^{+1.2}_{-0.85}$
083412.7+035856	1092	$0.60^{+3.21}_{-0.45}$	183^{+79}_{-50}	$2.5^{+1.7}_{-1.7}$	$1.55^{+0.65}_{-0.75}$	$1.69^{+0.81}_{-0.84}$
083422.7+034537	3240	$2.5^{+8.3}_{-3.5}$	62^{+64}_{-64}	$2.6^{+1.7}_{-1.7}$	$1.51^{+0.79}_{-0.79}$	$2.15^{+0.50}_{-0.50}$
083427.0-015612	12633	$0.42^{+1.11}_{-0.27}$	224^{+76}_{-52}	$2.9^{+1.4}_{-1.4}$	$1.54^{+0.66}_{-0.77}$	$0.82^{+0.51}_{-0.51}$
083431.0+034208	8206	$0.124^{+0.62}_{-0.028}$	510^{+160}_{-160}	$2.4^{+1.7}_{-1.7}$	$1.59^{+0.63}_{-0.77}$	$0.24^{+0.26}_{-0.17}$
083435.6+050159	4593	$0.39^{+2.30}_{-0.24}$	128^{+84}_{-94}	$2.3^{+1.7}_{-1.7}$	$1.53^{+0.69}_{-0.86}$	$1.15^{+0.56}_{-0.89}$
083457.7+052033	9892	$4.0^{+12.3}_{-3.6}$	88^{+52}_{-35}	$2.6^{+1.7}_{-1.7}$	$1.64^{+0.60}_{-0.79}$	$0.93^{+0.77}_{-0.65}$
083503.2+010756	3874	$0.48^{+1.82}_{-0.32}$	213^{+90}_{-60}	$2.8^{+1.5}_{-1.8}$	$1.50^{+0.69}_{-0.77}$	$1.51^{+0.29}_{-0.33}$
083509.0+001542	1360	30^{+6}_{-22}	91^{+37}_{-47}	$2.6^{+1.6}_{-1.7}$	$1.67^{+0.67}_{-0.67}$	$0.78^{+0.34}_{-0.34}$
083532.5+030911	3198	$0.44^{+5.84}_{-3.14}$	101^{+54}_{-54}	$2.5^{+1.7}_{-1.7}$	$1.41^{+0.67}_{-0.73}$	$2.24^{+0.50}_{-0.59}$
083615.7+024420	12572	$1.04^{+1.31}_{-1.11}$	95^{+65}_{-56}	$2.7^{+1.7}_{-1.8}$	$1.61^{+0.79}_{-0.79}$	$1.39^{+0.34}_{-0.34}$
083626.4+043821	5783	$1.9^{+13.9}_{-1.6}$	100^{+77}_{-39}	$2.7^{+1.6}_{-1.7}$	$1.53^{+0.69}_{-0.69}$	$1.74^{+0.34}_{-0.78}$
083651.3+030002	197	$5.7^{+20.9}_{-20.8}$	112^{+66}_{-52}	$1.25^{+1.11}_{-0.90}$	$0.61^{+0.32}_{-0.39}$	$1.72^{+0.16}_{-0.31}$
083654.6+025954	16471	$5.7^{+3.8}_{-3.8}$	112^{+66}_{-66}	$1.25^{+1.10}_{-0.90}$	$0.61^{+0.32}_{-0.39}$	$1.72^{+0.16}_{-0.16}$
083713.3+034110	10475	$3.0^{+20.2}_{-2.4}$	107^{+52}_{-45}	$2.6^{+1.7}_{-1.7}$	$1.70^{+0.58}_{-0.83}$	$1.11^{+0.74}_{-0.74}$
083723.6+012413	4731	$0.63^{+3.45}_{-3.45}$	179^{+82}_{-70}	$2.3^{+1.7}_{-1.8}$	$1.52^{+0.80}_{-0.80}$	$1.57^{+0.33}_{-0.60}$
083743.8-014128	5321	$3.6^{+3.1}_{-3.1}$	108^{+70}_{-57}	$2.3^{+1.8}_{-1.8}$	$1.30^{+0.68}_{-0.68}$	$1.42^{+0.48}_{-0.85}$
083757.1-014217	6303	$1.11^{+32.53}_{-0.83}$	61^{+99}_{-47}	$2.4^{+1.8}_{-1.8}$	$1.53^{+0.67}_{-0.75}$	$1.37^{+0.36}_{-0.94}$
083759.5-003643	2456	$0.193^{+0.390}_{-0.063}$	178^{+52}_{-46}	$1.6^{+2.0}_{-1.6}$	$0.76^{+0.83}_{-0.95}$	$2.28^{+0.19}_{-0.19}$
083802.9+015626	4511	$4.9^{+9.9}_{-3.9}$	126^{+62}_{-48}	$2.5^{+1.8}_{-1.7}$	$1.36^{+0.78}_{-0.76}$	$0.93^{+0.53}_{-0.58}$
083806.9-003600	5386	$0.188^{+0.261}_{-0.072}$	420^{+150}_{-160}	$3.0^{+1.6}_{-2.1}$	$1.55^{+0.62}_{-0.82}$	$0.53^{+0.58}_{-0.37}$
083807.6+002501	19692	$0.34^{+0.47}_{-0.16}$	373^{+99}_{-99}	$2.7^{+1.6}_{-1.7}$	$1.58^{+0.64}_{-0.75}$	$0.76^{+0.55}_{-0.53}$
083809.4-020450	10843	$5.4^{+36.0}_{-4.8}$	66^{+108}_{-36}	$3.1^{+1.5}_{-2.3}$	$1.58^{+0.68}_{-0.94}$	$1.10^{+0.17}_{-0.80}$
083810.1+031520	3035	$0.168^{+0.453}_{-0.063}$	176^{+62}_{-62}	$0.61^{+1.92}_{-0.49}$	$0.458^{+0.498}_{-0.097}$	$2.14^{+0.19}_{-0.70}$
083811.8-015934	53	$7.2^{+10.9}_{-5.1}$	98^{+40}_{-35}	$2.6^{+1.6}_{-1.7}$	$1.57^{+0.75}_{-0.78}$	$2.39^{+0.19}_{-0.19}$
083817.4+041821	6136	$0.173^{+0.340}_{-0.072}$	260^{+94}_{-94}	$2.0^{+1.9}_{-1.9}$	$1.03^{+0.91}_{-0.53}$	$1.68^{+0.21}_{-0.26}$
083817.5-021704	6195	$0.46^{+1.06}_{-0.41}$	252^{+89}_{-88}	$2.1^{+1.7}_{-1.7}$	$1.16^{+0.83}_{-0.83}$	$1.56^{+0.25}_{-0.25}$
083834.1+020643	3905	$2.3^{+1.7}_{-1.7}$	134^{+48}_{-48}	$1.9^{+2.1}_{-1.4}$	$1.31^{+0.81}_{-0.66}$	$1.41^{+0.43}_{-0.57}$
083840.3+044416	8186	$0.41^{+1.84}_{-0.76}$	207^{+94}_{-81}	$2.4^{+1.8}_{-1.8}$	$1.42^{+0.72}_{-0.72}$	$1.28^{+0.36}_{-0.63}$
083840.6-004134	7463	$0.52^{+1.01}_{-0.33}$	231^{+90}_{-80}	$2.5^{+1.7}_{-1.7}$	$1.64^{+0.63}_{-0.63}$	$0.72^{+0.51}_{-0.49}$
083856.9+030743	7902	$3.8^{+20.2}_{-20.2}$	73^{+78}_{-34}	$2.5^{+1.6}_{-1.6}$	$1.66^{+0.80}_{-0.80}$	$1.32^{+0.27}_{-0.96}$
083857.5+020846	1806	$0.76^{+1.86}_{-0.42}$	266^{+109}_{-99}	$2.3^{+1.8}_{-1.8}$	$1.40^{+0.73}_{-0.70}$	$1.49^{+0.23}_{-0.34}$
083858.5-015032	6026	$0.96^{+0.82}_{-0.82}$	84^{+44}_{-44}	$2.4^{+1.8}_{-1.8}$	$1.73^{+0.94}_{-0.94}$	$1.52^{+0.10}_{-0.10}$
083859.3+022841	3315	$2.0^{+15.3}_{-1.7}$	113^{+68}_{-68}	$2.5^{+1.8}_{-1.7}$	$1.59^{+0.63}_{-0.75}$	$1.64^{+0.44}_{-0.87}$
083900.6+020057	736	$4.2^{+2.1}_{-1.01}$	85^{+28}_{-33}	$2.4^{+1.7}_{-1.7}$	$0.80^{+0.89}_{-0.89}$	$2.07^{+0.23}_{-0.32}$
083903.5-011454	7445	$1.05^{+2.34}_{-0.79}$	181^{+79}_{-62}	$2.7^{+1.6}_{-1.8}$	$1.59^{+0.63}_{-0.74}$	$0.89^{+0.65}_{-0.60}$
083914.7-021226	5360	$12.7^{+46.3}_{-9.2}$	34^{+10}_{-10}	$1.56^{+0.50}_{-0.46}$	$0.47^{+0.23}_{-0.19}$	$1.55^{+0.64}_{-0.86}$
083916.7-020552	7669	$5.6^{+6.5}_{-3.0}$	42.4^{+72}_{-72}	$0.61^{+0.26}_{-0.28}$	$0.61^{+0.16}_{-0.16}$	$1.34^{+0.37}_{-0.36}$
083917.9-020839	15489	$0.30^{+1.02}_{-0.18}$	199^{+86}_{-70}	$2.0^{+1.9}_{-1.9}$	$1.68^{+0.63}_{-0.78}$	$1.03^{+0.60}_{-0.65}$
083921.0-014149	12407	$1.9^{+2.7}_{-1.7}$	146^{+45}_{-40}	$2.53^{+1.25}_{-1.25}$	$0.88^{+0.60}_{-0.39}$	$0.80^{+0.57}_{-0.47}$
083927.0-021357	10377	$0.31^{+1.06}_{-0.16}$	190^{+100}_{-120}	$2.9^{+1.6}_{-1.6}$	$1.41^{+0.80}_{-0.80}</math$	

Table 5: continued.

Cluster (eFEDS J+)	ID_SRC	n_0 10^{-7} cm^{-6}	r_s arcsec	ϵ	β	α
083936.0+011445	2898	$1.7^{+51.0}_{-1.6}$	83^{+91}_{-43}	$2.5^{+1.8}_{-1.7}$	$1.32^{+0.77}_{-0.68}$	$1.86^{+0.43}_{-1.11}$
083937.8+014631	7652	$1.4^{+6.7}_{-0.7}$	136^{+64}_{-50}	$2.7^{+1.6}_{-1.7}$	$1.65^{+0.68}_{-0.77}$	$1.31^{+0.50}_{-0.72}$
083940.8+010416	2832	$0.24^{+0.51}_{-0.42}$	247^{+76}_{-83}	$2.5^{+1.7}_{-1.7}$	$1.28^{+0.81}_{-0.64}$	$1.82^{+0.18}_{-0.25}$
083945.5+031556	7213	$5.3^{+57.9}_{-5.1}$	47^{+22}_{-22}	$2.6^{+1.7}_{-1.7}$	$1.67^{+0.88}_{-0.77}$	$1.62^{+0.37}_{-1.08}$
083955.0+022425	3270	$0.62^{+1.85}_{-0.48}$	153^{+97}_{-58}	$2.5^{+1.7}_{-1.6}$	$1.34^{+0.83}_{-0.66}$	$0.80^{+0.62}_{-0.55}$
084000.0-013109	7217	$1.06^{+4.80}_{-0.73}$	150^{+50}_{-50}	$1.6^{+2.1}_{-1.6}$	$0.82^{+0.88}_{-0.39}$	$1.27^{+0.38}_{-0.68}$
084001.6+042452	4839	$0.50^{+0.37}_{-0.35}$	128^{+57}_{-54}	$2.3^{+1.9}_{-1.7}$	$1.49^{+0.66}_{-0.76}$	$1.91^{+0.70}_{-0.70}$
084003.2+003008	2568	$0.68^{+18.55}_{-0.53}$	57^{+111}_{-46}	$2.7^{+1.6}_{-1.6}$	$1.53^{+0.69}_{-0.76}$	$1.33^{+1.54}_{-0.00}$
084004.8+013751	10272	$1.9^{+6.6}_{-1.5}$	98^{+34}_{-34}	$2.7^{+1.6}_{-1.6}$	$1.73^{+0.88}_{-0.84}$	$1.05^{+0.00}_{-0.00}$
084006.1+025913	2388	$1.4^{+6.4}_{-1.1}$	159^{+76}_{-61}	$2.5^{+1.8}_{-1.7}$	$1.67^{+0.83}_{-0.78}$	$1.52^{+0.33}_{-0.62}$
084011.6+034837	5544	12^{+49}_{-11}	60^{+41}_{-41}	$2.4^{+1.6}_{-1.6}$	$1.43^{+0.70}_{-0.70}$	$1.34^{+0.81}_{-0.89}$
084016.6+033951	6282	$5.2^{+26.8}_{-4.7}$	83^{+59}_{-36}	$2.6^{+1.8}_{-1.8}$	$1.64^{+0.59}_{-0.77}$	$1.19^{+0.79}_{-0.77}$
084021.6-022948	5406	$0.134^{+0.158}_{-0.040}$	307^{+113}_{-94}	$2.3^{+1.9}_{-1.8}$	$1.05^{+0.96}_{-0.56}$	$1.42^{+0.27}_{-0.35}$
084021.6+020132	5639	$1.13^{+2.90}_{-0.96}$	181^{+76}_{-62}	$2.6^{+1.8}_{-1.8}$	$1.62^{+0.60}_{-0.67}$	$0.92^{+0.54}_{-0.57}$
084034.5+023638	250	$0.49^{+0.26}_{-0.26}$	156^{+45}_{-45}	$2.0^{+2.0}_{-1.4}$	$0.89^{+0.82}_{-0.37}$	$2.56^{+0.16}_{-0.17}$
084035.8+044036	5844	16^{+110}_{-15}	53^{+45}_{-23}	$2.4^{+1.9}_{-1.8}$	$1.54^{+0.66}_{-0.71}$	$1.64^{+0.86}_{-1.18}$
084044.7+024108	8131	$6.1^{+28.2}_{-7.7}$	111^{+75}_{-75}	$2.7^{+1.6}_{-1.6}$	$1.53^{+0.66}_{-0.66}$	$1.23^{+0.57}_{-0.71}$
084051.7+014122	7662	$2.6^{+6.6}_{-2.1}$	142^{+71}_{-47}	$2.8^{+1.5}_{-1.7}$	$1.67^{+0.78}_{-0.78}$	$1.00^{+0.54}_{-0.62}$
084058.4+050407	7625	27^{+176}_{-25}	62^{+36}_{-31}	$2.6^{+1.7}_{-1.7}$	$1.60^{+0.61}_{-0.61}$	$1.30^{+1.04}_{-0.24}$
084102.1+044734	6014	$0.202^{+0.612}_{-0.094}$	237^{+61}_{-88}	$2.1^{+1.9}_{-1.9}$	$1.35^{+0.76}_{-0.76}$	$1.56^{+0.41}_{-0.41}$
084105.5+031639	1906	$0.68^{+2.64}_{-0.51}$	181^{+86}_{-69}	$2.6^{+1.6}_{-1.6}$	$1.53^{+0.63}_{-0.72}$	$1.79^{+0.24}_{-0.42}$
084107.2+050459	4300	17^{+65}_{-35}	38^{+21}_{-14}	$1.32^{+1.01}_{-0.89}$	$0.79^{+0.36}_{-0.39}$	$1.53^{+0.73}_{-0.77}$
084110.8+005200	5702	$2.2^{+3.7}_{-2.0}$	64^{+52}_{-32}	$3.1^{+1.5}_{-1.5}$	$1.79^{+0.78}_{-0.82}$	$1.67^{+0.82}_{-1.22}$
084111.8-001946	7983	$2.7^{+5.8}_{-2.1}$	148^{+66}_{-53}	$2.5^{+1.7}_{-1.6}$	$1.63^{+0.83}_{-0.68}$	$0.75^{+0.64}_{-0.52}$
084116.5+020700	9822	$6.8^{+51.1}_{-5.9}$	53^{+33}_{-31}	$1.47^{+1.01}_{-0.90}$	$0.96^{+0.64}_{-0.44}$	$1.10^{+0.10}_{-0.74}$
084124.1-023350	9149	$0.85^{+0.09}_{-0.65}$	136^{+61}_{-56}	$2.6^{+1.6}_{-1.6}$	$1.56^{+0.63}_{-0.71}$	$1.43^{+0.43}_{-0.75}$
084124.7+004636	6605	$1.9^{+11.4}_{-1.6}$	91^{+42}_{-39}	$2.8^{+1.5}_{-1.5}$	$1.30^{+0.78}_{-0.66}$	$1.65^{+0.54}_{-0.84}$
084129.0+002645	5591	$0.215^{+0.178}_{-0.098}$	163^{+71}_{-51}	$0.25^{+0.87}_{-0.49}$	$0.383^{+0.135}_{-0.097}$	$2.09^{+0.20}_{-0.22}$
084134.1+043503	7544	$0.51^{+4.0}_{-0.34}$	140^{+110}_{-100}	$2.6^{+1.9}_{-1.9}$	$1.52^{+0.69}_{-0.75}$	$0.95^{+0.66}_{-0.66}$
084135.0+010150	1644	$2.3^{+22.8}_{-2.0}$	92^{+51}_{-38}	$2.4^{+1.7}_{-1.7}$	$1.69^{+0.58}_{-0.70}$	$1.98^{+0.39}_{-0.73}$
084135.7-005048	4430	$3.4^{+2.2}_{-2.9}$	58^{+24}_{-24}	$2.5^{+1.7}_{-1.7}$	$1.46^{+0.70}_{-0.72}$	$2.00^{+0.71}_{-0.97}$
084142.9+002841	8433	$0.30^{+2.11}_{-0.19}$	204^{+98}_{-93}	$1.9^{+2.1}_{-1.4}$	$1.32^{+0.73}_{-0.69}$	$1.36^{+0.33}_{-0.82}$
084146.3-021339	18047	$0.61^{+2.48}_{-1.77}$	143^{+88}_{-77}	$2.5^{+1.6}_{-1.7}$	$1.57^{+0.65}_{-0.65}$	$1.09^{+0.54}_{-0.65}$
084146.5+045612	2796	$0.45^{+1.77}_{-0.24}$	240^{+170}_{-140}	$2.2^{+1.9}_{-1.6}$	$1.45^{+0.78}_{-0.80}$	$0.65^{+0.46}_{-0.46}$
084148.1+004911	3008	$2.2^{+63.2}_{-1.9}$	76^{+60}_{-37}	$3.0^{+1.5}_{-1.4}$	$1.26^{+0.93}_{-0.66}$	$2.00^{+0.48}_{-1.35}$
084151.3-003358	3706	$1.07^{+17.2}_{-7.4}$	214^{+64}_{-59}	$3.0^{+1.6}_{-1.4}$	$1.67^{+0.66}_{-0.66}$	$0.73^{+0.52}_{-0.52}$
084151.7+004351	6543	$9.2^{+3.7}_{-3.3}$	49^{+38}_{-30}	$1.8^{+1.8}_{-1.8}$	$2.02^{+0.38}_{-0.85}$	$0.92^{+0.44}_{-0.71}$
084151.9-010156	6071	$5.5^{+13.2}_{-11.3}$	78^{+35}_{-35}	$2.6^{+1.6}_{-1.6}$	$1.57^{+0.66}_{-0.71}$	$0.88^{+0.63}_{-0.63}$
084201.3+040534	6988	$5.6^{+52.3}_{-5.2}$	55^{+25}_{-23}	$2.7^{+1.5}_{-1.5}$	$1.62^{+0.74}_{-0.74}$	$1.80^{+0.12}_{-0.12}$
084201.8+005941	3334	$0.37^{+2.96}_{-0.20}$	88^{+116}_{-65}	$2.6^{+1.8}_{-1.8}$	$1.65^{+0.64}_{-0.95}$	$1.00^{+0.72}_{-0.72}$
084210.5+020558	7967	$0.87^{+2.06}_{-0.72}$	60^{+101}_{-45}	$2.5^{+1.7}_{-1.7}$	$1.58^{+0.62}_{-0.83}$	$1.27^{+0.34}_{-0.88}$
084220.9+013844	3295	$0.52^{+2.22}_{-0.33}$	273^{+92}_{-92}	$2.5^{+1.7}_{-1.7}$	$1.63^{+0.62}_{-0.80}$	$1.41^{+0.27}_{-0.42}$
084223.1+003340	4993	$7.6^{+17.7}_{-6.8}$	63^{+58}_{-38}	$2.7^{+1.6}_{-1.6}$	$1.60^{+0.62}_{-0.74}$	$2.1^{+1.3}_{-1.3}$
084240.7-011643	2859	$0.87^{+3.25}_{-1.6}$	38^{+48}_{-24}	$2.6^{+1.6}_{-1.6}$	$1.68^{+0.61}_{-0.81}$	$2.66^{+0.39}_{-0.52}$
084246.9-000917	4861	$3.2^{+3.9}_{-2.2}$	170^{+44}_{-46}	$3.0^{+1.4}_{-1.4}$	$1.72^{+0.72}_{-0.72}$	$0.58^{+0.50}_{-0.41}$
084253.7+002006	6903	$5.6^{+35.7}_{-35.7}$	57^{+45}_{-22}	$1.9^{+2.2}_{-1.8}$	$1.65^{+0.60}_{-0.73}$	$1.17^{+0.10}_{-0.85}$
084255.6+042332	2475	$0.31^{+0.79}_{-0.16}$	207^{+59}_{-59}	$2.6^{+1.7}_{-1.7}$	$1.38^{+0.75}_{-0.75}$	$2.00^{+0.18}_{-0.18}$
084258.3-004037	4269	$0.158^{+0.247}_{-0.047}$	440^{+230}_{-290}	$2.1^{+1.9}_{-1.5}$	$1.21^{+0.68}_{-0.60}$	$0.32^{+0.24}_{-0.23}$
084301.4+025741	11065	$2.1^{+43.7}_{-1.9}$	58^{+46}_{-30}	$2.6^{+1.6}_{-1.6}$	$1.60^{+0.61}_{-0.72}$	$2.02^{+0.60}_{-0.61}$
084307.1+002839	3336	$3.7^{+14.4}_{-2.9}$	135^{+38}_{-43}	$2.8^{+1.7}_{-1.7}$	$1.57^{+0.64}_{-0.79}$	$1.15^{+0.53}_{-0.70}$
084324.2-001438	9590	$0.71^{+1.89}_{-0.52}$	202^{+91}_{-76}	$2.5^{+1.6}_{-1.6}$	$1.57^{+0.65}_{-0.80}$	$0.96^{+0.58}_{-0.66}$
084346.2+010833	12839	$0.37^{+0.68}_{-0.20}$	224^{+113}_{-74}	$2.4^{+1.3}_{-1.3}$	$1.49^{+0.58}_{-0.68}$	$0.84^{+0.64}_{-0.64}$
084349.1+040404	19985	$6.5^{+4.6}_{-4.3}$	168^{+65}_{-72}	$2.7^{+1.5}_{-1.9}$	$1.52^{+0.86}_{-0.86}$	$0.63^{+0.34}_{-0.42}$
084353.9+031402	19202	$0.98^{+3.57}_{-1.76}$	108^{+62}_{-44}	$2.3^{+1.7}_{-1.7}$	$1.48^{+0.67}_{-0.69}$	$1.03^{+0.62}_{-0.61}$
084412.6-020514	3396	$6.1^{+19.8}_{-14.4}$	71^{+38}_{-53}	$2.6^{+1.6}_{-1.6}$	$1.57^{+0.64}_{-0.80}$	$1.37^{+0.44}_{-0.44}$
084417.9+010415	1812	$3.3^{+9.0}_{-2.4}$	135^{+52}_{-51}	$2.0^{+1.9}_{-1.9}$	$1.28^{+0.88}_{-0.66}$	$1.33^{+0.32}_{-0.63}$
084430.8+021736	3541	$4.3^{+23.2}_{-17.4}$	95^{+46}_{-33}	$2.2^{+1.4}_{-1.4}$	$1.51^{+0.70}_{-0.68}$	$1.58^{+0.56}_{-0.56}$
084434.3+031026	4876	$3.2^{+7.4}_{-2.7}$	111^{+63}_{-68}	$2.7^{+1.6}_{-1.6}$	$1.62^{+0.61}_{-0.76}$	$1.29^{+0.81}_{-0.83}$
084438.5+041946	11610	$2.5^{+7.1}_{-2.1}$	122^{+61}_{-43}	$2.9^{+1.5}_{-1.8}$	$1.60^{+0.64}_{-0.75}$	$0.99^{+0.61}_{-0.65}$
084439.0+043302	5668	$5.2^{+25.4}_{-25.4}$	85^{+45}_{-45}	$3.0^{+1.7}_{-1.7}$	$1.82^{+0.43}_{-0.54}$	$1.21^{+0.76}_{-0.76}$
084441.3+021701	1778	$0.220^{+195}_{-0.056}$	233^{+57}_{-56}	$1.9^{+1.7}_{-1.7}$	$0.81^{+0.31}_{-0.31}$	$2.11^{+0.15}_{-0.15}$
084454.0+010021	4436	$0.40^{+1.0}_{-0.23}$	190^{+83}_{-89}	$2.5^{+1.6}_{-1.6}$	$1.50^{+0.62}_{-0.82}$	$1.63^{+0.31}_{-0.90}$
084459.2-011902	4768	$0.29^{+0.59}_{-0.16}$	240^{+100}_{-110}	$2.0^{+1.7}_{-1.7}$	$1.28^{+0.55}_{-0.55}$	$1.54^{+0.25}_{-0.49}$
084501.0+012728	1607	$2.4^{+4.5}_{-1.8}$	145^{+61}_{-48}	$2.7^{+1.6}_{-1.9}$	$1.62^{+0.59}_{-0.68}$	$1.35^{+0.47}_{-0.67}$
084528.6+032739	144	$3.6^{+4.5}_{-1.8}$	174^{+67}_{-51}	$1.9^{+1.9}_{-1.9}$	$1.01^{+0.55}_{-0.64}$	$1.67^{+0.13}_{-0.15}$
084531.6+022831	1039	$0.87^{+0.68}_{-0.48}$	269^{+66}_{-87}	$2.4^{+1.7}_{-1.7}$	$1.54^{+0.63}_{-0.69}$	$1.67^{+0.19}_{-0.29}$
084544.3-002914	2214	$3.8^{+10.6}_{-2.3}$	132^{+38}_{-55}	$3.4^{+1.2}_{-1.6}$	$0.62^{+0.34}_{-0.22}$	$1.18^{+0.60}_{-0.60}$
084545.2+005535	3660	$1.5^{+44.8}_{-10.5}$	59^{+104}_{-43}	$2.6^{+1.8}_{-1.8}$	$1.54^{+0.66}_{-0.77}$	$1.6^{+1.3}_{-1.3}$
084552.4+011714	5804	$1.5^{+10.5}_{-1.2}$	124^{+73}_{-76}	$2.7^{+1.6}_{-1.7}$	$1.54^{+0.70}_{-0.81}$	$1.28^{+0.89}_{-0.78}$
084557.6+041103	25781	$0.46^{+194}_{-1.0}$	155^{+83}_{-60}	$2.5^{+1.7}_{-1.7}$	$1.72^{+0.55}_{-0.80}$	$0.97^{+0.56}_{-0.66}$
084558.1+012443	9771	$1.29^{+0.91}_{-0.31}$	141^{+68}_{-58}	$2.8^{+1.6}_{-1.6}$	$1.60^{+0.60}_{-0.60}$	$1.04^{+0.31}_{-0.31}$
084559.7+031321	5281	$0.31^{+0.67}_{-0.28}$	164^{+75}_{-75}	$2.2^{+1.8}_{-1.8}$	$1.26^{+0.68}_{-0.68}$	<

Table 5: continued.

Cluster (eFEDS J+)	ID_SRC	n_0 10^{-7} cm^{-6}	r_s arcsec	ϵ	β	α
084647.4+044607	6656	0.46 ^{+2.09} _{-0.23}	185 ⁺⁷³ ₋₈₁	1.7 ^{+2.0}	0.88 ^{+0.93}	1.70 ^{+0.27}
084649.0+004946	11018	1.05 ^{+0.10} _{-0.81}	96 ⁺⁷⁴ ₋₆₅	2.5 ^{+1.7}	1.63 ^{+0.61} _{-0.81}	1.11 ^{+1.07} _{-0.76}
084655.7-003705	3712	3.5 ^{+40.4} _{-3.0}	102 ⁺⁶¹ ₋₅₅	2.7 ^{+1.6}	1.64 ^{+0.60} _{-0.81}	1.63 ^{+0.48} _{-0.93}
084657.6-011314	9845	4.8 ^{+1.1} _{-1.7}	86 ⁺⁵⁴ ₋₃₈	2.7 ^{+1.7}	1.65 ^{+0.60} _{-0.77}	1.16 ^{+0.74} _{-0.74}
084717.7+033421	10507	1.9 ^{+24.8} _{-1.6}	52 ⁺⁶⁴ ₋₃₆	2.4 ^{+1.8}	1.61 ^{+0.60} _{-0.80}	1.43 ^{+1.32} _{-0.99}
084729.7+013053	5053	0.72 ^{+3.65} _{-0.50}	185 ⁺⁸² ₋₅₀	2.0 ^{+2.0}	1.61 ^{+0.62} _{-0.69}	1.40 ^{+0.38} _{-0.69}
084751.7+025522	4736	2.1 ^{+1.0} _{-0.9}	96 ⁺⁵⁸ ₋₃₃	2.7 ^{+1.6}	1.57 ^{+0.65} _{-0.74}	1.45 ^{+0.56} _{-0.83}
084759.1+014903	4709	2.6 ^{+48.4} _{-2.4}	77 ⁺⁸⁸ ₋₅₅	2.5 ^{+1.8}	1.61 ^{+0.64} _{-0.71}	1.51 ^{+0.40} _{-0.71}
084823.2+041205	2437	0.89 ^{+8.46} _{-2.9}	128 ⁺⁵⁷ ₋₄₆	1.9 ^{+1.7}	0.99 ^{+0.51} _{-0.71}	2.29 ^{+0.26} _{-0.24}
084833.2-012216	1073	2.2 ^{+1.5} _{-1.5}	177 ⁺⁶⁸ ₋₆₄	2.5 ^{+1.7}	1.67 ^{+0.73} _{-0.73}	1.64 ^{+0.35} _{-0.35}
084852.9+035939	10165	5.1 ^{+27.9} _{-4.5}	79 ⁺⁵² ₋₃₄	2.5 ^{+1.9}	1.59 ^{+0.64} _{-0.77}	1.25 ^{+0.68} _{-0.82}
084905.3+021435	7831	0.48 ^{+3.45} _{-0.29}	200 ⁺¹³⁰ ₋₁₀₀	2.2 ^{+1.8}	1.51 ^{+0.69} _{-0.81}	0.98 ^{+0.34} _{-0.67}
084910.6+024117	9790	5.0 ^{+4.4} _{-3.3}	70 ⁺⁵² ₋₄₀	2.4 ^{+1.7}	1.61 ^{+0.62} _{-0.80}	1.61 ^{+0.88} _{-0.96}
084925.4+013840	14327	1.7 ^{+4.8} _{-1.3}	162 ⁺⁷⁴ ₋₆₄	2.6 ^{+1.6}	1.58 ^{+0.64} _{-0.71}	1.03 ^{+0.46} _{-0.91}
084934.9+014437	32680	0.40 ^{+1.47} _{-0.21}	209 ⁺¹¹⁵ ₋₈₈	2.0 ^{+1.9}	1.13 ^{+0.91} _{-0.60}	1.16 ^{+0.54} _{-0.54}
084939.6-005126	2261	0.42 ^{+1.28} _{-1.2}	205 ⁺⁶⁹ ₋₈₅	1.9 ^{+1.9}	1.00 ^{+0.87} _{-0.50}	1.94 ^{+0.20} _{-0.28}
084957.4+004524	8524	5.8 ^{+15.6} _{-4.9}	70 ⁺⁸⁸ ₋₆₀	2.5 ^{+1.7}	1.47 ^{+0.72} _{-0.73}	1.5 ^{+1.0} _{-1.0}
085018.3+020018	5464	4.2 ^{+58.4} _{-3.7}	81 ⁺⁶¹ ₋₃₈	2.6 ^{+1.6}	1.48 ^{+0.71} _{-0.70}	1.78 ^{+0.31} _{-0.94}
085020.4+032819	6529	4.3 ^{+8.9} _{-3.1}	127 ⁺⁴⁸ ₋₃₅	2.8 ^{+1.7}	1.64 ^{+0.58} _{-0.60}	0.85 ^{+0.59} _{-0.60}
085022.2+001607	8602	0.202 ^{+0.232} _{-0.065}	540 ⁺¹⁹⁰ ₋₁₃₀	2.6 ^{+1.6}	1.40 ^{+0.74} _{-0.74}	0.57 ^{+0.40} _{-0.37}
085027.8+001503	1023	4.1 ^{+2.4} _{-2.4}	121 ⁺⁶⁶ ₋₃₈	0.84 ^{+0.68} _{-0.58}	0.51 ^{+0.16} _{-0.12}	1.31 ^{+0.25} _{-0.51}
085030.5+003330	6125	0.41 ^{+2.49} _{-1.3}	184 ⁺⁹⁶ ₋₁₀₅	0.66 ^{+0.68} _{-0.48}	0.51 ^{+0.34} _{-0.30}	1.70 ^{+0.24} _{-0.43}
085051.8+015331	8679	1.8 ^{+3.3} _{-1.4}	126 ⁺⁵⁷ ₋₄₆	2.6 ^{+1.5}	1.67 ^{+0.55} _{-0.74}	1.33 ^{+0.35} _{-0.86}
085056.4+005607	3556	0.85 ^{+5.42} _{-0.63}	156 ⁺⁸⁸ ₋₉₁	2.7 ^{+1.6}	1.58 ^{+0.62} _{-0.82}	1.27 ^{+1.09} _{-0.79}
085119.9+022951	2101	2.7 ^{+1.3} _{-2.1}	166 ⁺⁸⁴ ₋₆₁	2.3 ^{+1.8}	1.43 ^{+0.74} _{-0.68}	1.41 ^{+0.38} _{-0.66}
085121.2+012856	11156	1.4 ^{+6.4} _{-1.2}	136 ⁺⁶⁹ ₋₅₁	2.6 ^{+1.8}	1.58 ^{+0.68} _{-0.72}	1.19 ^{+0.55} _{-0.76}
085128.4+011501	7355	0.57 ^{+1.57} _{-0.38}	80 ⁺¹³⁵ ₋₆₃	2.7 ^{+1.5}	1.58 ^{+0.65} _{-0.74}	0.93 ^{+1.30} _{-0.67}
085130.0-004609	18314	0.82 ^{+3.1} _{-0.92}	171 ⁺⁷⁵ ₋₅₉	2.7 ^{+1.7}	1.61 ^{+0.62} _{-0.81}	1.20 ^{+0.62} _{-0.68}
085131.0+045239	863	0.55 ^{+1.38} _{-0.27}	224 ⁺⁵⁹ ₋₇₇	2.5 ^{+1.7}	1.57 ^{+0.60} _{-0.70}	2.09 ^{+0.13} _{-0.21}
085138.2-003537	4508	0.65 ^{+2.24} _{-1.6}	168 ⁺¹⁰⁶ ₋₆₇	2.8 ^{+1.4}	1.50 ^{+0.72} _{-0.69}	0.83 ^{+0.76} _{-0.58}
085141.9+021438	7280	1.14 ^{+1.88} _{-0.94}	65 ⁺⁷⁷ ₋₄₄	2.4 ^{+1.8}	1.63 ^{+0.60} _{-0.78}	1.5 ^{+1.1} _{-1.02}
085204.5+012132	6636	1.6 ^{+5.9} _{-1.2}	171 ⁺⁸² ₋₆₆	2.4 ^{+1.8}	1.56 ^{+0.64} _{-0.83}	1.24 ^{+0.45} _{-0.64}
085217.0-010131	339	1.21 ^{+4.15} _{-0.92}	240 ⁺⁸⁷ ₋₇₉	2.4 ^{+1.8}	1.75 ^{+0.53} _{-0.76}	1.81 ^{+0.41} _{-0.58}
085230.6+002457	2524	1.05 ^{+1.0} _{-0.69}	212 ⁺⁸⁰ ₋₆₀	2.0 ^{+1.9}	1.37 ^{+0.72} _{-0.73}	1.38 ^{+0.42} _{-0.59}
085231.1-011230	4810	1.05 ^{+1.86} _{-0.82}	142 ⁺⁷⁴ ₋₅₄	2.4 ^{+1.8}	1.49 ^{+0.67} _{-0.78}	1.62 ^{+0.37} _{-0.73}
085239.6+003240	5477	2.0 ^{+1.7} _{-0.7}	99 ⁺⁷⁸ ₋₄₈	2.2 ^{+1.7}	1.53 ^{+0.68} _{-0.85}	1.68 ^{+0.99} _{-0.38}
085245.7-020519	5790	0.65 ^{+1.75} _{-0.40}	101 ⁺⁵¹ ₋₅₁	2.5 ^{+1.8}	1.37 ^{+0.69} _{-0.79}	2.20 ^{+0.49} _{-0.49}
085255.1-013737	1376	0.45 ^{+2.32} _{-0.34}	199 ⁺¹⁰⁶ ₋₇₇	2.6 ^{+1.6}	1.58 ^{+0.64} _{-0.80}	1.34 ^{+0.36} _{-0.70}
085256.8+052741	6642	14 ^{+10.0} ₋₁₃	47 ⁺⁷³ ₋₂₆	2.7 ^{+1.6}	1.58 ^{+0.80} _{-0.80}	1.83 ^{+1.16} _{-0.54}
085325.6+030834	9042	2.5 ^{+36.7} _{-2.2}	67 ⁺⁴¹ ₋₂₇	2.8 ^{+1.5}	1.73 ^{+0.56} _{-0.74}	1.75 ^{+0.70} _{-1.02}
085327.2-002117	6003	0.59 ^{+2.43} _{-0.41}	201 ⁺⁸⁷ ₋₇₁	2.6 ^{+1.7}	1.52 ^{+0.66} _{-0.69}	1.40 ^{+0.35} _{-0.63}
085335.2+032214	8596	1.5 ^{+1.1} _{-1.2}	121 ⁺⁶⁰ ₋₅₀	2.7 ^{+1.5}	1.55 ^{+0.65} _{-0.73}	1.36 ^{+0.31} _{-0.81}
085340.5+022411	9213	2.8 ^{+4.8} _{-2.4}	140 ⁺⁷⁹ ₋₅₉	2.2 ^{+1.8}	1.38 ^{+0.79} _{-0.82}	0.77 ^{+0.70} _{-0.54}
085412.8-022123	1458	1.39 ^{+5.34} _{-0.63}	196 ⁺⁶² ₋₅₈	2.7 ^{+1.8}	1.53 ^{+0.68} _{-0.71}	1.81 ^{+0.68} _{-0.49}
085419.5-000925	1294	0.49 ^{+1.01} _{-0.30}	179 ⁺⁷¹ ₋₈₄	0.96 ^{+1.45} _{-0.70}	0.54 ^{+0.13} _{-0.13}	1.97 ^{+0.32} _{-0.32}
085433.0+004009	3675	3.1 ^{+61.4} _{-28.80}	37 ⁺²⁹ ₋₁₆	3.4 ^{+1.1} _{-1.8}	1.59 ^{+0.65} _{-0.75}	2.58 ^{+0.97} _{-0.53}
085434.5-014038	8094	0.64 ^{+1.40} _{-0.46}	159 ⁺⁷¹ ₋₅₅	2.5 ^{+1.7}	1.44 ^{+0.70} _{-0.75}	1.50 ^{+0.67} _{-0.67}
085436.6+003835	328	10.7 ^{+9.9} _{-4.5}	104 ⁺¹⁸ ₋₂₄	0.62 ^{+0.58} _{-0.42}	0.57 ^{+0.11} _{-0.12}	1.39 ^{+0.23} _{-0.25}
085438.5+001211	5390	0.58 ^{+1.43} _{-0.44}	107 ⁺⁹⁵ ₋₆₃	2.2 ^{+1.7}	1.37 ^{+0.79} _{-0.78}	1.53 ^{+0.64} _{-0.84}
085440.4-020931	7700	6.5 ^{+6.0} _{-4.7}	57 ⁺⁴¹ ₋₂₅	2.5 ^{+1.7}	1.62 ^{+0.69} _{-0.69}	1.45 ^{+0.99} _{-0.99}
085447.0-012132	2079	2.0 ^{+5.4} _{-1.2}	181 ⁺⁷³ ₋₅₆	2.5 ^{+1.7}	1.59 ^{+0.65} _{-0.76}	1.21 ^{+0.38} _{-0.52}
085508.9-003445	2810	2.0 ^{+1.9} _{-0.9}	57 ⁺²⁶ ₋₂₆	2.7 ^{+1.8}	1.73 ^{+0.55} _{-0.77}	2.33 ^{+1.57} _{-1.27}
085517.2+013508	6746	0.67 ^{+2.25} _{-0.49}	263 ⁺¹⁰⁶ ₋₉₄	2.6 ^{+1.4}	1.63 ^{+0.43} _{-0.67}	1.13 ^{+0.40} _{-0.65}
085519.1-014315	5909	0.69 ^{+10.07} _{-0.56}	66 ⁺¹⁰⁶ ₋₅₁	2.7 ^{+1.6}	1.56 ^{+0.66} _{-0.75}	1.04 ^{+1.34} _{-0.74}
085524.3+015012	23313	0.24 ^{+1.39} _{-1.12}	300 ⁺¹³⁰ ₋₁₀₀	2.4 ^{+1.8}	1.57 ^{+0.64} _{-0.82}	0.82 ^{+0.44} _{-0.46}
085530.1-010634	1797	10.7 ^{+34.5} _{-9.0}	108 ⁺⁶⁴ ₋₄₁	2.6 ^{+1.7}	1.57 ^{+0.86} _{-0.86}	1.17 ^{+0.56} _{-0.70}
085541.2+002740	5589	0.72 ^{+3.59} _{-1.53}	84 ⁺⁸⁶ ₋₆₁	3.2 ^{+1.8}	1.70 ^{+0.57} _{-0.77}	1.14 ^{+0.30} _{-0.31}
085542.6+032807	8925	0.96 ^{+6.4} _{-0.64}	73 ⁺¹³ ₋₅₆	2.7 ^{+1.8}	1.44 ^{+0.73} _{-0.77}	1.10 ^{+0.35} _{-0.80}
085547.0+025458	8799	2.7 ^{+6.4} _{-2.2}	53 ⁺⁸⁶ ₋₃₆	2.3 ^{+1.9}	1.72 ^{+0.54} _{-0.86}	1.6 ^{+1.6} _{-1.1}
085604.8+002520	8826	0.78 ^{+1.38} _{-0.68}	280 ⁺¹³⁰ ₋₁₀	2.1 ^{+1.6}	1.02 ^{+1.01} _{-0.51}	0.85 ^{+0.54} _{-0.44}
085616.1-013945	8922	0.85 ^{+1.31} _{-0.66}	21 ⁺³⁸ ₋₁₆	3.0 ^{+1.6}	1.72 ^{+0.86} _{-0.86}	1.02 ^{+0.56} _{-0.73}
085620.7+014649	569	1.08 ^{+3.52} _{-0.76}	173 ⁺⁶² ₋₅₉	2.5 ^{+1.7}	1.49 ^{+0.63} _{-0.64}	2.09 ^{+0.20} _{-0.31}
085623.6-013612	16370	0.81 ^{+1.66} _{-0.66}	139 ⁺⁹³ ₋₆₈	2.7 ^{+1.7}	1.57 ^{+0.64} _{-0.64}	1.29 ^{+0.35} _{-0.81}
085624.3+004632	32576	2.2 ^{+3.65} _{-1.8}	123 ⁺³⁸ ₋₄₃	2.3 ^{+1.8}	1.74 ^{+0.55} _{-0.76}	0.90 ^{+0.63} _{-0.64}
085626.2+021348	5697	0.183 ^{+0.344} _{-0.073}	295 ⁺⁹⁰ ₋₉₀	2.1 ^{+1.9}	1.18 ^{+0.87} _{-0.59}	1.53 ^{+0.31} _{-0.44}
085627.2+014217	1385	18 ⁺³² ₋₁₅	99 ⁺⁶⁷ ₋₃₁	2.6 ^{+1.7}	1.55 ^{+0.54} _{-0.77}	0.82 ^{+0.64} _{-0.58}
085635.0+031342	24300	0.76 ^{+10.36} _{-0.59}	53 ⁺⁸⁷ ₋₄₂	2.6 ^{+1.7}	1.69 ^{+0.56} _{-0.83}	1.28 ^{+1.58} _{-0.86}
085650.4-022200	5261	1.02 ^{+2.65} _{-1.81}	162 ⁺⁶² ₋₄₆	2.6 ^{+1.6}	1.70 ^{+0.55} _{-0.76}	1.12 ^{+0.54} _{-0.34}
085705.9+011453	3128	1.6 ^{+1.2} _{-1.2}	218 ⁺⁸⁸ ₋₇₄	2.6 ^{+1.7}	1.48 ^{+0.74} _{-0.74}	1.07 ^{+0.34} _{-0.68}
085728.3+032354	6278	0.81 ^{+3.52} _{-0.58}	167 ⁺⁷⁵ ₋₇₀	2.1 ^{+1.9}	0.93 ^{+0.83} _{-0.46}	1.25 ^{+0.44} _{-0.64}
085740.1-020037	7884	1.05 ^{+0.88} _{-0.82}	155 ⁺⁹⁷ ₋₈₆	2.5 ^{+1.7}	1.55 ^{+0.65} ₋	

Table 5: continued.

Cluster (eFEDS J+)	ID_SRC	n_0 10^{-7} cm^{-6}	r_s arcsec	ϵ	β	α
085841.8-020541	2367	$0.52^{+0.92}_{-0.41}$	126^{+78}_{-59}	$2.6^{+1.6}_{-1.8}$	$1.38^{+0.73}_{-0.67}$	$1.87^{+0.32}_{-0.68}$
085849.8+022800	715	$0.186^{+0.785}_{-0.083}$	241^{+89}_{-120}	$1.6^{+2.1}_{-1.7}$	$0.74^{+0.75}_{-0.31}$	$2.24^{+0.30}_{-0.30}$
085901.1-012025	3527	$7.4^{+30.6}_{-6.2}$	101^{+70}_{-39}	$2.6^{+1.7}_{-1.7}$	$1.60^{+0.65}_{-0.75}$	$1.23^{+0.69}_{-0.79}$
085901.5+010649	2757	$1.23^{+5.00}_{-0.92}$	151^{+55}_{-50}	$2.4^{+1.7}_{-1.7}$	$1.55^{+0.67}_{-0.77}$	$1.55^{+0.37}_{-0.44}$
085907.3-005056	16320	$0.211^{+0.478}_{-0.098}$	330^{+140}_{-120}	$2.4^{+1.8}_{-1.8}$	$1.34^{+0.88}_{-0.76}$	$0.75^{+0.24}_{-0.52}$
085913.1+031334	485	$0.203^{+0.445}_{-0.082}$	149^{+41}_{-42}	$1.5^{+2.2}_{-1.7}$	$0.67^{+1.22}_{-0.70}$	$2.64^{+0.16}_{-0.13}$
085931.9+030839	360	$0.97^{+0.22}_{-0.51}$	243^{+79}_{-76}	$2.4^{+1.7}_{-1.7}$	$1.46^{+0.66}_{-0.66}$	$1.82^{+0.14}_{-0.14}$
085939.1-004932	6894	$1.28^{+3.47}_{-1.00}$	162^{+75}_{-64}	$2.6^{+1.7}_{-1.7}$	$1.65^{+0.61}_{-0.79}$	$0.98^{+0.55}_{-0.65}$
085948.9+041120	1350	$0.28^{+1.00}_{-0.46}$	204^{+84}_{-61}	$2.3^{+1.8}_{-1.8}$	$1.36^{+0.74}_{-0.74}$	$2.10^{+0.25}_{-0.25}$
085950.1-001221	4539	$0.82^{+0.65}_{-0.65}$	174^{+89}_{-70}	$2.4^{+1.7}_{-1.7}$	$1.56^{+0.63}_{-0.73}$	$1.42^{+0.37}_{-0.71}$
085954.2-013308	13823	$1.9^{+54.2}_{-1.7}$	56^{+73}_{-38}	$2.3^{+1.8}_{-1.8}$	$1.54^{+0.64}_{-0.76}$	$2.0^{+0.16}_{-0.29}$
090004.3+033324	7945	$4.3^{+17.9}_{-3.6}$	91^{+31}_{-32}	$2.6^{+1.7}_{-1.7}$	$1.62^{+0.62}_{-0.71}$	$1.12^{+0.73}_{-0.73}$
090010.4+023631	10878	$0.83^{+3.31}_{-0.64}$	162^{+77}_{-68}	$2.6^{+1.6}_{-1.9}$	$1.46^{+0.68}_{-0.71}$	$1.11^{+0.52}_{-0.63}$
090020.8-002602	1315	$0.88^{+25.63}_{-0.07}$	81^{+101}_{-59}	$2.3^{+1.7}_{-1.7}$	$1.54^{+0.67}_{-0.80}$	$1.4^{+0.30}_{-0.30}$
090033.7+033932	2407	$0.82^{+0.55}_{-0.61}$	180^{+130}_{-110}	$2.4^{+1.8}_{-1.8}$	$1.43^{+0.73}_{-0.74}$	$1.12^{+0.39}_{-0.68}$
090034.1-010649	1652	$0.85^{+0.43}_{-0.66}$	179^{+84}_{-61}	$2.4^{+1.7}_{-1.6}$	$1.69^{+0.56}_{-0.76}$	$1.08^{+0.46}_{-0.59}$
090044.6-011104	8508	$0.32^{+8.25}_{-0.55}$	58^{+31}_{-31}	$2.7^{+1.6}_{-1.5}$	$1.61^{+0.64}_{-0.78}$	$2.27^{+0.11}_{-0.97}$
090051.6-003457	9834	$0.70^{+3.19}_{-0.54}$	133^{+65}_{-61}	$2.9^{+1.8}_{-1.9}$	$1.54^{+0.67}_{-0.71}$	$1.05^{+0.72}_{-0.67}$
090053.0-002837	9310	$1.3^{+5.5}_{-1.2}$	114^{+67}_{-41}	$2.4^{+1.7}_{-1.6}$	$1.55^{+0.66}_{-0.77}$	$1.19^{+0.64}_{-0.80}$
090059.3+035925	983	$1.9^{+12.9}_{-1.6}$	120^{+69}_{-49}	$2.3^{+1.8}_{-1.8}$	$1.50^{+0.69}_{-0.73}$	$1.92^{+0.35}_{-0.52}$
090104.4+011643	3171	$3.9^{+8.8}_{-3.0}$	142^{+67}_{-47}	$2.8^{+1.7}_{-1.8}$	$1.63^{+0.59}_{-0.74}$	$0.96^{+0.50}_{-0.58}$
090105.2-012525	11836	$1.11^{+21.5}_{-0.78}$	169^{+62}_{-59}	$2.7^{+1.5}_{-1.9}$	$1.48^{+0.64}_{-0.70}$	$0.82^{+0.53}_{-0.57}$
090115.3+005040	8881	$2.4^{+3.5}_{-2.0}$	144^{+81}_{-77}	$2.5^{+1.7}_{-1.7}$	$1.55^{+0.67}_{-0.80}$	$0.77^{+0.67}_{-0.53}$
090119.0+030204	7017	$3.4^{+18.1}_{-2.9}$	79^{+53}_{-41}	$1.6^{+1.0}_{-1.0}$	$0.72^{+0.99}_{-0.28}$	$1.36^{+0.82}_{-0.76}$
090121.9-003709	1600	$1.47^{+11.3}_{-1.2}$	117^{+74}_{-51}	$2.3^{+2.0}_{-2.0}$	$1.68^{+0.63}_{-0.63}$	$1.48^{+0.60}_{-0.60}$
090129.1-013853	1104	39^{+12}_{-14}	60^{+15}_{-12}	$0.56^{+0.37}_{-0.36}$	$0.527^{+0.74}_{-0.92}$	$0.49^{+0.39}_{-0.39}$
090131.1+030056	152	$15.3^{+21.8}_{-6.7}$	93^{+14}_{-18}	$1.50^{+0.88}_{-0.83}$	$0.52^{+0.13}_{-0.12}$	$1.27^{+0.31}_{-0.60}$
090133.2+021651	4181	$0.44^{+1.13}_{-0.28}$	214^{+77}_{-76}	$2.6^{+1.6}_{-1.6}$	$1.64^{+0.58}_{-0.72}$	$1.26^{+0.37}_{-0.46}$
090135.5-010540	10870	$0.74^{+0.23}_{-0.54}$	101^{+61}_{-44}	$2.6^{+1.7}_{-1.7}$	$1.53^{+0.67}_{-0.78}$	$1.59^{+0.94}_{-0.86}$
090137.7+030253	15914	$0.56^{+0.57}_{-0.38}$	124^{+79}_{-63}	$2.6^{+1.4}_{-1.4}$	$1.59^{+0.55}_{-0.58}$	$1.01^{+0.60}_{-0.59}$
090140.9-012132	2412	$0.75^{+10.04}_{-0.58}$	241^{+91}_{-68}	$3.1^{+2.1}_{-2.1}$	$1.66^{+0.65}_{-0.65}$	$0.81^{+0.45}_{-0.51}$
090144.7+040827	3199	$1.5^{+11.3}_{-1.1}$	130^{+60}_{-56}	$2.5^{+1.7}_{-1.8}$	$1.43^{+0.64}_{-0.76}$	$1.88^{+0.32}_{-0.61}$
090146.2-013756	4232	$5.8^{+35.6}_{-5.6}$	88^{+45}_{-39}	$2.4^{+1.7}_{-1.7}$	$1.65^{+0.62}_{-0.72}$	$1.56^{+0.88}_{-0.88}$
090153.9-012209	2048	$3.0^{+1.6}_{-1.8}$	123^{+39}_{-39}	$2.5^{+1.8}_{-1.4}$	$1.20^{+0.78}_{-0.52}$	$1.02^{+0.46}_{-0.46}$
090200.5+022339	3800	$0.70^{+2.86}_{-0.47}$	218^{+88}_{-86}	$2.4^{+1.8}_{-1.8}$	$1.43^{+0.74}_{-0.70}$	$1.43^{+0.30}_{-0.60}$
090210.6+032513	431	$0.89^{+0.69}_{-0.69}$	43^{+38}_{-39}	$2.8^{+1.7}_{-1.9}$	$1.53^{+0.66}_{-0.69}$	$3.28^{+0.73}_{-0.73}$
090223.3+015205	6840	$2.7^{+16.1}_{-2.4}$	37^{+13}_{-18}	$2.6^{+1.9}_{-1.8}$	$1.72^{+0.85}_{-0.85}$	$2.55^{+0.73}_{-1.34}$
090224.4-005150	9893	$2.2^{+10.4}_{-2.0}$	94^{+68}_{-68}	$2.6^{+1.7}_{-1.8}$	$1.58^{+0.65}_{-0.78}$	$1.28^{+0.59}_{-0.82}$
090248.5+044005	4121	$2.9^{+1.0}_{-2.4}$	104^{+34}_{-39}	$2.8^{+1.8}_{-1.8}$	$1.56^{+0.65}_{-0.67}$	$1.30^{+0.38}_{-0.38}$
090255.2+030220	5489	$0.73^{+3.02}_{-0.54}$	220^{+110}_{-100}	$2.3^{+1.8}_{-1.8}$	$1.22^{+0.90}_{-0.68}$	$1.19^{+0.46}_{-0.67}$
090255.5+044036	4348	$1.6^{+17.2}_{-1.7}$	125^{+65}_{-53}	$0.97^{+0.73}_{-0.72}$	$1.16^{+0.90}_{-0.62}$	$1.65^{+0.41}_{-0.87}$
090256.2+014625	5655	$0.30^{+0.97}_{-0.18}$	215^{+70}_{-70}	$2.1^{+1.7}_{-1.7}$	$1.58^{+0.67}_{-0.70}$	$1.58^{+0.49}_{-0.49}$
090257.4+004819	1712	$1.8^{+3.04}_{-1.6}$	73^{+59}_{-35}	$2.7^{+1.7}_{-1.8}$	$1.53^{+0.67}_{-0.74}$	$1.98^{+0.49}_{-0.49}$
090323.7+030738	2083	$4.1^{+30.1}_{-1.9}$	103^{+84}_{-84}	$1.5^{+2.3}_{-1.3}$	$0.74^{+1.07}_{-0.70}$	$1.45^{+0.44}_{-0.37}$
090327.2+032545	4771	$0.71^{+1.93}_{-0.56}$	120^{+66}_{-55}	$2.2^{+1.9}_{-1.9}$	$1.54^{+0.68}_{-0.72}$	$1.80^{+0.37}_{-0.12}$
090328.7-013622	4487	$1.7^{+5.9}_{-1.4}$	166^{+73}_{-62}	$2.1^{+1.8}_{-1.5}$	$1.67^{+0.56}_{-0.76}$	$1.18^{+0.55}_{-0.80}$
090333.8+043950	9404	$2.3^{+3.8}_{-1.8}$	136^{+61}_{-55}	$2.5^{+1.7}_{-1.8}$	$1.56^{+0.58}_{-0.76}$	$0.88^{+0.56}_{-0.54}$
090335.0+022006	8941	$1.7^{+13.5}_{-1.5}$	75^{+52}_{-34}	$2.7^{+1.7}_{-1.8}$	$1.66^{+0.59}_{-0.73}$	$1.46^{+0.73}_{-0.89}$
090336.7+033124	12221	$1.5^{+7.3}_{-1.2}$	122^{+55}_{-46}	$3.0^{+1.3}_{-1.3}$	$1.69^{+0.55}_{-0.85}$	$1.37^{+0.59}_{-0.85}$
090408.6+012555	5774	$0.49^{+0.66}_{-0.28}$	200^{+130}_{-110}	$2.5^{+1.7}_{-1.7}$	$1.47^{+0.68}_{-0.73}$	$0.77^{+0.50}_{-0.50}$
090409.7+003831	9877	$1.3^{+4.5}_{-1.1}$	143^{+76}_{-54}	$2.6^{+1.7}_{-1.8}$	$1.53^{+0.66}_{-0.73}$	$1.02^{+0.59}_{-0.69}$
090417.0+040439	13330	$0.57^{+1.74}_{-0.29}$	227^{+98}_{-75}	$2.3^{+1.8}_{-1.6}$	$1.61^{+0.63}_{-0.63}$	$1.14^{+0.39}_{-0.69}$
090418.6+020642	3590	1.6^{+40}_{-14}	84^{+49}_{-30}	$2.6^{+1.7}_{-1.7}$	$1.61^{+0.63}_{-0.76}$	$1.02^{+0.62}_{-0.66}$
090419.1-010436	12660	$0.82^{+3.05}_{-0.65}$	144^{+68}_{-53}	$2.8^{+1.5}_{-1.8}$	$1.68^{+0.56}_{-0.73}$	$1.18^{+0.52}_{-0.79}$
090430.7+042648	1075	$0.92^{+3.88}_{-0.48}$	107^{+47}_{-48}	$2.3^{+1.8}_{-1.8}$	$0.97^{+0.90}_{-0.44}$	$2.39^{+0.22}_{-0.38}$
090452.4+033326	2931	$0.34^{+1.6}_{-0.17}$	228^{+81}_{-104}	$1.9^{+1.7}_{-1.7}$	$0.98^{+0.60}_{-0.52}$	$1.85^{+0.33}_{-0.33}$
090504.0+043440	354	$3.7^{+8.2}_{-2.0}$	194^{+68}_{-75}	$2.8^{+1.6}_{-1.6}$	$1.29^{+0.84}_{-0.79}$	$1.52^{+0.20}_{-0.33}$
090540.7+013219	3585	$7.5^{+4.6}_{-5.7}$	117^{+71}_{-32}	$2.7^{+1.6}_{-1.6}$	$1.70^{+0.74}_{-0.74}$	$0.89^{+0.62}_{-0.62}$
090553.5+002244	5170	$0.50^{+2.41}_{-0.34}$	124^{+51}_{-49}	$2.5^{+1.7}_{-1.7}$	$1.55^{+0.64}_{-0.74}$	$2.05^{+0.30}_{-0.46}$
090600.3-002521	9359	$2.1^{+8.5}_{-1.8}$	110^{+35}_{-39}	$2.4^{+1.7}_{-1.7}$	$1.51^{+0.66}_{-0.66}$	$1.26^{+0.59}_{-0.73}$
090601.0+000055	3259	$0.149^{+0.346}_{-0.051}$	230^{+99}_{-97}	$0.99^{+1.59}_{-0.75}$	$0.59^{+0.20}_{-0.20}$	$1.97^{+0.19}_{-0.19}$
090609.4+042924	11420	$0.67^{+3.54}_{-0.50}$	142^{+67}_{-54}	$2.6^{+1.6}_{-1.7}$	$1.46^{+0.70}_{-0.70}$	$1.42^{+0.45}_{-0.72}$
090614.6-010819	5854	$1.75^{+1.6}_{-1.5}$	82^{+85}_{-85}	$2.7^{+1.7}_{-1.7}$	$1.39^{+0.64}_{-0.64}$	$2.01^{+0.39}_{-0.80}$
090627.5+035846	10162	$0.183^{+0.319}_{-0.083}$	340^{+210}_{-160}	$2.6^{+1.8}_{-1.8}$	$1.37^{+0.75}_{-0.71}$	$0.63^{+0.39}_{-0.39}$
090628.9-012938	2424	$1.3^{+4.5}_{-1.0}$	158^{+69}_{-62}	$2.9^{+1.5}_{-1.8}$	$1.70^{+0.55}_{-0.75}$	$1.44^{+0.36}_{-0.59}$
090634.9+045033	8384	$5.27^{+26.0}_{-4.2}$	106^{+45}_{-37}	$3.0^{+2.0}_{-2.0}$	$1.54^{+0.66}_{-0.74}$	$1.56^{+0.36}_{-0.89}$
090636.9+010852	7086	$2.1^{+12.5}_{-1.8}$	134^{+58}_{-55}	$2.6^{+1.7}_{-1.7}$	$1.58^{+0.63}_{-0.77}$	$1.38^{+0.44}_{-0.79}$
090644.8+011124	5858	$1.00^{+11.06}_{-0.12}$	87^{+40}_{-38}	$3.0^{+1.4}_{-1.4}$	$1.37^{+0.72}_{-0.72}$	$2.12^{+0.44}_{-0.44}$
090656.3+044717	12153	$0.33^{+0.37}_{-0.17}$	460^{+120}_{-100}	$2.3^{+1.8}_{-1.8}$	$1.57^{+0.64}_{-0.64}$	$0.98^{+0.37}_{-0.37}$
090700.7+011032	9463	22^{+124}_{-20}	51^{+33}_{-30}	$1.6^{+1.1}_{-1.1}$	$1.89^{+0.46}_{-0.73}$	$1.27^{+0.11}_{-0.85}$
090703.9+010756	13484	$1.4^{+10.8}_{-1.1}$	42^{+37}_{-28}	$1.6^{+1.4}_{-1.4}$	$2.04^{+0.33}_{-0.67}$	$2.0^{+0.11}_{-1.1}$
090718.6+035258	6439	$8.6^{+18.2}_{-7.1}$	105^{+37}_{-30}	$2.7^{+1.6}_{-1.6$		

Table 5: continued.

Cluster (eFEDS J+)	ID_SRC	n_0 10^{-7} cm^{-6}	r_s arcsec	ϵ	β	α
090752.9+013407	2074	$0.36^{+1.74}_{-0.25}$	211^{+86}_{-78}	$2.4^{+1.9}_{-1.8}$	$1.46^{+0.75}_{-0.87}$	$1.67^{+0.59}_{-0.23}$
090754.5+005738	5219	$1.14^{+2.31}_{-0.85}$	156^{+74}_{-61}	$2.3^{+1.8}_{-1.6}$	$1.51^{+0.67}_{-0.79}$	$1.56^{+0.36}_{-0.36}$
090757.5+025427	9569	$6.8^{+31.2}_{-6.1}$	92^{+61}_{-41}	$2.7^{+1.6}_{-1.9}$	$1.46^{+0.81}_{-0.88}$	$1.17^{+0.71}_{-0.89}$
090803.8+020045	2234	$0.53^{+0.92}_{-0.37}$	148^{+87}_{-61}	$2.4^{+1.7}_{-1.7}$	$1.53^{+0.64}_{-0.78}$	$2.13^{+0.32}_{-0.32}$
090805.9+011952	7084	$4.4^{+2.51}_{-3.8}$	91^{+50}_{-33}	$2.7^{+1.8}_{-1.8}$	$1.64^{+0.60}_{-0.74}$	$1.33^{+0.59}_{-0.83}$
090806.4+032613	12592	$2.7^{+2.2}_{-2.0}$	96^{+64}_{-40}	$2.5^{+1.8}_{-1.8}$	$1.70^{+0.57}_{-0.78}$	$1.17^{+0.70}_{-0.70}$
090806.9+042351	6554	$0.200^{+0.465}_{-0.099}$	315^{+106}_{-97}	$2.4^{+1.7}_{-1.7}$	$1.36^{+0.67}_{-0.78}$	$1.38^{+0.24}_{-0.37}$
090811.6-014811	3984	$0.67^{+1.22}_{-0.47}$	154^{+73}_{-68}	$3.4^{+1.7}_{-2.0}$	$1.52^{+0.68}_{-0.73}$	$1.81^{+0.33}_{-0.92}$
090816.3+033416	11470	$0.33^{+0.20}_{-0.17}$	178^{+70}_{-70}	$2.4^{+2.0}_{-1.7}$	$1.26^{+0.60}_{-0.67}$	$1.60^{+0.39}_{-0.56}$
090817.2-013034	15548	$0.39^{+1.91}_{-0.29}$	174^{+85}_{-74}	$2.7^{+1.5}_{-1.8}$	$1.53^{+0.68}_{-0.79}$	$1.17^{+0.47}_{-0.72}$
090821.6-014115	16287	$0.49^{+2.53}_{-1.39}$	148^{+87}_{-69}	$2.2^{+1.8}_{-1.8}$	$1.53^{+0.73}_{-0.82}$	$1.35^{+0.48}_{-0.85}$
090821.9+025141	8248	$2.0^{+1.0}_{-1.6}$	130^{+66}_{-69}	$2.8^{+2.0}_{-1.8}$	$1.50^{+0.81}_{-0.81}$	$1.18^{+0.64}_{-0.76}$
090838.0+015226	1479	$0.29^{+0.57}_{-0.17}$	222^{+86}_{-83}	$1.8^{+2.1}_{-1.9}$	$0.86^{+0.86}_{-0.88}$	$1.98^{+0.16}_{-0.20}$
090843.9-013034	4974	$0.40^{+0.05}_{-0.20}$	149^{+81}_{-77}	$1.7^{+2.1}_{-1.7}$	$1.35^{+0.38}_{-0.61}$	$1.32^{+0.37}_{-0.37}$
090849.7+042241	2460	35^{+21}_{-25}	91^{+25}_{-22}	$2.9^{+1.5}_{-1.5}$	$1.80^{+0.50}_{-0.58}$	$0.65^{+0.39}_{-0.43}$
090913.8-001214	885	$0.82^{+1.27}_{-0.46}$	232^{+67}_{-71}	$2.9^{+1.8}_{-1.9}$	$1.67^{+0.58}_{-0.75}$	$1.68^{+0.19}_{-0.23}$
090915.3-010104	2004	$0.57^{+0.35}_{-0.33}$	204^{+66}_{-69}	$2.3^{+1.8}_{-1.8}$	$1.41^{+0.61}_{-0.70}$	$1.96^{+0.44}_{-0.59}$
090916.0-015540	5772	$1.5^{+3.3}_{-1.1}$	161^{+67}_{-48}	$2.8^{+1.6}_{-1.6}$	$1.75^{+0.59}_{-0.80}$	$0.96^{+0.33}_{-0.62}$
090930.6+034055	638	$0.49^{+1.72}_{-1.28}$	108^{+42}_{-34}	$2.3^{+1.6}_{-1.6}$	$1.12^{+0.81}_{-0.52}$	$2.79^{+0.26}_{-0.26}$
090932.5-005020	3523	$2.9^{+2.6}_{-2.3}$	113^{+51}_{-51}	$2.5^{+1.6}_{-1.6}$	$1.51^{+0.73}_{-0.73}$	$1.93^{+0.32}_{-0.64}$
090938.1+040816	13180	$0.83^{+3.60}_{-0.66}$	147^{+78}_{-60}	$2.7^{+1.6}_{-1.8}$	$1.48^{+0.69}_{-0.70}$	$1.30^{+0.46}_{-0.68}$
091011.7+013914	13622	$0.42^{+1.68}_{-0.89}$	205^{+86}_{-81}	$2.4^{+1.8}_{-1.8}$	$1.45^{+0.70}_{-0.73}$	$1.30^{+0.34}_{-0.63}$
091032.4+035301	8750	$4.5^{+0.28}_{-3.9}$	103^{+34}_{-30}	$2.6^{+1.9}_{-1.9}$	$1.50^{+0.86}_{-0.85}$	$0.74^{+0.33}_{-0.53}$
091033.8+005100	510	$0.22^{+0.62}_{-0.11}$	171^{+34}_{-34}	$2.3^{+1.7}_{-1.7}$	$1.21^{+0.81}_{-0.66}$	$2.43^{+0.17}_{-0.19}$
091057.2+041730	206	$2.7^{+2.4}_{-2.4}$	105^{+85}_{-85}	$2.6^{+1.6}_{-1.6}$	$1.54^{+0.68}_{-0.68}$	$1.39^{+0.52}_{-0.56}$
091104.1+052237	11694	$1.11^{+0.37}_{-0.89}$	132^{+78}_{-56}	$2.3^{+1.7}_{-1.6}$	$1.36^{+0.59}_{-0.74}$	$1.32^{+0.47}_{-0.79}$
091108.0-015422	5376	23^{+168}_{-21}	43^{+28}_{-20}	$2.5^{+1.6}_{-1.6}$	$1.49^{+0.69}_{-0.73}$	$1.59^{+0.99}_{-0.04}$
091110.0+040015	6021	$1.7^{+2.7}_{-1.4}$	120^{+62}_{-41}	$2.2^{+2.0}_{-1.7}$	$1.68^{+0.70}_{-0.79}$	$1.12^{+0.03}_{-0.24}$
091117.1+030441	15328	$0.199^{+0.276}_{-0.088}$	370^{+110}_{-110}	$2.5^{+1.7}_{-1.7}$	$1.29^{+0.80}_{-0.80}$	$1.05^{+0.38}_{-0.40}$
091135.9+034626	3774	$8.2^{+3.1}_{-6.9}$	114^{+52}_{-52}	$2.4^{+1.6}_{-1.6}$	$1.62^{+0.54}_{-0.54}$	$1.23^{+0.60}_{-0.66}$
091139.3-014144	5511	$4.6^{+2.0}_{-2.0}$	96^{+51}_{-32}	$2.8^{+1.5}_{-1.8}$	$1.71^{+0.57}_{-0.77}$	$1.31^{+0.37}_{-0.73}$
091159.7+031036	9374	$0.27^{+0.48}_{-0.16}$	215^{+86}_{-86}	$2.9^{+1.7}_{-1.7}$	$1.36^{+0.71}_{-0.69}$	$1.49^{+0.35}_{-0.76}$
091213.4-021621	7699	$3.4^{+1.6}_{-3.0}$	81^{+47}_{-59}	$2.9^{+1.4}_{-1.4}$	$1.49^{+0.65}_{-0.65}$	$1.50^{+0.05}_{-0.27}$
091214.1+022443	18040	$0.34^{+1.39}_{-0.22}$	151^{+89}_{-89}	$2.5^{+1.8}_{-1.7}$	$1.59^{+0.63}_{-0.79}$	$1.01^{+0.94}_{-0.67}$
091215.3-021743	626	$3.4^{+5.4}_{-5.4}$	280^{+67}_{-67}	$2.5^{+1.7}_{-1.7}$	$1.67^{+0.57}_{-0.67}$	$1.30^{+0.20}_{-0.29}$
091248.2+002446	11837	$0.30^{+0.13}_{-0.13}$	227^{+89}_{-84}	$2.4^{+1.7}_{-1.7}$	$1.36^{+0.80}_{-0.72}$	$0.99^{+0.44}_{-0.59}$
091254.4+032028	1415	$13.7^{+0.88}_{-0.88}$	93^{+31}_{-26}	$2.7^{+1.8}_{-1.8}$	$1.64^{+0.55}_{-0.69}$	$1.22^{+0.48}_{-0.67}$
091300.9-013152	7531	$2.7^{+22.1}_{-21}$	95^{+61}_{-41}	$2.7^{+1.6}_{-1.6}$	$1.56^{+0.65}_{-0.80}$	$1.45^{+0.36}_{-0.99}$
091302.1+035000	1277	$1.8^{+1.4}_{-1.4}$	178^{+33}_{-61}	$2.8^{+1.4}_{-1.9}$	$1.76^{+0.51}_{-0.75}$	$1.05^{+0.32}_{-0.69}$
091305.9+035021	3797	$1.8^{+4.8}_{-4.8}$	178^{+83}_{-61}	$2.8^{+1.4}_{-1.9}$	$1.76^{+0.51}_{-0.75}$	$1.05^{+0.52}_{-0.69}$
091315.0+034850	593	$0.42^{+0.66}_{-0.24}$	216^{+72}_{-70}	$2.0^{+2.0}_{-1.4}$	$0.97^{+0.73}_{-0.40}$	$2.13^{+0.14}_{-0.16}$
091320.3+032834	2977	$1.03^{+14.98}_{-0.84}$	96^{+55}_{-46}	$2.3^{+1.8}_{-1.8}$	$1.51^{+0.65}_{-0.74}$	$2.13^{+0.33}_{-0.64}$
091322.9+040617	9801	$0.201^{+0.225}_{-0.098}$	430^{+110}_{-100}	$2.6^{+1.9}_{-1.9}$	$1.76^{+0.51}_{-0.68}$	$0.71^{+0.41}_{-0.45}$
091331.0+024513	3488	$44^{+8.0}_{-38}$	40^{+30}_{-13}	$2.9^{+1.5}_{-1.5}$	$1.73^{+0.51}_{-0.72}$	$0.83^{+0.30}_{-0.30}$
091336.6+031723	5541	$1.5^{+2.5}_{-1.0}$	144^{+45}_{-45}	$0.97^{+1.21}_{-0.69}$	$0.65^{+0.34}_{-0.22}$	$1.04^{+0.39}_{-0.37}$
091351.1-004507	1319	$1.6^{+4.1}_{-4.1}$	182^{+76}_{-75}	$2.4^{+1.6}_{-1.8}$	$1.45^{+0.75}_{-0.68}$	$1.47^{+0.31}_{-0.43}$
091354.7+025323	16902	$0.81^{+0.63}_{-0.63}$	137^{+54}_{-54}	$2.4^{+1.7}_{-1.7}$	$1.48^{+0.77}_{-0.73}$	$1.15^{+0.69}_{-0.69}$
091358.1+025707	940	$1.8^{+8.3}_{-8.3}$	109^{+66}_{-47}	$2.8^{+1.6}_{-1.8}$	$1.35^{+0.75}_{-0.67}$	$1.10^{+0.94}_{-0.77}$
091402.7-010208	5561	$0.57^{+3.99}_{-0.10}$	138^{+62}_{-62}	$2.5^{+1.7}_{-1.7}$	$1.41^{+0.75}_{-0.77}$	$1.80^{+0.33}_{-0.62}$
091403.3+013846	1465	$0.150^{+0.155}_{-0.149}$	284^{+68}_{-74}	$1.8^{+1.9}_{-1.9}$	$0.73^{+0.53}_{-0.27}$	$2.00^{+0.14}_{-0.14}$
091412.6+001856	1844	$0.55^{+1.13}_{-0.30}$	215^{+56}_{-49}	$2.0^{+1.6}_{-1.6}$	$0.89^{+0.63}_{-0.37}$	$1.60^{+0.28}_{-0.47}$
091414.9+022709	1424	$1.7^{+2.5}_{-2.5}$	79^{+48}_{-35}	$1.47^{+1.4}_{-1.49}$	$1.55^{+0.88}_{-0.88}$	$1.90^{+0.56}_{-0.56}$
091417.7+031159	396	$0.108^{+0.225}_{-0.039}$	103^{+30}_{-32}	$2.5^{+2.0}_{-1.5}$	$1.28^{+0.84}_{-0.73}$	$3.02^{+0.28}_{-0.25}$
091423.9+022833	7735	$0.47^{+1.33}_{-1.31}$	226^{+88}_{-88}	$2.0^{+1.9}_{-1.8}$	$1.07^{+0.48}_{-0.44}$	$1.14^{+0.40}_{-0.67}$
091431.6+010910	4637	$1.9^{+5.2}_{-5.2}$	70^{+38}_{-38}	$2.5^{+1.8}_{-1.7}$	$1.47^{+0.47}_{-0.67}$	$2.08^{+0.13}_{-0.13}$
091433.8+022718	3159	$0.195^{+0.800}_{-0.089}$	222^{+77}_{-66}	$3.1^{+1.4}_{-1.4}$	$1.56^{+0.80}_{-0.71}$	$1.84^{+0.25}_{-0.41}$
091439.5-014416	6130	$0.166^{+0.040}_{-0.07}$	242^{+90}_{-87}	$2.1^{+1.6}_{-1.6}$	$1.18^{+0.86}_{-0.65}$	$1.64^{+0.37}_{-0.37}$
091445.7+032755	8636	$0.64^{+2.56}_{-0.46}$	196^{+62}_{-67}	$2.4^{+1.7}_{-1.7}$	$1.61^{+0.63}_{-0.89}$	$1.24^{+0.42}_{-0.69}$
091445.8+042621	13299	71^{+15}_{-30}	70^{+15}_{-15}	$3.64^{+1.00}_{-1.92}$	$0.69^{+0.32}_{-0.22}$	$0.53^{+0.27}_{-0.28}$
091446.1+001047	1917	$0.31^{+0.088}_{-0.076}$	200^{+61}_{-61}	$2.5^{+1.7}_{-1.7}$	$1.39^{+0.64}_{-0.64}$	$2.10^{+0.17}_{-0.22}$
091450.6-022606	2154	$0.47^{+0.38}_{-0.33}$	150^{+66}_{-68}	$2.6^{+1.7}_{-1.7}$	$1.39^{+0.65}_{-0.72}$	$2.04^{+0.23}_{-0.40}$
091453.6+041613	372	$4.9^{+17.0}_{-3.0}$	106^{+38}_{-33}	$0.92^{+0.95}_{-0.60}$	$0.56^{+0.16}_{-0.15}$	$1.93^{+0.42}_{-0.05}$
091509.5+051521	6244	$1.4^{+3.7}_{-3.7}$	250^{+140}_{-140}	$2.0^{+1.8}_{-1.4}$	$1.18^{+0.90}_{-0.90}$	$1.10^{+0.37}_{-0.37}$
091512.2+043506	4253	$6.7^{+40.7}_{-6.2}$	65^{+40}_{-24}	$2.8^{+1.5}_{-1.5}$	$1.61^{+0.62}_{-0.73}$	$1.40^{+0.77}_{-0.89}$
091517.4-005909	13537	$0.33^{+0.69}_{-0.69}$	234^{+95}_{-85}	$2.7^{+1.7}_{-1.7}$	$1.47^{+0.75}_{-0.75}$	$0.78^{+0.51}_{-0.51}$
091520.5+045203	14354	$0.87^{+0.63}_{-0.13}$	116^{+55}_{-55}	$2.2^{+2.0}_{-1.8}$	$1.53^{+0.66}_{-0.88}$	$1.33^{+0.78}_{-0.78}$
091522.5+041201	14525	$1.5^{+2.8}_{-1.2}$	108^{+68}_{-67}	$2.3^{+1.8}_{-1.8}$	$1.72^{+0.57}_{-0.86}$	$1.20^{+0.63}_{-0.72}$
091543.5-004944	10164	$5.1^{+11.1}_{-4.8}$	48^{+40}_{-31}	$2.6^{+1.7}_{-1.7}$	$1.62^{+0.63}_{-0.71}$	$1.72^{+0.31}_{-1.09}$
091553.1+040545	12204	$0.63^{+8.07}_{-0.46}$	72^{+55}_{-33}	$3.0^{+1.5}_{-2.0}$	$1.69^{+0.57}_{-0.78}$	$1.92^{+0.76}_{-1.08}$
091555.6-013248	888	$1.5^{+4.8}_{-4.8}$	186^{+93}_{-78}	$2.1^{+1.7}_{-1.7}$	$1.35^{+0.78}_{-0.66}$	$1.69^{+0.24}_{-0.34}$
091601.8+000831	9930	$1.7^{+1.7}_{-1.7}$	147^{+74}_{-74}	$2.6^{+1.5}_{-1.5}$	$1.63^{+0.62}_{-0.72}$	$0.98^{+0.59}_{-0.59}$
091609.4+013519	8107	$0.34^{+1.65}_{-0.21}$	219^{+124}_{-97}	$2.3^{+1.8}_{-1.8}$	$1.42^{+0.$	

Table 5: continued.

Cluster (eFEDS J+)	ID_SRC	n_0 10^{-7} cm^{-6}	r_s arcsec	ϵ	β	α
091648.1+030506	5300	4.7 $^{+29.0}_{-4.2}$	89 $^{+56}_{-57}$	2.5 $^{+1.6}_{-1.7}$	1.46 $^{+0.75}_{-0.74}$	1.52 $^{+0.56}_{-0.84}$
091655.7-011158	11550	1.14 $^{+8.59}_{-0.93}$	91 $^{+72}_{-56}$	2.6 $^{+1.6}_{-1.7}$	1.44 $^{+0.74}_{-0.68}$	1.42 $^{+1.10}_{-0.89}$
091722.4+010118	1526	1.3 $^{+5.1}_{-1.0}$	157 $^{+77}_{-62}$	2.3 $^{+1.8}_{-1.9}$	1.53 $^{+0.70}_{-0.63}$	1.73 $^{+0.29}_{-0.44}$
091741.1+024518	10140	0.38 $^{+0.30}_{-0.24}$	170 $^{+150}_{-110}$	2.6 $^{+1.7}_{-1.7}$	1.53 $^{+0.66}_{-0.77}$	0.86 $^{+0.59}_{-0.59}$
091749.4+014621	9976	0.42 $^{+1.16}_{-0.27}$	267 $^{+91}_{-83}$	2.7 $^{+1.7}_{-1.7}$	1.64 $^{+0.59}_{-0.73}$	1.22 $^{+0.33}_{-0.57}$
091757.1+050915	1934	22 $^{+20}_{-20}$	110 $^{+71}_{-58}$	2.7 $^{+1.6}_{-1.6}$	1.56 $^{+0.65}_{-0.62}$	1.06 $^{+0.70}_{-0.70}$
091806.0-003228	3910	29 $^{+11}_{-27}$	42 $^{+27}_{-16}$	2.9 $^{+1.8}_{-1.8}$	1.63 $^{+0.77}_{-0.78}$	1.09 $^{+0.96}_{-0.76}$
091842.2+034754	10019	2.2 $^{+31.0}_{-1.9}$	76 $^{+60}_{-40}$	3.0 $^{+1.4}_{-1.4}$	1.56 $^{+0.64}_{-0.81}$	1.39 $^{+0.97}_{-0.93}$
091849.0+021204	994	1.12 $^{+0.93}_{-0.80}$	250 $^{+140}_{-140}$	1.7 $^{+1.8}_{-1.8}$	1.33 $^{+0.80}_{-0.71}$	1.35 $^{+0.27}_{-0.27}$
091850.7+030942	19979	0.98 $^{+0.66}_{-0.66}$	179 $^{+91}_{-75}$	2.6 $^{+1.7}_{-1.7}$	1.68 $^{+0.58}_{-0.83}$	1.18 $^{+0.33}_{-0.64}$
091851.7+021432	4105	0.42 $^{+0.93}_{-0.28}$	185 $^{+108}_{-94}$	2.9 $^{+1.4}_{-1.4}$	1.40 $^{+0.70}_{-0.68}$	1.05 $^{+0.65}_{-0.64}$
091855.8+004916	12125	5.1 $^{+1.3}_{-4.3}$	99 $^{+61}_{-36}$	2.7 $^{+1.5}_{-1.5}$	1.55 $^{+0.66}_{-0.74}$	1.08 $^{+0.66}_{-0.67}$
091858.0+024946	7194	0.55 $^{+1.57}_{-0.38}$	231 $^{+81}_{-76}$	2.8 $^{+1.7}_{-1.8}$	1.56 $^{+0.64}_{-0.73}$	1.29 $^{+0.35}_{-0.57}$
091900.0+035311	5545	0.52 $^{+2.23}_{-1.77}$	211 $^{+95}_{-81}$	2.5 $^{+1.8}_{-1.8}$	1.51 $^{+0.69}_{-0.71}$	1.46 $^{+0.57}_{-0.57}$
091925.6-010430	4254	3.9 $^{+7.4}_{-7.4}$	76 $^{+78}_{-39}$	2.4 $^{+1.7}_{-1.7}$	1.36 $^{+0.81}_{-0.76}$	1.72 $^{+0.33}_{-1.17}$
091934.6+033941	1892	44 $^{+195}_{-195}$	41 $^{+31}_{-15}$	2.6 $^{+1.8}_{-2.0}$	1.29 $^{+0.76}_{-0.59}$	1.27 $^{+1.07}_{-0.93}$
091936.6+042553	11376	2.0 $^{+10.6}_{-10.6}$	77 $^{+55}_{-52}$	2.5 $^{+1.8}_{-1.8}$	1.57 $^{+0.76}_{-0.73}$	1.36 $^{+0.68}_{-0.81}$
091957.7+035012	4131	7.2 $^{+13.2}_{-6.1}$	105 $^{+66}_{-42}$	2.2 $^{+1.8}_{-1.8}$	1.38 $^{+0.80}_{-0.78}$	0.99 $^{+0.64}_{-0.66}$
092002.1+010219	150	1.85 $^{+2.35}_{-0.89}$	241 $^{+46}_{-43}$	2.1 $^{+1.9}_{-1.9}$	0.78 $^{+0.54}_{-0.30}$	2.13 $^{+0.16}_{-0.19}$
092004.3+010023	11754	16 $^{+41}_{-37}$	81 $^{+37}_{-37}$	0.39 $^{+0.73}_{-0.29}$	1.92 $^{+0.59}_{-0.59}$	0.18 $^{+0.39}_{-0.34}$
092022.0+030106	6534	1.18 $^{+18.46}_{-0.98}$	66 $^{+92}_{-46}$	2.6 $^{+1.7}_{-1.8}$	1.51 $^{+0.70}_{-0.82}$	1.97 $^{+1.14}_{-1.22}$
092022.8+045012	5320	0.249 $^{+0.78}_{-0.78}$	202 $^{+68}_{-68}$	1.6 $^{+2.1}_{-2.1}$	0.80 $^{+0.76}_{-0.76}$	1.96 $^{+0.22}_{-0.22}$
092023.2+013444	222	0.75 $^{+0.66}_{-0.52}$	161 $^{+62}_{-67}$	2.3 $^{+2.0}_{-2.0}$	1.34 $^{+0.68}_{-0.68}$	2.44 $^{+0.13}_{-0.21}$
092031.3+024710	18068	1.7 $^{+6.0}_{-1.5}$	98 $^{+55}_{-44}$	2.3 $^{+1.8}_{-1.8}$	1.46 $^{+0.74}_{-0.75}$	1.10 $^{+0.74}_{-0.74}$
092031.8+040621	4115	4.2 $^{+30.4}_{-9.9}$	91 $^{+38}_{-38}$	2.5 $^{+1.7}_{-1.7}$	1.60 $^{+0.55}_{-0.67}$	1.60 $^{+0.73}_{-0.88}$
092037.0-011506	5739	0.36 $^{+0.87}_{-0.23}$	247 $^{+85}_{-76}$	2.6 $^{+1.7}_{-1.7}$	1.52 $^{+0.68}_{-0.73}$	1.39 $^{+0.44}_{-0.44}$
092037.9+033528	6467	1.16 $^{+22.4}_{-0.98}$	74 $^{+77}_{-49}$	2.6 $^{+1.6}_{-1.6}$	1.57 $^{+0.58}_{-0.70}$	1.8 $^{+1.2}_{-0.88}$
092039.1+004725	6669	0.67 $^{+0.88}_{-0.51}$	113 $^{+49}_{-35}$	2.4 $^{+1.7}_{-1.7}$	1.38 $^{+0.66}_{-0.68}$	1.92 $^{+0.38}_{-0.62}$
092041.1+041117	10334	2.7 $^{+28.5}_{-2.4}$	75 $^{+65}_{-35}$	2.5 $^{+1.9}_{-1.5}$	1.55 $^{+0.66}_{-0.70}$	1.55 $^{+0.62}_{-1.01}$
092046.2+002849	1915	0.166 $^{+0.739}_{-0.070}$	259 $^{+94}_{-137}$	1.10 $^{+1.98}_{-0.83}$	0.60 $^{+0.67}_{-0.59}$	1.96 $^{+0.14}_{-0.20}$
092049.5+024513	489	2.8 $^{+45}_{-1.6}$	153 $^{+52}_{-45}$	1.34 $^{+0.92}_{-0.92}$	0.69 $^{+0.38}_{-0.22}$	1.53 $^{+0.17}_{-0.23}$
092053.4+021125	18194	0.23 $^{+0.32}_{-0.13}$	260 $^{+110}_{-100}$	2.7 $^{+1.7}_{-1.8}$	1.53 $^{+0.66}_{-0.71}$	0.90 $^{+0.47}_{-0.52}$
092105.0+004452	6459	3.4 $^{+28.6}_{-3.1}$	75 $^{+59}_{-33}$	3.1 $^{+1.8}_{-1.8}$	1.55 $^{+0.79}_{-0.74}$	1.46 $^{+0.98}_{-0.98}$
092121.2+031726	100	26 $^{+21}_{-21}$	93 $^{+103}_{-32}$	1.11 $^{+1.15}_{-0.80}$	0.80 $^{+0.70}_{-0.57}$	1.20 $^{+0.34}_{-0.42}$
092133.2+043431	9512	1.8 $^{+7.1}_{-1.5}$	119 $^{+56}_{-35}$	2.9 $^{+1.5}_{-1.5}$	1.65 $^{+0.58}_{-0.77}$	1.20 $^{+0.55}_{-0.73}$
092134.4+015832	810	0.59 $^{+14.5}_{-0.46}$	210 $^{+65}_{-94}$	2.5 $^{+1.7}_{-1.7}$	1.39 $^{+0.66}_{-0.74}$	1.64 $^{+0.49}_{-0.83}$
092135.4+005128	7447	0.72 $^{+0.53}_{-0.53}$	121 $^{+95}_{-76}$	2.5 $^{+1.7}_{-1.7}$	1.55 $^{+0.65}_{-0.71}$	1.37 $^{+0.94}_{-0.90}$
092136.4-001449	4168	2.0 $^{+0.44}_{-1.5}$	161 $^{+80}_{-58}$	2.8 $^{+1.5}_{-1.5}$	1.67 $^{+0.57}_{-0.80}$	1.18 $^{+0.48}_{-0.67}$
092202.2+034520	5347	4.4 $^{+48}_{-18}$	128 $^{+28}_{-27}$	1.8 $^{+1.4}_{-1.4}$	0.74 $^{+0.50}_{-0.50}$	0.54 $^{+0.64}_{-0.34}$
092209.3+034628	367	47 $^{+13}_{-13}$	58 $^{+14}_{-14}$	0.47 $^{+0.68}_{-0.35}$	0.60 $^{+0.12}_{-0.13}$	0.50 $^{+0.33}_{-0.33}$
092212.0-002731	857	0.63 $^{+0.92}_{-0.98}$	299 $^{+111}_{-85}$	2.0 $^{+1.7}_{-1.7}$	1.46 $^{+0.68}_{-0.69}$	1.62 $^{+0.18}_{-0.21}$
092220.4+034806	4014	9.0 $^{+9.8}_{-5.6}$	77 $^{+18}_{-18}$	1.19 $^{+0.84}_{-0.84}$	0.86 $^{+0.34}_{-0.30}$	0.56 $^{+0.66}_{-0.40}$
092235.8-002443	3133	11.2 $^{+8.8}_{-4.8}$	97 $^{+31}_{-36}$	1.12 $^{+0.50}_{-0.66}$	0.62 $^{+0.88}_{-0.23}$	1.06 $^{+0.54}_{-0.50}$
092241.9+020719	1535	1.6 $^{+1.3}_{-1.3}$	154 $^{+80}_{-84}$	2.6 $^{+1.7}_{-1.7}$	1.61 $^{+0.44}_{-0.73}$	1.22 $^{+0.53}_{-0.66}$
092246.2+034251	2216	7.3 $^{+11.0}_{-4.6}$	78 $^{+23}_{-17}$	1.06 $^{+0.99}_{-0.74}$	0.90 $^{+0.29}_{-0.28}$	1.04 $^{+0.68}_{-0.66}$
092246.4+042424	5348	1.7 $^{+14.9}_{-5.5}$	109 $^{+79}_{-57}$	2.3 $^{+1.7}_{-1.6}$	1.41 $^{+0.73}_{-0.71}$	1.62 $^{+0.46}_{-0.96}$
092258.2+032041	4833	4.8 $^{+26.8}_{-4.4}$	87 $^{+57}_{-36}$	2.6 $^{+1.7}_{-1.7}$	1.54 $^{+0.63}_{-0.67}$	1.32 $^{+0.64}_{-0.79}$
092302.6+034002	9076	0.26 $^{+0.62}_{-0.16}$	283 $^{+112}_{-92}$	2.3 $^{+1.7}_{-1.7}$	1.53 $^{+0.65}_{-0.75}$	0.95 $^{+0.44}_{-0.54}$
092312.0+000355	6657	0.40 $^{+0.92}_{-0.47}$	77 $^{+184}_{-64}$	2.5 $^{+1.7}_{-1.7}$	1.53 $^{+0.65}_{-0.63}$	0.98 $^{+1.57}_{-0.73}$
092328.2+043107	6063	13 $^{+11}_{-11}$	88 $^{+41}_{-26}$	2.7 $^{+1.6}_{-1.6}$	1.71 $^{+0.71}_{-0.71}$	0.70 $^{+0.55}_{-0.53}$
092333.1-001917	7637	12 $^{+44}_{-11}$	79 $^{+39}_{-29}$	2.9 $^{+1.5}_{-1.5}$	1.58 $^{+0.62}_{-0.73}$	1.11 $^{+0.73}_{-0.73}$
092335.1+012907	4806	0.49 $^{+1.02}_{-0.27}$	272 $^{+116}_{-94}$	2.5 $^{+1.7}_{-1.7}$	1.54 $^{+0.69}_{-0.82}$	0.80 $^{+0.82}_{-0.81}$
092339.0+052654	1894	40 $^{+788}_{-38}$	62 $^{+58}_{-33}$	3.0 $^{+1.4}_{-1.8}$	1.64 $^{+0.60}_{-0.75}$	2.5 $^{+0.81}_{-1.4}$
092346.8-005330	11530	1.22 $^{+2.80}_{-0.95}$	162 $^{+68}_{-55}$	2.6 $^{+1.7}_{-1.8}$	1.66 $^{+0.59}_{-0.72}$	1.00 $^{+0.53}_{-0.61}$
092402.2+054205	7973	4.91 $^{+19.4}_{-16.6}$	142 $^{+63}_{-60}$	2.6 $^{+1.7}_{-1.7}$	1.44 $^{+0.72}_{-0.72}$	1.10 $^{+0.71}_{-0.71}$
092405.0-013059	298	1.6 $^{+4.9}_{-1.1}$	163 $^{+67}_{-66}$	2.4 $^{+1.7}_{-1.7}$	1.44 $^{+0.75}_{-0.67}$	1.61 $^{+0.24}_{-0.37}$
092409.4+040057	1437	0.34 $^{+0.67}_{-0.19}$	322 $^{+96}_{-96}$	2.6 $^{+1.7}_{-1.7}$	1.62 $^{+0.64}_{-0.64}$	1.58 $^{+0.39}_{-0.39}$
092421.9-005103	8544	0.47 $^{+0.86}_{-0.34}$	139 $^{+56}_{-56}$	2.8 $^{+1.8}_{-1.8}$	1.44 $^{+0.65}_{-0.72}$	1.66 $^{+0.32}_{-0.71}$
092454.7+014901	7841	0.98 $^{+10.90}_{-0.80}$	96 $^{+60}_{-47}$	2.7 $^{+1.6}_{-1.7}$	1.51 $^{+0.70}_{-0.75}$	1.63 $^{+0.53}_{-0.88}$
092502.6+022612	7060	2.7 $^{+19.4}_{-2.4}$	93 $^{+56}_{-40}$	2.5 $^{+1.7}_{-1.7}$	1.65 $^{+0.58}_{-0.58}$	1.40 $^{+0.61}_{-0.87}$
092504.3-005602	11531	2.2 $^{+52.3}_{-52.3}$	67 $^{+64}_{-43}$	2.7 $^{+1.6}_{-1.6}$	1.65 $^{+0.55}_{-0.81}$	1.6 $^{+0.77}_{-1.0}$
092510.0-014830	5079	2.7 $^{+19.4}_{-21.2}$	78 $^{+38}_{-43}$	2.9 $^{+1.5}_{-1.5}$	1.22 $^{+0.64}_{-0.50}$	1.91 $^{+0.48}_{-0.69}$
092511.8-011436	9471	0.97 $^{+0.82}_{-0.82}$	139 $^{+77}_{-52}$	2.1 $^{+1.5}_{-1.5}$	1.68 $^{+0.62}_{-0.92}$	1.18 $^{+0.57}_{-0.79}$
092522.1-013148	6653	0.90 $^{+0.70}_{-0.70}$	154 $^{+74}_{-60}$	2.3 $^{+1.5}_{-1.5}$	1.65 $^{+0.61}_{-0.75}$	1.37 $^{+0.40}_{-0.68}$
092533.6-014205	1483	2.3 $^{+9.9}_{-1.0}$	115 $^{+51}_{-52}$	1.7 $^{+1.7}_{-1.5}$	1.06 $^{+0.82}_{-0.82}$	1.46 $^{+0.36}_{-0.64}$
092546.3-014347	566	1.17 $^{+1.96}_{-0.67}$	224 $^{+38}_{-69}$	2.2 $^{+1.5}_{-1.5}$	1.65 $^{+0.54}_{-0.51}$	1.46 $^{+0.28}_{-0.34}$
092548.9-011725	5488	0.80 $^{+2.64}_{-0.63}$	206 $^{+88}_{-69}$	2.6 $^{+1.7}_{-1.7}$	1.64 $^{+0.60}_{-0.78}$	1.09 $^{+0.50}_{-0.65}$
092553.3+015519	991	0.51 $^{+3.88}_{-1.96}$	105 $^{+65}_{-55}$	2.6 $^{+1.6}_{-1.6}$	1.50 $^{+0.61}_{-0.70}$	0.99 $^{+0.22}_{-0.68}$
092555.6+004311	6732	1.7 $^{+1.8}_{-1.0}$	258 $^{+81}_{-82}$	2.6 $^{+1.6}_{-1.8}$	1.60 $^{+0.73}_{-0.73}$	0.62 $^{+0.41}_{-0.41}$
092619.9+021207	8160	2.4 $^{+11.1}_{-11.1}$	113 $^{+66}_{-40}$	2.8 $^{+1.5}_{-1.8$		

Table 5: continued.

Cluster (eFEDS J+)	ID_SRC	n_0 10^{-7} cm^{-6}	r_s arcsec	ϵ	β	α
092648.0+050124	6875	$3.0^{+14.7}_{-2.6}$	158^{+101}_{-53}	$2.3^{+1.7}_{-1.5}$	$1.65^{+0.61}_{-0.86}$	$1.40^{+0.48}_{-0.70}$
092650.5+035755	671	$2.1^{+50.9}_{-56}$	96^{+51}_{-51}	$2.5^{+1.9}_{-1.8}$	$1.42^{+0.81}_{-0.76}$	$2.22^{+0.32}_{-0.83}$
092711.5+011735	10285	$2.0^{+8.2}_{-1.7}$	117^{+61}_{-45}	$2.7^{+1.8}_{-1.8}$	$1.55^{+0.65}_{-0.72}$	$1.17^{+0.59}_{-0.73}$
092735.3+014423	266	$0.25^{+0.13}_{-0.12}$	217^{+57}_{-53}	$2.7^{+1.8}_{-1.8}$	$1.11^{+0.69}_{-0.69}$	$2.15^{+0.31}_{-0.68}$
092737.7+020607	1924	$4.6^{+9.0}_{-3.3}$	159^{+70}_{-58}	$2.3^{+1.7}_{-1.5}$	$1.50^{+0.69}_{-0.72}$	$0.91^{+0.45}_{-0.53}$
092739.7-010427	2636	$0.67^{+1.87}_{-0.16}$	260^{+94}_{-40}	$2.8^{+1.6}_{-1.8}$	$1.51^{+0.69}_{-0.77}$	$1.14^{+0.42}_{-0.64}$
092740.1-002922	3454	$0.22^{+1.00}_{-0.11}$	160^{+62}_{-66}	$2.5^{+1.7}_{-1.7}$	$1.08^{+0.87}_{-0.87}$	$2.16^{+0.24}_{-0.27}$
092740.1+042038	4999	$0.167^{+0.18}_{-0.063}$	300^{+230}_{-190}	$2.8^{+1.5}_{-1.7}$	$1.40^{+0.81}_{-0.80}$	$0.44^{+0.99}_{-0.34}$
092740.7-015320	7063	$0.57^{+0.33}_{-0.23}$	154^{+71}_{-60}	$2.5^{+1.7}_{-1.7}$	$1.52^{+0.67}_{-0.77}$	$1.60^{+0.35}_{-0.59}$
092744.6+045630	17315	$2.0^{+1.7}_{-1.7}$	81^{+54}_{-33}	$2.6^{+1.6}_{-1.7}$	$1.70^{+0.80}_{-0.80}$	$1.30^{+0.66}_{-0.84}$
092755.9+000439	10316	$9.4^{+38.6}_{-8.0}$	86^{+49}_{-31}	$2.8^{+1.5}_{-1.8}$	$1.60^{+0.75}_{-0.75}$	$1.16^{+0.68}_{-0.77}$
092803.4+010953	1527	$0.42^{+0.33}_{-0.27}$	138^{+57}_{-58}	$2.1^{+1.8}_{-1.8}$	$1.29^{+0.88}_{-0.70}$	$2.35^{+0.20}_{-0.23}$
092807.5-001353	13561	$1.11^{+13.17}_{-0.83}$	93^{+48}_{-37}	$2.3^{+1.6}_{-1.8}$	$1.49^{+0.67}_{-0.68}$	$1.76^{+0.71}_{-0.71}$
092807.7-012704	6687	$2.0^{+6.5}_{-1.5}$	80^{+170}_{-62}	$2.5^{+1.7}_{-1.7}$	$1.50^{+0.69}_{-0.79}$	$1.12^{+0.45}_{-0.89}$
092813.0-004508	13305	$1.8^{+1.4}_{-1.4}$	148^{+49}_{-49}	$2.4^{+1.8}_{-1.8}$	$1.49^{+0.69}_{-0.70}$	$0.81^{+0.54}_{-0.54}$
092821.1+041941	7167	$0.45^{+1.85}_{-0.32}$	130^{+140}_{-100}	$2.9^{+1.8}_{-2.0}$	$1.80^{+0.51}_{-0.79}$	$0.82^{+0.90}_{-0.59}$
092821.2+042149	666	$2.4^{+1.0}_{-1.6}$	180^{+75}_{-75}	$1.9^{+2.2}_{-1.8}$	$1.86^{+0.53}_{-0.53}$	$1.46^{+0.33}_{-0.74}$
092828.3-000955	845	$0.93^{+4.51}_{-0.72}$	131^{+69}_{-63}	$2.7^{+1.6}_{-1.7}$	$1.14^{+0.68}_{-0.51}$	$1.26^{+0.71}_{-0.85}$
092832.4+041517	4192	$1.3^{+6.8}_{-1.5}$	114^{+73}_{-56}	$2.3^{+1.8}_{-1.8}$	$1.47^{+0.75}_{-0.70}$	$1.51^{+0.91}_{-0.96}$
092844.0+005318	8858	$1.14^{+3.81}_{-0.92}$	158^{+56}_{-56}	$2.7^{+1.5}_{-1.8}$	$1.62^{+0.61}_{-0.77}$	$1.03^{+0.57}_{-0.67}$
092846.5+000056	10287	$0.76^{+2.05}_{-0.57}$	210^{+91}_{-71}	$2.6^{+1.6}_{-1.8}$	$1.61^{+0.61}_{-0.76}$	$0.99^{+0.45}_{-0.61}$
092859.0+040532	4029	$0.33^{+1.57}_{-0.30}$	265^{+74}_{-59}	$2.5^{+1.6}_{-1.8}$	$1.30^{+0.70}_{-0.38}$	$1.53^{+0.20}_{-0.27}$
092900.0-003920	5593	$0.26^{+0.12}_{-0.13}$	159^{+60}_{-60}	$2.5^{+1.6}_{-1.6}$	$1.37^{+0.66}_{-0.58}$	$1.82^{+0.38}_{-0.86}$
092910.2+022034	5092	11^{+31}_{-10}	76^{+47}_{-47}	$2.7^{+1.7}_{-1.8}$	$1.64^{+0.59}_{-0.59}$	$1.06^{+0.30}_{-0.80}$
092911.0+021118	10090	$1.27^{+2.6}_{-1.0}$	43^{+32}_{-32}	$2.8^{+1.6}_{-1.8}$	$1.66^{+0.58}_{-0.62}$	$1.87^{+0.57}_{-1.2}$
092915.2+002427	8178	$0.77^{+0.39}_{-0.39}$	177^{+77}_{-62}	$2.7^{+1.8}_{-1.7}$	$1.54^{+0.67}_{-0.77}$	$1.34^{+0.40}_{-0.68}$
092915.7-001357	1549	$0.21^{+0.36}_{-0.10}$	178^{+52}_{-62}	$2.0^{+2.1}_{-1.4}$	$1.07^{+0.91}_{-0.56}$	$2.27^{+0.16}_{-0.18}$
092918.3+044925	6602	$4.6^{+8.5}_{-3.6}$	115^{+55}_{-33}	$2.8^{+1.5}_{-1.8}$	$1.71^{+0.66}_{-0.73}$	$0.86^{+0.64}_{-0.64}$
092921.7+040040	609	$2.1^{+15.7}_{-1.8}$	108^{+63}_{-43}	$2.7^{+1.7}_{-1.7}$	$1.56^{+0.63}_{-0.72}$	$2.16^{+0.31}_{-0.51}$
092928.3+042411	3563	$1.3^{+7.9}_{-1.4}$	133^{+52}_{-51}	$2.5^{+1.7}_{-1.8}$	$1.54^{+0.68}_{-0.75}$	$1.59^{+0.42}_{-0.74}$
092941.7+023026	7770	$0.38^{+0.98}_{-0.38}$	260^{+150}_{-100}	$2.2^{+1.8}_{-1.8}$	$1.41^{+0.61}_{-0.73}$	$0.66^{+0.44}_{-0.44}$
092953.5+002801	12565	$0.70^{+1.49}_{-0.51}$	208^{+72}_{-69}	$2.7^{+1.7}_{-1.8}$	$1.65^{+0.60}_{-0.73}$	$0.89^{+0.58}_{-0.64}$
092955.8-003403	1967	$0.204^{+0.288}_{-0.191}$	283^{+88}_{-32}	$2.8^{+1.6}_{-1.7}$	$1.22^{+0.86}_{-0.66}$	$1.88^{+0.16}_{-0.19}$
093003.3+035630	288	$5.9^{+12.19}_{-4.0}$	103^{+26}_{-28}	$2.5^{+1.6}_{-1.6}$	$1.56^{+0.62}_{-0.66}$	$1.89^{+0.28}_{-0.35}$
093009.0+040144	536	14^{+98}_{-12}	78^{+48}_{-42}	$1.9^{+1.8}_{-1.4}$	$1.04^{+0.97}_{-0.50}$	$1.63^{+0.45}_{-0.77}$
093011.2+031648	16215	$2.8^{+5.0}_{-3.5}$	66^{+56}_{-40}	$2.6^{+1.6}_{-1.8}$	$1.50^{+0.69}_{-0.78}$	$1.86^{+0.39}_{-0.99}$
093012.0+030202	7539	$3.1^{+20.0}_{-2.8}$	77^{+48}_{-33}	$2.6^{+1.6}_{-1.8}$	$1.59^{+0.64}_{-0.76}$	$1.47^{+0.69}_{-0.92}$
093022.1+021835	8763	$0.68^{+3.69}_{-0.74}$	163^{+70}_{-65}	$2.9^{+1.4}_{-1.8}$	$1.40^{+0.72}_{-0.72}$	$1.61^{+0.37}_{-0.62}$
093025.3+021714	1003	$0.59^{+0.34}_{-0.34}$	233^{+60}_{-60}	$3.2^{+1.6}_{-1.9}$	$1.58^{+0.63}_{-0.63}$	$1.83^{+0.20}_{-0.29}$
093025.7-020507	1064	$1.23^{+0.40}_{-0.40}$	130^{+60}_{-60}	$2.5^{+1.7}_{-1.7}$	$0.86^{+0.64}_{-0.36}$	$1.38^{+0.45}_{-0.83}$
093049.2-003714	1823	$0.94^{+0.49}_{-0.71}$	198^{+57}_{-57}	$2.3^{+1.7}_{-1.7}$	$1.39^{+0.71}_{-0.71}$	$1.39^{+0.38}_{-0.60}$
093056.9+034825	4579	$0.186^{+0.0556}_{-0.071}$	214^{+65}_{-65}	$2.4^{+1.7}_{-1.7}$	$1.18^{+0.82}_{-0.68}$	$1.85^{+0.25}_{-0.37}$
093117.4-015643	11648	$3.8^{+11.0}_{-2.8}$	42^{+16}_{-15}	$1.25^{+0.35}_{-0.35}$	$0.68^{+0.26}_{-0.18}$	$0.97^{+0.63}_{-0.57}$
093138.7-020933	5201	$0.87^{+3.41}_{-0.73}$	161^{+88}_{-88}	$2.7^{+1.7}_{-1.7}$	$1.62^{+0.63}_{-0.63}$	$1.19^{+0.50}_{-0.75}$
093141.2-004717	1705	$0.60^{+0.46}_{-0.14}$	119^{+54}_{-56}	$2.1^{+2.0}_{-1.5}$	$1.52^{+0.80}_{-0.86}$	$2.00^{+0.10}_{-1.01}$
093149.8-020143	6494	$0.143^{+0.505}_{-0.089}$	259^{+106}_{-97}	$3.2^{+1.3}_{-1.3}$	$1.37^{+0.84}_{-0.71}$	$1.35^{+0.30}_{-0.52}$
093151.3-002212	836	$1.28^{+0.97}_{-0.95}$	150^{+59}_{-59}	$2.6^{+1.7}_{-1.7}$	$1.57^{+0.66}_{-0.80}$	$1.91^{+0.24}_{-0.24}$
093207.5-021317	1674	$0.49^{+0.46}_{-0.38}$	108^{+57}_{-53}	$2.3^{+1.9}_{-1.6}$	$1.30^{+0.78}_{-0.68}$	$2.29^{+0.25}_{-0.50}$
093222.0+012412	7346	$1.67^{+4.2}_{-2.4}$	52^{+41}_{-41}	$2.3^{+1.7}_{-1.5}$	$1.62^{+0.59}_{-0.69}$	$2.15^{+0.84}_{-0.43}$
093231.0+010617	4873	11^{+41}_{-11}	86^{+33}_{-33}	$2.8^{+1.6}_{-1.8}$	$1.56^{+0.79}_{-0.79}$	$1.06^{+0.75}_{-0.75}$
093232.8-015152	10734	$0.43^{+1.54}_{-0.46}$	165^{+90}_{-73}	$2.3^{+1.8}_{-1.6}$	$1.59^{+0.63}_{-0.78}$	$1.00^{+0.65}_{-0.62}$
093253.8+025917	5631	$1.17^{+0.85}_{-0.85}$	86^{+31}_{-31}	$2.6^{+1.6}_{-1.8}$	$1.46^{+0.60}_{-0.68}$	$1.60^{+0.27}_{-0.97}$
093301.3+024301	12582	$2.2^{+1.9}_{-1.9}$	64^{+40}_{-40}	$2.4^{+1.8}_{-1.8}$	$1.58^{+0.63}_{-0.81}$	$1.25^{+0.88}_{-0.87}$
093302.7-010145	5763	$2.8^{+5.6}_{-2.1}$	144^{+64}_{-47}	$2.8^{+1.6}_{-1.8}$	$1.47^{+0.70}_{-0.74}$	$0.90^{+0.55}_{-0.58}$
093316.6+004619	13784	$0.47^{+3.95}_{-0.33}$	92^{+103}_{-75}	$2.3^{+1.8}_{-1.8}$	$1.54^{+0.63}_{-0.74}$	$0.98^{+0.71}_{-0.49}$
093329.3+000334	5618	$1.7^{+8.1}_{-1.5}$	120^{+69}_{-44}	$2.5^{+1.7}_{-1.7}$	$1.47^{+0.84}_{-0.69}$	$1.38^{+0.77}_{-0.72}$
093332.1+020933	6577	$5.6^{+52.8}_{-3.0}$	71^{+46}_{-35}	$2.6^{+1.7}_{-1.7}$	$1.49^{+0.68}_{-0.68}$	$1.69^{+0.65}_{-0.98}$
093403.5-001422	900	$2.2^{+1.5}_{-1.5}$	129^{+72}_{-44}	$1.8^{+1.9}_{-1.9}$	$0.77^{+0.88}_{-0.88}$	$1.65^{+0.30}_{-0.66}$
093431.3-002309	1641	$0.85^{+3.58}_{-0.56}$	201^{+75}_{-89}	$2.3^{+1.8}_{-1.8}$	$1.16^{+0.83}_{-0.55}$	$1.63^{+0.27}_{-0.48}$
093436.1+051533	9995	$2.7^{+5.1}_{-1.9}$	182^{+70}_{-70}	$2.7^{+1.6}_{-1.6}$	$1.64^{+0.62}_{-0.62}$	$0.92^{+0.51}_{-0.58}$
093456.1+031518	7091	$4.9^{+13.9}_{-4.3}$	94^{+53}_{-32}	$2.5^{+1.8}_{-1.8}$	$1.62^{+0.76}_{-0.76}$	$0.99^{+0.68}_{-0.68}$
093500.7+005417	649	$11.1^{+38.2}_{-7.7}$	113^{+43}_{-43}	$2.4^{+1.8}_{-1.8}$	$1.61^{+0.65}_{-0.82}$	$1.19^{+0.38}_{-0.72}$
093513.0+004757	213	$18.5^{+38.7}_{-20.7}$	111^{+35}_{-35}	$1.49^{+0.95}_{-0.95}$	$0.77^{+0.85}_{-0.85}$	$0.93^{+0.31}_{-0.48}$
093520.7+003448	4394	$0.34^{+0.88}_{-0.20}$	209^{+71}_{-79}	$2.5^{+1.8}_{-1.8}$	$1.40^{+0.75}_{-0.79}$	$1.73^{+0.38}_{-0.48}$
093520.9+023234	82	$3.0^{+3.5}_{-1.3}$	132^{+28}_{-35}	$2.7^{+1.5}_{-1.6}$	$0.87^{+0.52}_{-0.74}$	$2.26^{+0.11}_{-0.13}$
093522.2+032329	1242	$3.7^{+2.6}_{-2.6}$	133^{+39}_{-36}	$2.2^{+1.9}_{-1.9}$	$1.33^{+0.84}_{-0.74}$	$1.34^{+0.58}_{-0.55}$
093525.6+023445	12009	$1.32^{+0.91}_{-0.91}$	201^{+65}_{-57}	$2.7^{+1.6}_{-1.6}$	$1.22^{+0.92}_{-0.63}$	$0.77^{+0.57}_{-0.52}$
093525.9+035101	3773	$4.2^{+38.9}_{-3.4}$	76^{+57}_{-57}	$2.4^{+1.8}_{-1.8}$	$1.50^{+0.68}_{-0.68}$	$1.89^{+0.34}_{-0.38}$
093531.4+022710	2609	$2.1^{+3.4}_{-1.8}$	130^{+70}_{-52}	$2.2^{+1.9}_{-1.9}$	$1.23^{+0.64}_{-0.65}$	$1.40^{+0.34}_{-0.80}$
093544.2-000339	6324	$1.18^{+3.87}_{-0.89}$	164^{+71}_{-52}	$2.8^{+1.5}_{-1.9}$	$1.57^{+0.68}_{-0.76}$	$1.31^{+0.46}_{-0.72}$
093546.3-000115	1761	$0.25^{+0.38}_{-0.10}$	187^{+35}_{-57}	$2.2^{+1.9}_{-1.9}$	$0.99^{+0.89}_{-0.89}$	$2.24^{+0.20}_{-0.20}$
093612.7+001650	4455	$0.56^{+1.72}_{-0.35}$	205^{+69}_{-74}	$2.4^{+1.8}_{-1.8}$	$1.42^{+0.92}_{-0.47}$	$1.$

Table 5: continued.

Cluster (eFEDS J+)	ID_SRC	n_0 10^{-7} cm^{-6}	r_s arcsec	ϵ	β	α
093744.1+024536	3372	$1.46^{+8.19}_{-0.87}$	155^{+59}_{-60}	$2.1^{+1.8}_{-1.4}$	$1.31^{+0.82}_{-0.95}$	$2.05^{+0.26}_{-0.35}$
093830.5+041523	10322	$0.21^{+0.11}_{-0.11}$	280^{+100}_{-100}	$2.5^{+1.4}_{-1.6}$	$1.28^{+0.67}_{-0.64}$	$1.26^{+0.39}_{-0.44}$
093938.3+042218	1594	$2.7^{+10.8}_{-10.5}$	139^{+62}_{-53}	$2.5^{+1.7}_{-1.7}$	$1.55^{+0.68}_{-0.66}$	$1.45^{+0.37}_{-0.56}$
094005.9+031329	4689	$6.6^{+19.5}_{-6.1}$	77^{+39}_{-39}	$2.5^{+1.6}_{-1.7}$	$1.52^{+0.69}_{-0.80}$	$1.73^{+0.31}_{-0.96}$
094007.3+035754	11337	$4.0^{+18.1}_{-3.4}$	105^{+65}_{-41}	$2.5^{+1.7}_{-1.7}$	$1.48^{+0.69}_{-0.69}$	$1.08^{+0.62}_{-0.74}$

Notes. Column 1: cluster name. Column 2: unique source ID presented in the eFEDS source catalog (Brunner et al. 2021). Columns 3, 4, 5, 6, 7: parameters of the Vikhlinin et al. (2006) model, n_0^2 , r_s , ϵ , β , α respectively.